CH_4 Reforming for Synthesis Gas Production over Supported Ni Catalysts

by

Hoon Sub Song

A thesis

presented to the University of Waterloo

in fulfillment of the

thesis requirement for the degree of

Master of Applied Science

in

Chemical Engineering

Waterloo, Ontario, Canada, 2010

Author's Declaration

I hereby declare that I am the sole author of this thesis. This is a true copy of the thesis, including any required final revisions, as accepted by my examiners.

I understand that my thesis may be made electronically available to the public.

Abstract

Partial oxidation of CH_4, CO_2 reforming of CH_4, and oxidative CO_2 reforming of CH_4 to produce synthesis gas at 700℃ over supported Ni catalysts have been studied. A Ni/Mg-Al catalyst was prepared by the solid phase crystallization (*spc*-) method starting from a hydrotalcite-type (HT) anionic precursor. From XRD analysis, only $Ni_{0.5}Mg_{2.5}Al$ catalyst consists of the layered hydrotalcite-type structure; not $Ni_{0.5}Ca_{2.5}Al$ and Ni/Al_2O_3 catalysts. By TPR test, the $Ni_{0.5}Mg_{2.5}Al$-HT catalyst requires a high reduction temperature than the $Ni_{0.5}Ca_{2.5}Al$ catalyst. It implies that the $Ni_{0.5}Mg_{2.5}Al$-HT which has a layered structure shows the stronger interaction strength between the molecules. It might increase the resistance of coke formation on the surface of the catalyst. For the reaction tests, the $Ni_{0.5}Ca_{2.5}Al$ showed the highest initial activity for synthesis gas production for all reactions; but, its activity was decreased quickly due to coke formation except during the partial oxidation of CH_4. The $Ni_{0.5}Mg_{2.5}Al$-HT showed a relatively higher reactivity compared to the equilibrium level than Ni/Al_2O_3 catalyst; and it shows very stable reactivity than other catalysts. By TPO test, the $Ni_{0.5}Mg_{2.5}Al$-HT has the lower amount of coke formed during the reaction than the $Ni_{0.5}Ca_{2.5}Al$ catalyst. It confirms that the $Ni_{0.5}Mg_{2.5}Al$-HT catalyst has stronger resistance to coke formation; and it leads to provide stable reactivity in any reforming conditions at high temperature. Therefore, the $Ni_{0.5}Mg_{2.5}Al$-HT catalyst was the most promising catalyst in terms of activity and stability for partial oxidation, CO_2 reforming, and oxidative CO_2 reforming of CH_4.

The $Ni_{0.5}Mg_{2.5}Al$-HT catalyst was used to investigate the CO_2 reforming of CH_4 kinetics. With increasing CH_4 partial pressures at constant CO_2 partial pressure, the rates of CH_4 consumption were increased. However, with increasing CO_2 partial pressure at constant CH_4 partial pressure, CH_4 consumption rates was increased at lower CO_2 partial pressure, but turned to independent at higher CO_2 partial pressure. When the partial pressure of H_2 was increased, the CO formation rate was decreased; it confirmed that the reverse water-gas shift (RWGS) reaction was occurring during the CO_2 reforming of CH_4 reaction. In addition, the reaction kinetic expression was proposed when the CH_4 dissociation step was considered as a rate-limiting step.

Acknowledgements

First of all, I have to thank my supervisors, Dr. Eric Croiset and Dr. Bill Epling, who showed great confidence in me, and provided me with a great deal of support. Also, I would like to thank Dr. John R. Grace (University of British Columbia, BC) who gave me the first chance to start the research experience. It changed my whole life. I really appreciate it.

I would like to thank the all staffs in the Department of Chemical Engineering for various supports, especially Lorna. Thank you!

I would like to thank my family, especially mom, and friends, Young-jae Kim, Hyun-ju Chang, Tak-dong Kim, Eun-mi Kim, Suk-woo Lee, Kyung-ju Kim, Mi-ok Park, Young-ho Seo, Myung-hee Woo, and Dr. Ho-young Hwang. You made my Waterloo life much more enjoyable.

I would like to show my special thanks to my lovely lady, Su-jeong Park, who always stands on my side. You always give me true happiness. “tkfkdgo! skdhk rufghsgownffo?”

Lastly, I really appreciate Dr. Anthony Sang-young Shin, Dr. Sung-chan Nam (Korea Institute of Energy Research, Korea) and Mr. Yiyoung Choi who showed true attention for me. Without your help, I doubt I would complete my MASc and I cannot imagine how my Waterloo life would be. I will never forget!!

THANK YOU VERY MUCH EVERYONE!!

Table of Contents

List of Figures

List of Tables

Chapter 1. Introduction

The high price and limited availability of oil is a growing concern. In addition, the combustion of oil to generate energy negatively impacts the environment by, for example, increasing global warming. Recently, there has been significant interest in reducing the use of oil. Natural gas is an abundant energy source, but most of it is located in remote areas. Therefore, utilization of natural gas (mainly methane) to more useful and easily transportable liquids has been given high priority. The production of fuels such as Fischer-Tropsch products and methanol from methane can help reduce problems related to pollutants, such as sulphur compounds, heavy metals, and fine air born particles, associated with coal. Furthermore, its higher H/C ratio results in less C emissions in comparison to oil or coal.

Methanol can be produced from synthesis gas ($2H_2 + CO = CH_3OH$). In practice, synthesis gas production by standard reforming processes, such as methane steam reforming and CO_2 reforming of methane, has some problems. Both reforming reactions require an additional process to adjust the H_2/CO ratio (Oyama 2003) since both produce a synthesis gas ratio less than 2. Partial oxidation of methane that meets a H_2/CO ratio of 2 is difficult to control due to hot-spots and the risk of explosion (Tang, Lin and Tan 1998). On the contrary, in oxidative CO_2 reforming of CH_4 (co-feed CH_4, CO_2, and O_2), the H_2/CO ratio can feasibly be directly controlled by adjusting the feed ratio of O_2 and CO_2. Thus, the oxidative CO_2 reforming of CH_4 process is an interesting approach for synthesis gas production with a H_2/CO ratio that is required in the Fischer-Tropsch process and methanol synthesis.

Economical, highly active and stable catalysts are necessary to improve process efficiency and to reduce its operating costs. A catalyst that has high resistance to carbon deposition would also allow stable operation. In the reforming reaction, precious metal catalysts have high activity and are highly resistant to carbon deposition. However, due to their high cost and limited availability, precious metal catalysts are not economical solutions. Therefore, Ni-based catalysts have been commercially applied in industrial reforming processes, as they are less costly compared to noble metal catalysts (Bartholomew and Farrauto 2006) and are active in

reforming. However, the Ni-based catalysts have some problems, such as Ni particle sintering and coke deposition, which result in catalyst deactivation.

The main objective of this research is to develop a Ni-based catalyst which has high catalytic performance and stability in partial oxidation (exothermic reaction), carbon dioxide reforming (endothermic reaction) and oxidative carbon dioxide reforming (combined exothermic and endothermic reaction) of methane. In order to design better Ni-based catalysts, the effects of supports were investigated. The supports play important roles for the dispersion of active metal particles and resistance to sintering. They also affect the reactivity and coke resistance of the metal particles which participate in the catalytic reaction.

In this research, the catalytic reactivities for methane partial oxidation, carbon dioxide reforming of methane, and the combined process (oxidative CO_2 reforming of CH_4) were tested for 20 hrs. In addition, some catalyst characterization was done to explain the performance trends. Three different catalysts ($Ni_{0.5}Mg_{2.5}Al$, $Ni_{0.5}Ca_{2.5}Al$ and Ni/Al_2O_3) were tested. The $Ni_{0.5}Mg_{2.5}Al$ catalyst produced a hydrotalcite-type structure showed the highest resistance to the coke formation for the reactions of interest. After the reaction tests, kinetic studies were conducted over the $Ni_{0.5}Mg_{2.5}Al$-HT catalyst for CO_2 reforming of CH_4 reaction.

Chapter 2. Literature Review

Thermodynamic and kinetic studies are necessary to understand the relationships between process conditions (i.e. reaction temperatures and feed compositions) and the possible product distributions. There are three major pathways to produce synthesis gas (a mixture of H_2 and CO): (i) methane steam reforming, (ii) methane partial oxidation, and (iii) CO_2 reforming of methane. Each pathway has unique thermodynamic properties, and product compositions. In this chapter, the thermodynamic properties and the reaction kinetics for (i) methane partial oxidation, (ii) CO_2 reforming of methane and (iii) oxidative CO_2 reforming of methane are discussed.

2.1 Chemical Reaction Pathway and Catalytic Kinetic Study

2.1.1 Activation of methane

The proposed first step in the reforming reaction is the adsorption and dissociation of CH_4 on the active metal component of the catalyst. CH_4 dissociation (also called "CH_4 activation"), which is the breaking of one of the C-H bonds on the active metal site, is typically considered the rate-limiting step (Luntz and Harris 1991). The most typical transition metal (or active metal type) which has been used for reforming reactions is nickel, because of its price and high activity. CH_4 dissociation is structure sensitive, which may be a consequence of a change in the geometric active site distribution on the different metal surface structures. CH_4 decomposition preferentially occurs on small Ni crystallites (Kuijpers, et al. 1983), and decreases in the order Ni(110) > Ni(100) > Ni(111) (Beebe, et al. 1987).

When CH_4 dissociates on the active site, various CH_x species will form depending on the composition or structure of the catalysts. Possible CH_4 dissociation steps, during CO_2 reforming of CH_4 as an example, have been proposed (Osaki, et al. 1994) based on pulse surface reaction analysis (PSRA):

$$CO_{2,gas} \leftrightarrow CO_{ads} + O_{ads}$$ [Equation 1]

$$CH_{4,gas} \leftrightarrow CH_{x,ads} + \frac{1}{2}(4-x)H_{2,gas}$$ [Equation 2]

$$CH_{x,ads} + O_{ads} \leftrightarrow CO_{ads} + xH_{ads}$$ [Equation 3]

$$CO_{ads} \leftrightarrow CO_{gas}$$ [Equation 4]

$$xH_{ads} \leftrightarrow \frac{1}{2}xH_{2,gas}$$ [Equation 5]

Generally, CH_4 dissociation is regarded as a reversible reaction. Therefore, any H adsorbed on the catalyst could inhibit the CH_4 dissociation. At high temperature, more hydrogen on the catalyst further inhibits CH_4 dissociation and the rate reaches a constant value with surface hydrogen indicating that dissociation of CH_4 reaches an equilibrium state (Cui, et al. 2007).

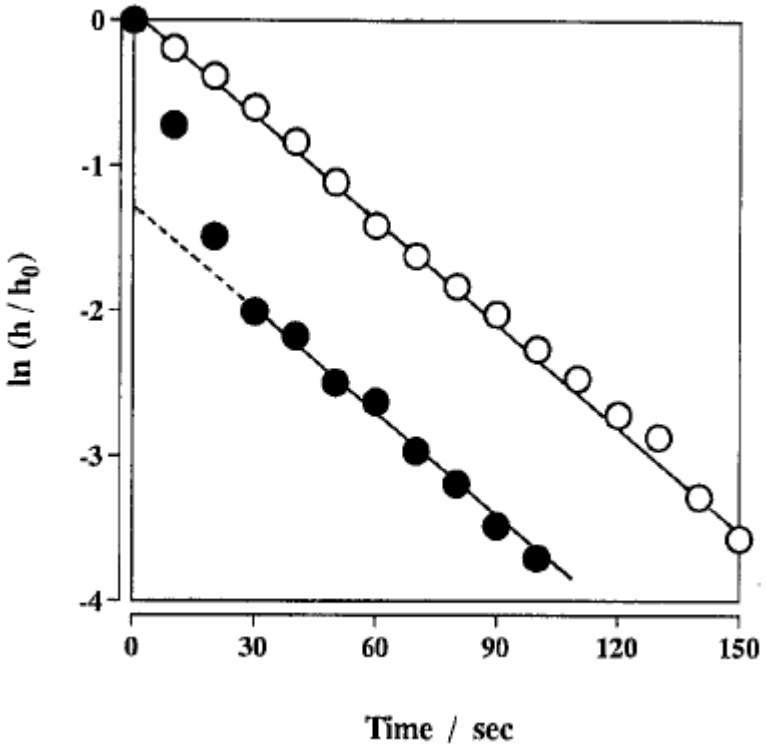

Figure 1: Relationship between ln *h* and *t* for CO (○)and H_2 (●) (Osaki, et al. 1994)

PSRA theory is based on the response of H_2 consumption (*h*) at a certain time (*t*) being proportional to the rate of production at t. If the reaction is first order with respect to the number of adsorbed CH_4 molecules, the relationship between ln*h* and *t* should yield a straight line, the slope of which is the rate constant. An Arrhenius plot of the rate constants calculated based on a first order assumption is shown in Figure 1, and the linearity indicates that the 1st order assumption is correct.

Table 1: CH_x species observed on Ni surface during CO_2 reforming of CH_4 (Osaki, et al. 1994)

Catalyst	x
Ni/MgO	2.7
Ni/ZnO	2.5
Ni/Al_2O_3	2.4
Ni/TiO_2	1.9
Ni/SiO_2	1.0

The surface CH_x intermediate species can be determined by investigating the number of hydrogen atoms involved (x H_{ads}). The hydrogen contents of CH_x intermediates for different catalysts are summarized in Table 1. Except for the Ni/SiO_2 catalyst, more than one hydrocarbon species (x > 1.0) exist on the surface since the value of x for each catalyst is not an integer; and the Ni/SiO_2 catalyst is the most hydrogen-deficient. Catalysts with lower values of x are more likely to form carbonaceous deposits. Therefore, these results indicate that the Ni/MgO catalyst should have a higher resistance to coke formation than the other catalysts.

2.1.2 Partial oxidation of CH_4

The partial oxidation of methane is a mildly exothermic reaction [Eq. 6]. The process can occur at very short residence time (τ = 3.6-72 ms) on the surface of transition metals (Basile, et al. 1998). The overall partial oxidation of CH_4 reaction is illustrated as:

$$CH_4 + 0.5O_2 \leftrightarrow 2H_2 + CO \quad \Delta H^{\circ}_{298K} = -22.6kJ/mol \qquad \text{[Equation 6]}$$

The synthesis gas ratio (H_2/CO) is 2, which is ideal for the methanol production process, if the reaction goes to completion and is carried out with a stoichiometric ratio of reactants. However, depending on the employed catalyst, temperature, pressure and the feed ratio (CH_4/O_2), the product distribution will vary.

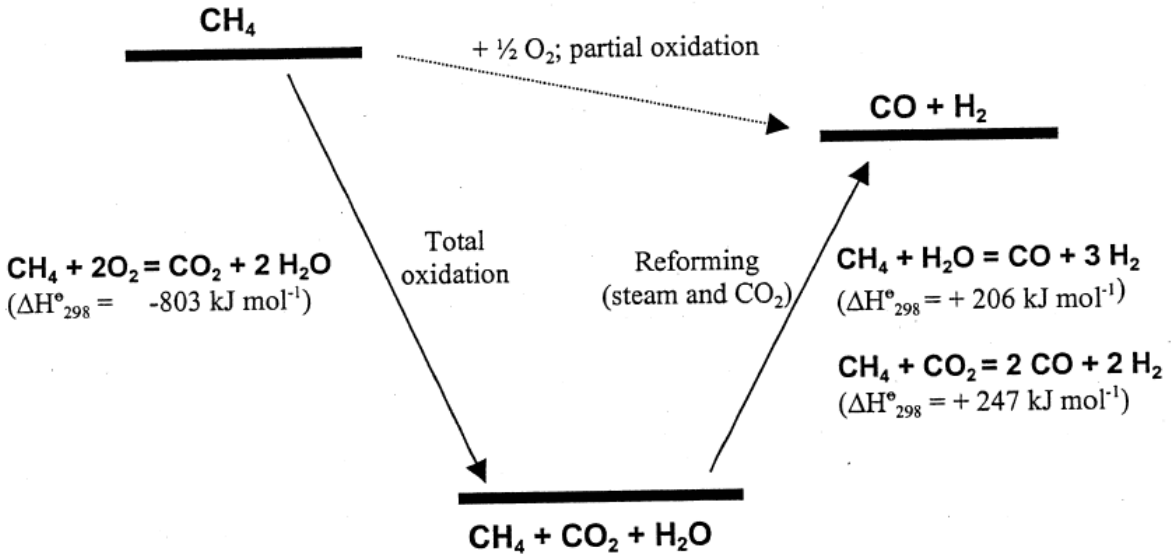

Figure 2: Thermodynamic representation of the partial oxidation of CH_4 (Zhu, et al. 2004) (York, et al. 2003)

Besides the direct partial oxidation of CH_4 [Eq. 6], other possible pathways are proposed in Figure 2. These reactions in more detail are described below:

(a) Total combustion of CH_4 in the oxygen-rich zone of the reactor yielding CO_2 and H_2O.

$$CH_4 + 2O_2 \rightarrow CO_2 + 2H_2O \qquad \Delta H^{\circ}_{298K} = -803\ kJ/mol \qquad \text{[Equation 7]}$$

(b) Reforming the remaining CH_4 with H_2O or CO_2

$$CH_4 + CO_2 \rightarrow 2CO + 2H_2 \qquad \Delta H^{\circ}_{298K} = +226\ kJ/mol \qquad \text{[Equation 8]}$$

$$CH_4 + H_2O \rightarrow CO + 3H_2 \qquad \Delta H^{\circ}_{298K} = +261\ kJ/mol \qquad \text{[Equation 9]}$$

Either the direct (for high temperature) or indirect (for low temperature) partial oxidation of CH_4 could occur depending on the reaction temperature. Figure 3 shows the effect of temperature and pressure on equilibrium product distribution with a stoichiometric feed mixture of CH_4 and O_2 (CH_4/O_2 = 2). With increasing pressure, higher temperatures are required to obtain high conversion and high selectivity to H_2 and CO.

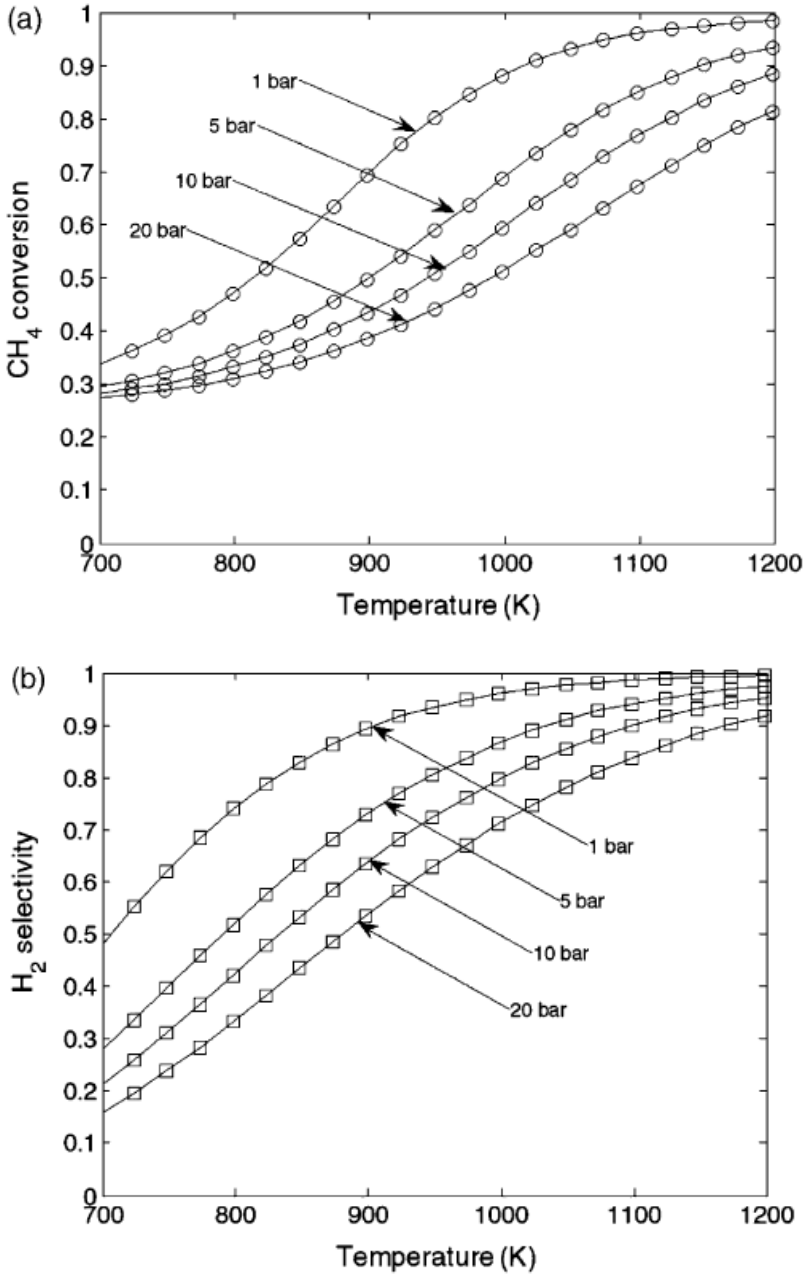

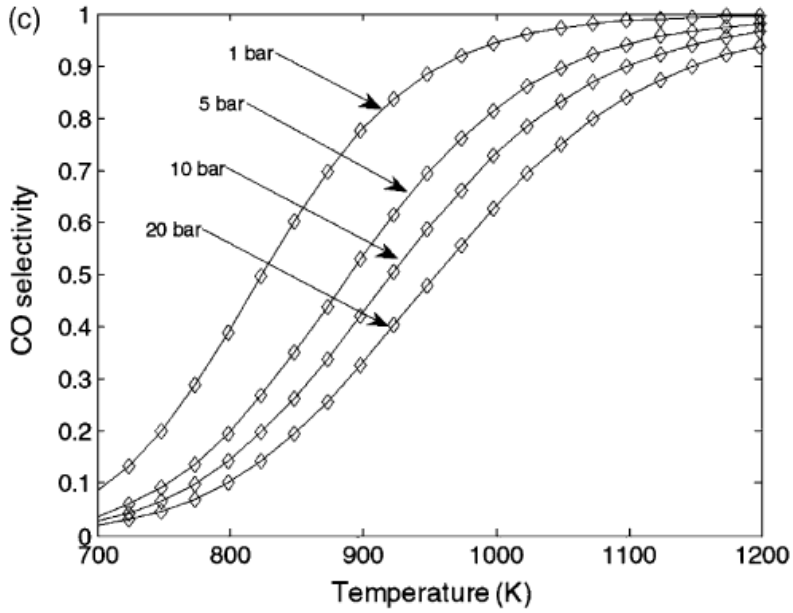

Figure 3: Thermodynamic equilibrium concentrations as a function of the temperature at 1-20 bar from HYSYS 3.2 simulation using $CH_4/O_2 = 2.0$ and air as oxidant (Enger, et al. 2008)

As mentioned above, methane partial oxidation is an exothermic reaction, and generates a very high temperature region (called "hot spot") in the catalyst bed. The "combustion (Eq. 7) and reforming reaction (Eq. 8 and Eq. 9)" pathway produces a temperature profile in the catalyst bed which generates the hot-spot at the front of the catalyst bed since the highly exothermic combustion is followed by the endothermic reforming reaction. This temperature profile is shown in Figure 4. A hot-spot generated at the front of the catalyst bed is difficult to remove from the reactor, particularly from large-scale equipment; thus the process also becomes very difficult to control (Ruckenstein and Hu 1995).

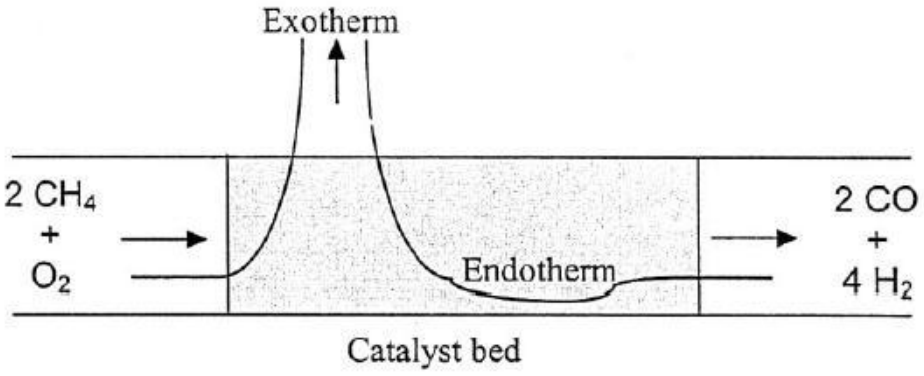

Figure 4: Temperature profile on a catalyst bed for partial oxidation of methane (York, et al. 2003)

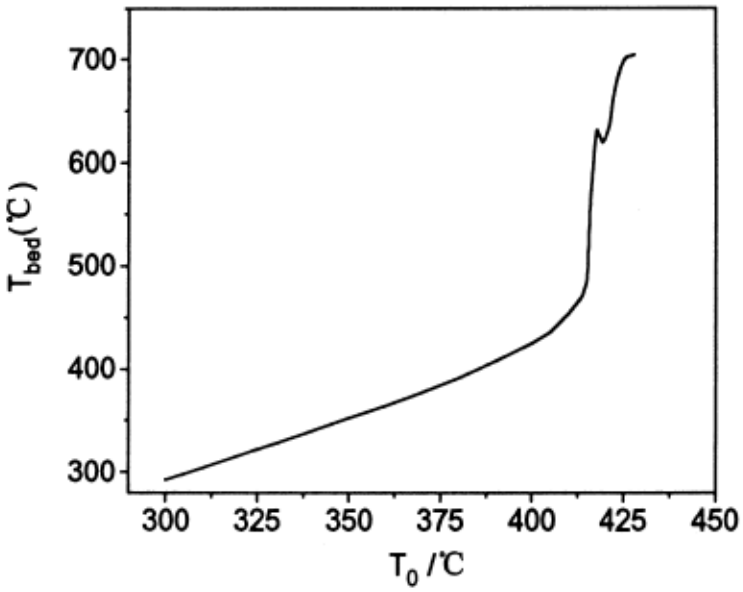

Figure 5: The temperature of the catalyst bed as a function of the furnace temperature. Ni^0 catalyst used, 100mg; CH_4/O_2 = 2.0 (no diluting gas); SV = $1.5*10^5$ h^{-1} (Jin, et al. 2000)

Jin and co-workers (2000) ran temperature-programmed experiments that describe the combination of reactions, with results shown in Figures 5 and 6. At 450℃, O_2 began to be consumed, and then the bed temperature sharply increased to 650℃ due to CH_4 combustion (Eq. 7). During CH_4 combustion, neither H_2 nor CO was detected (H_2O and CO_2 were generated instead). After the exothermic combustion stage, a short endothermic process (Eq. 8 and Eq. 9) was observed at a bed temperature of 650℃ (Figure 5). This behavior confirms that the overall partial oxidation of methane consists of two steps; the exothermic process from combustion of CH_4, followed by the endothermic process from the reforming processes.

CH_4 dissociation as the first step to produce synthesis gas requires reduced Ni^0 sites (Goula, et al. 1996). To confirm this, the oxygen species involved in the formation of CO were identified by CH_4 pulse tests over a Ni^0 catalyst that had been previously used in partial

oxidation reaction tests. When CH_4 was pulsed over the used Ni^0 catalyst, considerable amounts of CO were generated, but no CO_2 was detected. This indicates that some oxygen species was present on the Ni^0 surface after the CH_4/O_2 partial oxidation reaction. It was confirmed that a specific oxygen species on the Ni^0 surface, which was designated as $Ni^{\delta+}\ldots O^{\delta-}$, was the intermediate species in methane partial oxidation and plays an important role in the generation of CO (Jin, et al. 2000).

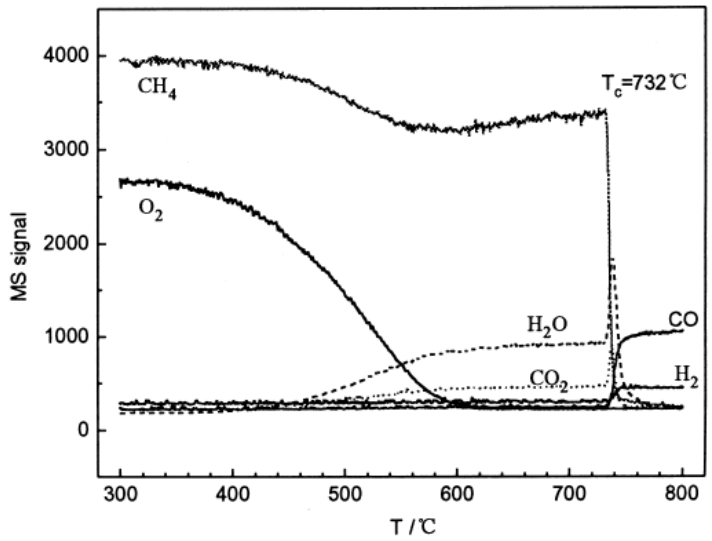

Figure 6: Temperature-programmed surface reaction (TPSR) responses for the interaction of CH_4/O_2/He flow with Ni^0 catalysts. CH_4/O_2/He=10/5/85; total flow rate: 100mL/min; catalyst amount: 200mg; from 25℃ to 800℃ with 10℃/min (Jin, et al. 2000)

Figure 6 shows the surface reaction profiles for the oxidation of methane on a Ni^0 metal surface. O_2 consumption, although slight, began at 320℃, and CH_4 consumption started at 400℃. Up to 400℃, product components, such as CO_2, H_2O, CO and H_2, were not detected. This suggests that the active Ni^0 surface were bing oxidized to NiO until 400℃. Then, when CH_4 began to be consumed at 400℃, some product components, such as H_2O and CO_2, were simultaneously detected due to CH_4 combustion. When the temperature of the catalyst bed reached 580℃, O_2 conversion approached 100% and remained complete at higher temperature. This suggests that the complete combustion (or oxidation) of CH_4 was occurring by 580℃. At 732℃, CH_4 conversion drastically increased, accompanied by a transient formation of additional

CO_2 and H_2O, and simultaneously, H_2 and CO formation sharply increased then remained almost constant (Jin, et al. 2000).

The proposed two steps (total oxidation of CH_4 followed by reforming reactions) for the methane partial oxidation reaction can be explained by the following mechanism (Jin, et al. 2000):

$$Ni^0 + O_2 \rightarrow NiO \qquad \text{[Equation 10]}$$

$$CH_4 + O_2 \rightarrow CO_2 + H_2O \quad (over\ NiO) \qquad \text{[Equation 11]}$$

$$CH_4 + NiO \rightarrow CO_2 + H_2O + Ni^0 \qquad \text{[Equation 12]}$$

$$CH_4 + Ni^0 \rightarrow Ni\cdots C + 4H \qquad \text{[Equation 13]}$$

$$H + H \rightarrow H_2 \qquad \text{[Equation 14]}$$

$$O_2 + Ni^0 \rightarrow Ni^{\delta+}\cdots O^{\delta-} \qquad \text{[Equation 15]}$$

$$Ni\cdots C + Ni^{\delta+}\cdots O^{\delta-} \rightarrow 2Ni^0 + CO \qquad \text{[Equation 16]}$$

$$2H + Ni^{\delta+}\cdots O^{\delta-} \rightarrow H_2O \qquad \text{[Equation 17]}$$

$$CO + Ni^{\delta+}\cdots O^{\delta-} \rightarrow CO_2 \qquad \text{[Equation 18]}$$

First, the active Ni^0 sites are oxidized to NiO, consuming O_2, and based on the data above this occurs up to 400℃ (Eq. 10). Between 400 to 625℃, the complete oxidation of CH_4 occurs (Eq. 11) producing CO_2 and H_2O. When the temperature of the catalyst bed reached 625℃, the transient reduction of NiO to Ni^0 by CH4 occurred (Eq. 12), and the temperature at that point slightly decreased since the reduction of NiO to active metal Ni^0 by CH_4 is endothermic. The dissociative activation of methane (Eq. 17) formed the surface Ni…C species and H_2. The surface Ni…C species further react with the $Ni^{\delta+}$…$O^{\delta-}$ species (Eq. 15). Then the primary products, CO and H_2, are produced (Eq. 16) (Jin, et al. 2000).

2.1.3 CO_2 reforming of CH_4

CO_2 reforming of CH_4 (also called "dry reforming of CH_4") is considered an environmentally friendly process due to the consumption of CO_2 (Eq. 19) as a feedstock (Li and Wang 2004). In addition, it is of industrial interest for the synthesis of liquid hydrocarbons in the Fischer-Tropsch synthesis network and for the preparation of high-purity CO (Trimm 1977) because of the low H_2/CO ratio (~ 1). Dry reforming of methane is:

$$CH_4 + CO_2 \rightarrow 2H_2 + 2CO \quad \Delta H^{\circ}_{298K} = +260.5 kJ/mol \quad \text{[Equation 19]}$$

A reverse water-gas-shift (RWGS) reaction (Eq. 20), which occurs simultaneously, influences the product synthesis gas ratio (H_2/CO), pushing it to less than 1 since the reverse RWGS reaction produces CO. The overall CO_2 reforming of CH_4 reaction is endothermic; therefore, this reaction requires a lot of heat to maintain high reactivity.

$$CO_2 + H_2 \rightarrow CO + H_2O \quad \Delta H^{\circ}_{298K} = +41.2 kJ/mol \quad \text{[Equation 20]}$$

Several other side reactions may also occur (Edwards and Maitra 1995).

$$CH_4 \rightarrow C + 2H_2 \quad \Delta H^{\circ}_{298K} = +75 kJ/mol \quad \text{[Equation 21]}$$

$$2CO \rightarrow C + CO_2 \quad \Delta H^{\circ}_{298K} = -171 kJ/mol \quad \text{[Equation 22]}$$

$$CO_2 + H_2 \rightarrow CO + H_2O \quad \Delta H^{\circ}_{298K} = +40 kJ/mol \quad \text{[Equation 23]}$$

$$C + H_2O \rightarrow CO + H_2 \quad \Delta H^{\circ}_{298K} = +131 kJ/mol \quad \text{[Equation 24]}$$

CO_2 reforming of CH_4 could result in the most severe catalyst conditions since no O_2 is involved, which would burn-off carbon deposited on the catalyst surface. To avoid carbon deposition, or at least reduce the amount of carbon produced during the CO_2 reforming of CH_4, the carbon formed by Eq. 21 could be consumed by the reverse Boudouard reaction (Eq. 22) and the steam/carbon gasification reaction (Eq. 24). The steam used for the gasification reaction is formed from the reverse water-gas-shift reaction (Eq. 20). The reactions which are related to form carbon (Eq. 21, Eq. 22, and the reverse of Eq. 24) are favored at low temperatures.

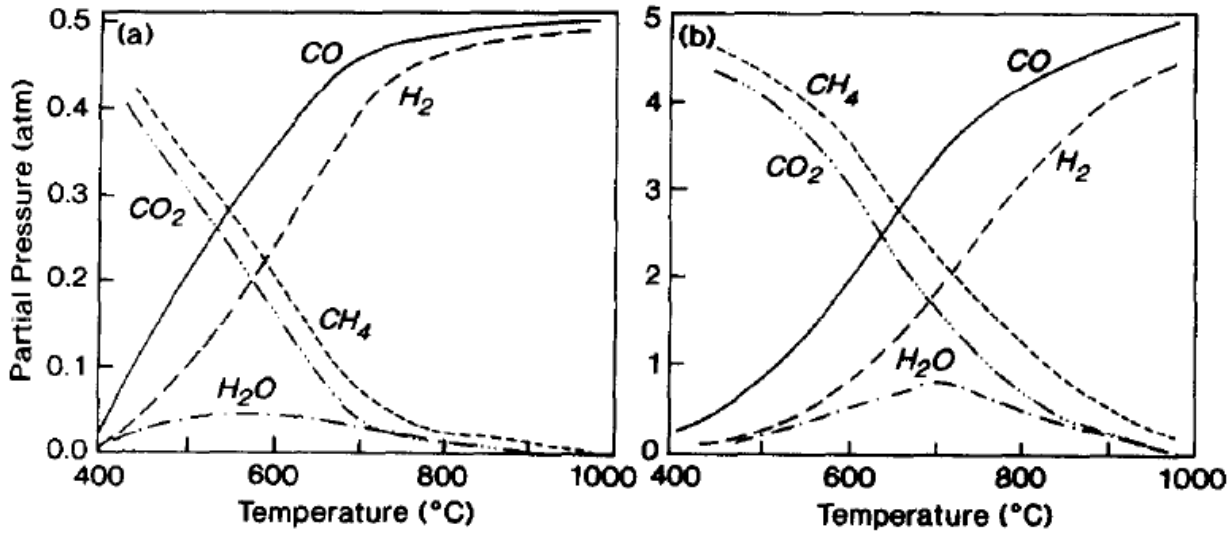

Figure 7: Equilibrium gas composition calculated for CO_2/CH_4 (1/1) system at (a) 1 atm and (b) 10 atm (Fraenkel, et al. 1986)

The equilibrium product compositions for the CO_2 reforming of CH_4 as a function of reaction temperature are shown in Figure 7. CH_4 and CO_2 conversions increase when the reaction temperature increases. Steam is also formed by the reverse water-gas-shift reaction (Eq. 20) at low temperature, but it effectively disappears when the temperature is above 900℃. Compared to 1 atm, the formation of water at 10 atm is more pronounced, extending well beyond 900℃.

2.1.4 Oxidative CO_2 reforming of CH_4

Methane partial oxidation is exothermic, and CO_2 reforming of methane is endothermic. Methane partial oxidation releases heat during the reaction; but it might generate a hot-spot along the catalyst bed. On the other hand, CO_2 reforming of methane requires significant heat to maintain reaction activity; but it consumes CO_2 as a feedstock which is attractive from an environmental point of view.

The possibility of combining the slightly exothermic methane partial oxidation reaction with the highly endothermic CO_2 reforming of methane reaction has been proposed (Ashcroft, et

al. 1991) and is here called oxidative CO_2 reforming of CH_4. This is based on the assumption that each process has advantages that are able to overcome each other's limitations and consequently enhance the overall reforming reaction performance (Amin and Yaw 2007). Oxidative CO_2 reforming of CH_4 may need a considerably lower amount of input heat to keep the catalyst bed at high temperatures because the combined process can facilitate heat transfer between those reactions. Secondly, by changing the feed composition ($CH_4/CO_2/O_2$), the product ratios (H_2/CO) and the selectivities can be controlled (Ruckenstein and Wang 2001). Finally, addition of oxygen to the CO_2 reforming of methane process is able to reduce the carbon deposition on the catalyst surface, and increase the methane conversion (Amin and Yaw 2007).

Oxidative CO_2 reforming of methane is a complex multi-reaction process. The possible reactions involved are:

$$CH_4 + \frac{1}{2}O_2 \leftrightarrow CO + 2H_2 \quad \Delta H_{298K} = -36kJ/mol \qquad \text{[Equation 25]}$$

$$CH_4 + 2O_2 \leftrightarrow CO_2 + 2H_2O \quad \Delta H_{298K} = -802kJ/mol \qquad \text{[Equation 26]}$$

$$CH_4 + CO_2 \leftrightarrow 2H_2 + 2CO \quad \Delta H_{298K} = +261kJ/mol \qquad \text{[Equation 27]}$$

$$CH_4 + H_2O \leftrightarrow CO + 3H_2 \quad \Delta H_{298K} = +206kJ/mol \qquad \text{[Equation 28]}$$

$$CO_2 + H_2 \leftrightarrow CO + H_2O \quad \Delta H_{298K} = +41kJ/mol \qquad \text{[Equation 29]}$$

Figure 8 shows the effect of O_2 addition on equilibrium reactant conversions as a function of temperature. Since CH_4 reacts with O_2 easily, the conversion of O_2 for each condition is 100%. CH_4 oxidation was dominant compared to the dry reforming of CH_4 in the combined oxidation and dry reforming of CH_4.

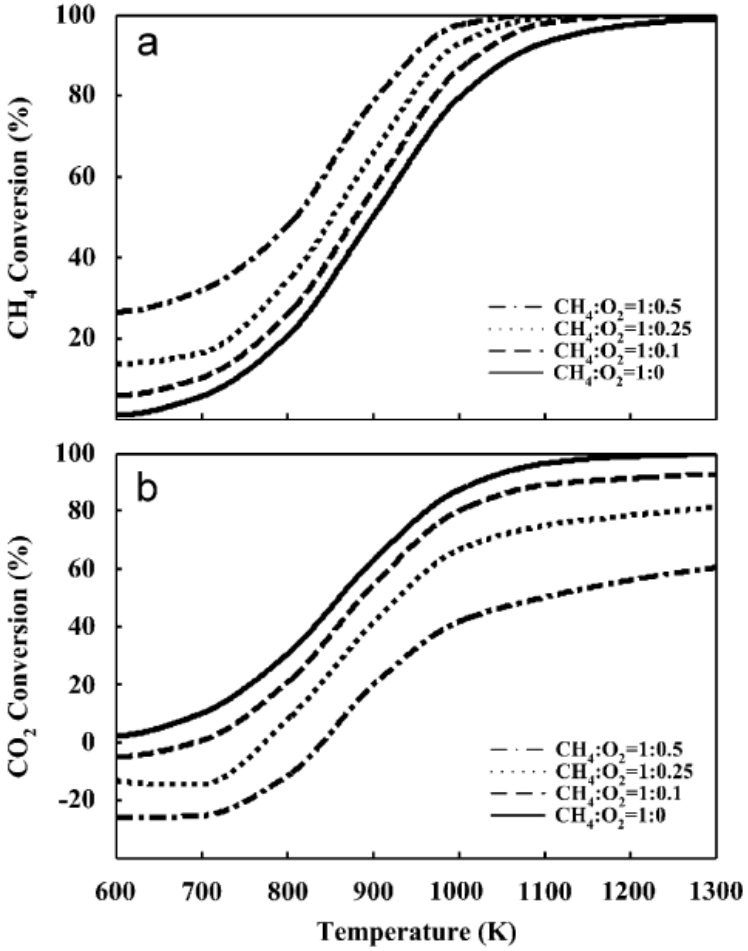

Figure 8: Effect of O_2 addition on equilibrium yields with $CH_4/CO_2 = 1$ (Amin and Yaw 2007)

With increasing O_2 content in the feed, CH_4 conversion increases, especially at temperatures below 1100K, since CH_4 is consumed in both oxidation and CO_2 reforming; thus CH_4 is considered the limiting reactant. On the other hand, increasing O_2 content leads to decreased CO_2 conversion (Tomishige, et al. 2004). Below 900K, the CO_2 conversions are negative values since the total combustion of CH_4 (Eq. 7) is the predominant reaction.

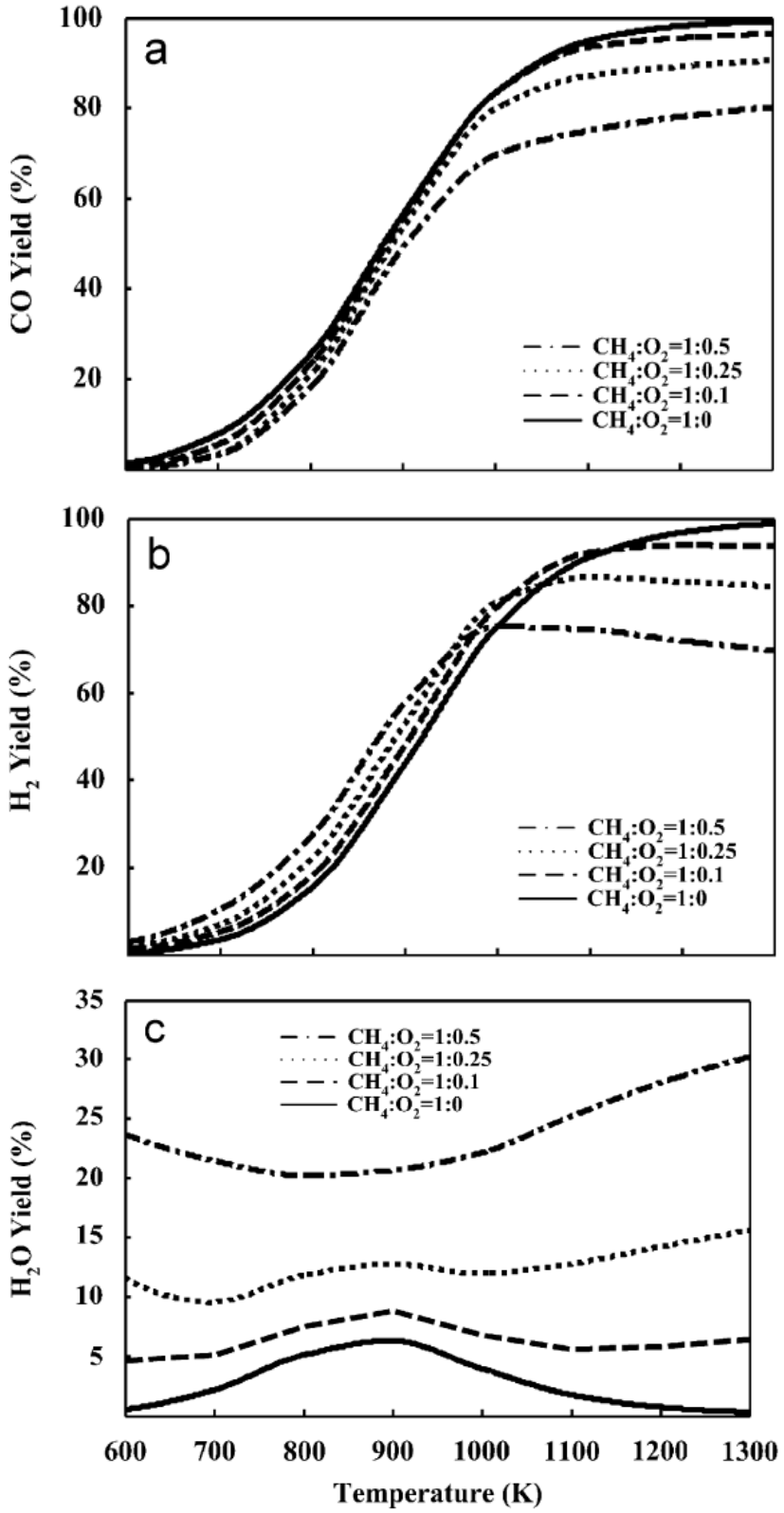

Figure 9: Effect of O_2 addition on equilibrium yields with $CH_4/CO_2 = 1$ (Amin and Yaw 2007)

The yields of CO and H_2 (the equilibrium products) are less sensitive to the addition of O_2 at temperatures below 1000K; however, the formation of H_2O increases drastically (Figure 9). As a result, with increasing O_2 content in the feed, CH_4 tends to be converted to CO_2 and H_2O (combustion of CH_4), which leads to reduced formation of H_2 and CO. When the reaction temperature is below 1000K, the H_2/CO ratio differs greatly depending on the O_2 content; however, above 1000K, the ratio is maintained at unity (Amin and Yaw 2007).

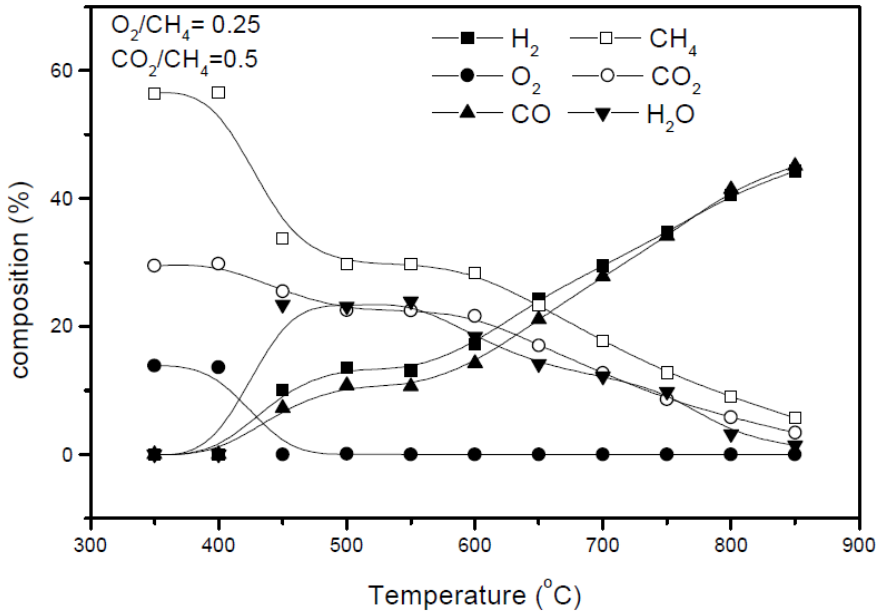

Figure 10: Composition profile for oxidative CO_2 reforming of methane as a function of temperature over the Pt/10%ZrO_2/Al_2O_3 catalyst (CH_4:CO_2:O_2 = 4:2:1) (Souza and Schmal 2003)

The profiles of the product gases for the oxidative CO_2 reforming of CH_4 are shown in Figure 10. Even at low temperature, the O_2 conversion is 100%. At 450°C, the production of steam starts and begins to decrease at 600°C. This profile also confirms that CH_4 combustion occurs at low temperature, which explains the H_2O production and decreased CO_2 conversion. It suggests that at low temperature (< 1000K) the partial oxidation of CH_4 and the reverse water-gas-shift reactions occur, while CO_2 reforming of CH_4 is dominant at high temperature (> 1000K) (Souza and Schmal 2003).

2.2 Catalyst Studies

A catalyst is a substance that affects the rate of a reaction but emerges from the process unchanged (Fogler 2006). A catalyst changes a reaction rate by reducing the activation energy, however, it does not affect the equilibrium distribution of products and reactants. This chapter discusses the materials, preparation methods, characteristics, and reaction mechanisms of catalysts for reforming reactions.

2.2.1 Materials

In general, catalytic properties are classified as dynamic, chemical, and physical (Bartholomew and Farrauto 2006). Dynamic properties include activity or selectivity, or the behavior of the catalyst toward the chemical reaction. Chemical properties include the chemical state of the active catalytic phase, such as acidity and oxidation state. Physical properties are the surface area, pore structure, density and mechanical properties.

A typical heterogeneous catalyst consists of three components: an active phase, a promoter, and a support. For reforming processes, transition metals (ex. Ni, Pt etc.) are used as the active phase. Promoters are added in very small quantities to increase reaction activity or stability, for example by enhancing or maintaining the catalytic surface area. Supports are used to disperse the active sites on the surface, and provide the thermal stability of these phases over long periods of time. For reforming reactions, high-surface area catalysts are used. Examples of these three catalyst components are listed in Table 2 and Figure 11.

Table 2: Components of a typical heterogeneous catalyst (Bartholomew and Farrauto 2006)

Component	Material types	Examples
Active phase	Metals	Noble metals: Pt, Pd; Base metals: Ni, Fe
	Metal oxides	transition metal oxides: MoO_2, CuO
	Metal sulfides	Transition metal sulfines: MoS_2, Ni_3S_2
Promoters	Metal oxides	Transition metal and Group IIIA: Al_2O_3, SiO_2, MgO, TiO_2
	Metal oxides	Alkali and alkaline earth: K_2O, PbO

Support	Metal oxides	Group IIIA, alkaline earth and transition metal oxides: Al_2O_3, SiO_2, MgO, Zeolites, and activated carbon

Transition metals which are used as active catalytic phases have the ability to catalyze chemical reactions because the transition metals can donate or accept electrons easily during the reactions (Somorjai 1994). For example, synthesis gas production by dissociation of CH_4 typically uses group VIII metal catalysts (Zhu, et al. 2004).

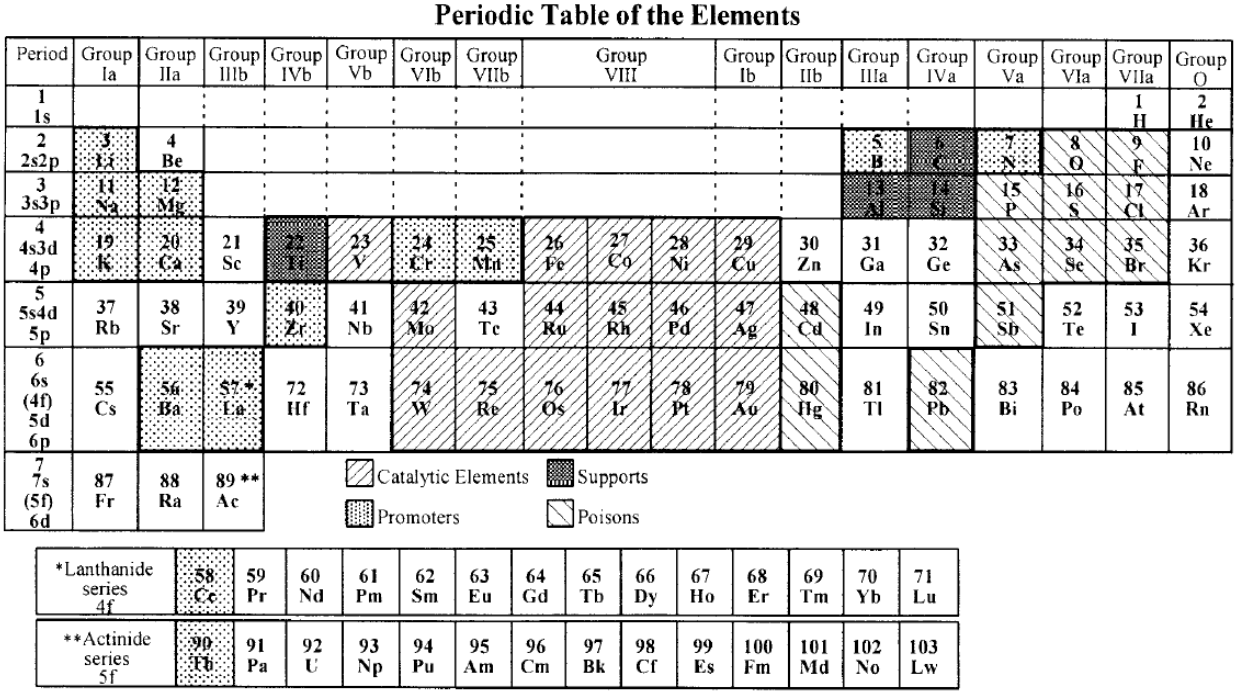

Figure 11: Elements of the period table finding application as catalytic phases, supports, and promoters (Bartholomew and Farrauto 2006)

The major roles of the supports are to prepare and preserve stable, well-dispersed catalytic phases during the reaction. They are typically porous, high surface area metal oxides or carbon. Examples of the supports (and surface area) are activated carbon (500-1500 m^2/g), zeolites (500-1000 m^2/g), activated clays (150-225 m^2/g), and activated Al_2O_3 (100-300 m^2/g) (Bartholomew and Farrauto 2006). Among those supports, alumina (Al_2O_3) is the most common commercial support due to its excellent thermal stability and wide range of chemical, physical, and catalytic properties. Al_2O_3 supports are used in alkene and benzene hydrogenations, catalytic reforming, hydro-treating, emission control, methanol synthesis and the water-gas-shift reactions (Oberlander 1984).

There are two kinds of promoters: textural and chemical promoters. Textural promoters are used to facilitate the preparation of well-dispersed catalytic phases and to maintain their well-dispersed state during reaction conditions. Chemical promoters, such as alkali and alkaline earth metals or metal oxides, are additives that enhance the activity or selectivity of the catalytic phase.

2.2.2 Catalyst preparation

Catalysts are prepared by the deposition of the active components on the surface of supports. The typical preparation methods are impregnation and precipitation. After the deposition of the active phase on the support, washing, drying, calcination, and activation steps are typically conducted to prepare the catalyst for reaction.

2.2.2.1 Impregnation method

The impregnation method is the simplest and most common method. A catalytic species is dispersed on a support by impregnating the pre-dried support with an aqueous or non-aqueous solution containing a salt (precursor) of the catalytic elements. The precursor salt solution is added slowly (drop-wise) to the support, where capillary forces of up to several hundred atmospheres draw the liquid into the pores (Bartholomew and Farrauto 2006). The precursor salt solution is added until the pores of the supports are saturated. This procedure is illustrated in Figure 12.

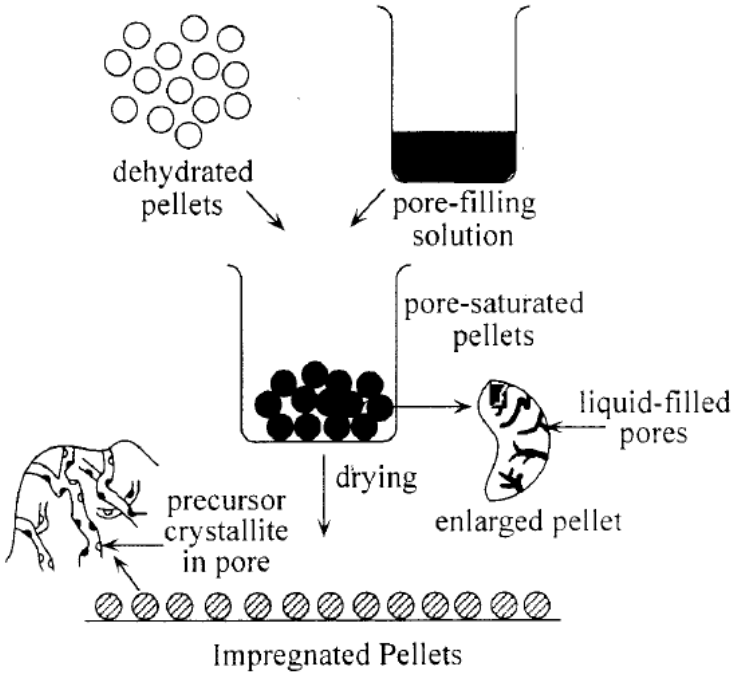

Figure 12: Schematic of steps in the preparation of supported catalysts by impregnation (Bartholomew and Farrauto 2006)

Crystallites of the precursor deposit in the pores when the impregnated catalysts are dried in air at 80 to 150℃. Depending on the drying rate, the catalyst properties can be varied (Figure 13). At low drying rates (or drying at low temperature), evaporation occurs at the meniscus; therefore most of the precursor will end up deposited at the deepest end of the pore in the pellet center (called an egg-yolk deposit). On the other hand, if the impregnated catalyst is dried quickly (or dried at high temperature), vaporization can occur from deep within the pores, forcing the precursor to be deposited closer to the pore entrance, which leads to what is called an eggshell deposit on the pellet.

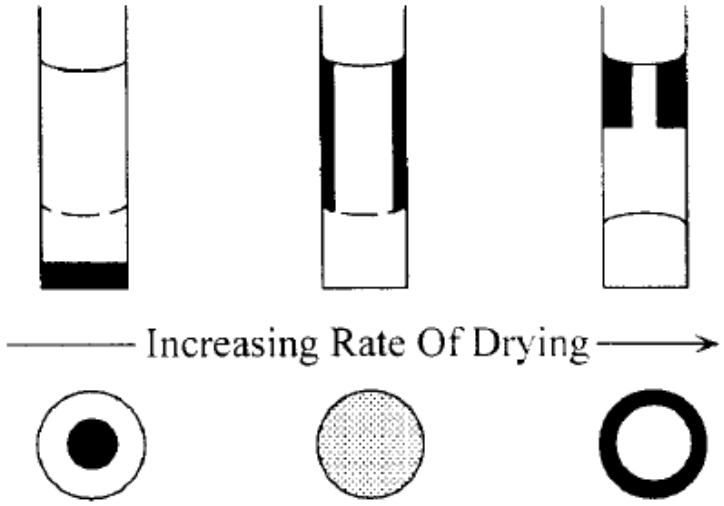

Figure 13: Pore and particle profiles after drying at different rates (Bartholomew and Farrauto 2006)

The advantages of the impregnation method include its relative simplicity, rapidity, and capability for depositing the precursor at high metal loadings. However, impregnation typically results in non-uniform deposits along the pores.

2.2.2.2 Precipitation method

In the precipitation method, the catalyst precursor is added in the form of a hydroxide or carbonate species in solution, which enters the pores. These precursors deposit on the surface of the support when the solution pH is adjusted through addition of a base, such as NaOH, NH_4OH, or Na_2CO_3. In addition, support and catalyst precursors can be co-precipitated together, such as in the co-precipitation of Ni hydroxide on alumina by mixing aqueous solutions of aluminum nitrate and nickel nitrate. Generally, support material in the form of pellets or powder is added to the salt solution, after which the alkali solution is usually added drop-wise, accompanied by rapid stirring of the slurry (Figure 14).

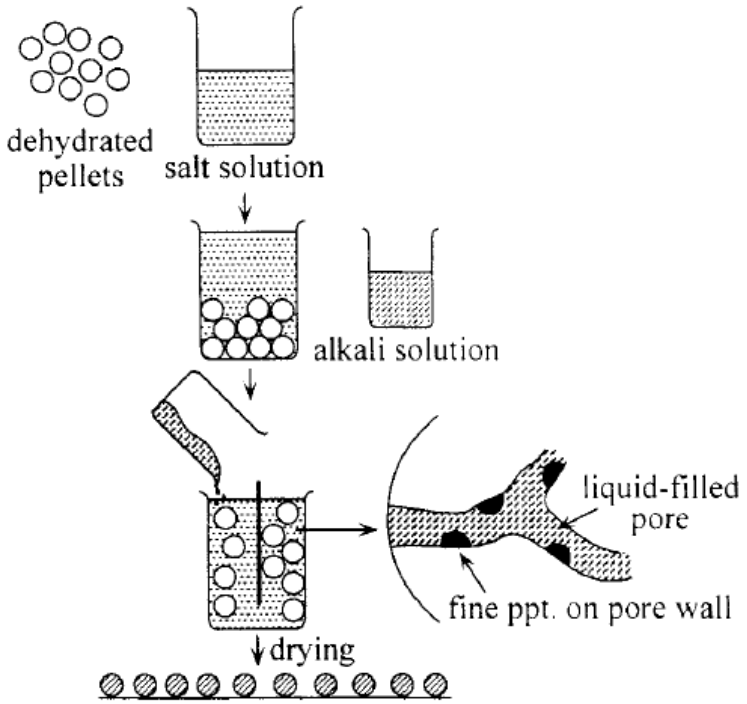

Figure 14: Schematic of steps in the preparation of supported catalysts by precipitation from alkali solution (Bartholomew and Farrauto 2006)

The precipitation method leads to more uniform, finely divided deposits, which can ultimately translate to a highly dispersed, high surface area catalyst of high activity. The precipitation method can be used to achieve moderately high loadings of the active components. To obtain a uniform, well-dispersed precipitate, the control of the precipitation rate inside the catalyst plays an important role. When precipitation is complete, the precursor-support material is washed with de-ionized water to remove undesirable, soluble ions; then dried and calcined to decompose the catalyst precursor.

It is well known that highly dispersed metal particles on the catalyst surface result in high activity and higher resistance to coke formation (Morioka, et al. 2001). With the incipient wetness impregnation method, it is difficult to produce homogeneous and reproducible catalysts for the target reactions (Takehira, et al. 2004) (Shishido, et al. 2002); and the fine particles tend to sinter at high temperature, resulting in catalyst deactivation. Therefore, the precipitation method, which can provide greater homogeneity and reproducibility, should be employed.

2.2.2.3 Calcination

The catalysts, either made by impregnation or precipitation, should be calcined to decompose the precursors, which will result in oxide or metal catalyst particles. Low temperature (≤ 200°C) calcination should be used for carbonate precursors because of the combustibility of the carbon. High temperature treatments can be used to decompose catalyst precursors on oxide supports since solid state reactions of metal oxides with the oxide carrier and extensive segregation of bimetallic components can be avoided.

However, calcination at high temperature decreases the activity of some catalysts. For example with a Ni/Al_2O_3 catalyst, a reaction between Ni^{2+} and Al_2O_3 can occur, forming a stable and inactive surface nickel aluminate. In addition, high temperature calcination causes sintering of the support and Ni crystallites, leading to decreased available catalytic surface area. Therefore, calcining the catalyst precursor at high temperature can provide greater thermal stability for applications at higher temperature, such as high-temperature methanation and steam reforming; however, it decreases the surface area of the catalyst and generates inactive phases by the reaction between the precursor and active phase.

2.2.2.4 Reduction

Reduction is the final step in the production of the reforming catalysts. Reduction is needed to convert oxides and/or catalyst precursor salts to the metal phase. Temperature is an important variable in the reduction process. Depending on the metal-support system, the optimum reduction temperature varies. Generally, supported noble metal catalysts are reduced easily at low temperature (250-350℃); whereas supported base metals require high reduction temperatures (350-500℃). In addition, impregnated catalysts are more easily reduced than precipitated catalysts.

2.2.3 Supported nickel-based catalysts

Three main types of catalysts have been investigated for the reforming processes. They are supported nickel, cobalt, and iron catalysts; supported noble metal catalysts; and transition metal carbide catalysts. Among them, supported nickel catalysts are the typical choice since Ni metal is an active component for synthesis gas production via methane reforming reactions. Co and Fe catalysts have much lower reactivity for reforming reactions (especially for partial oxidation of methane) since CoO and Fe_2O_3 have higher activity for complete oxidation of methane (York, Xiao and Green 2003). The order of activity for partial oxidation of methane is Ni >> Co > Fe (Slagtern and Olsbye 1994). However, under conditions where synthesis gas is produced, carbon deposition also occurs; and it leads to catalyst deactivation. To decrease the carbon deposition or increase the stability of the catalyst, modification of the supports is often studied.

Resistance to carbon deposition is a function of the support. As mentioned above, the most typical catalyst for the reforming reaction is Ni/Al_2O_3 due to its low cost and high turnover frequency (Zhang, et al. 2000). However, due to the formation of an inactive solid solution, $NiAl_2O_4$, carbon deposition and nickel sintering, catalyst deactivation occurs with time on stream (Zhu, et al. 2009). Ni catalysts on different supports, such as MgO, CaO, and CeO_2, show different resistances to coke formation (Tang, et al. 1998). Compared with other supports, only MgO-supported Ni catalysts showed high resistance to carbon deposition under severe conditions (Figure 15); the CaO and CeO_2 supports had similar, higher rates of carbon formation. It is well known that Ni/MgO produces a solid-solution after the calcination step (Hu and Ruckenstein 1996), which is an inactive phase for the reforming reaction. However, it helps stabilize small nickel particles and the Ni-Ni bonds on the reduced surfaces. Furthermore, surface reconstruction by bond relaxation decreased and inhibited carbon diffusion into the nickel lattice and subsequent growth of carbon whiskers (Enger, et al. 2008).

Deposition of carbonaceous materials occurs easily on support acid sites and over metallic sites. Increasing the catalyst basicity by adding basic components (Miao, et al. 1997), such as Li or Mg, decreases carbon deposition in the pores of the catalyst (Tang, et al. 1995).

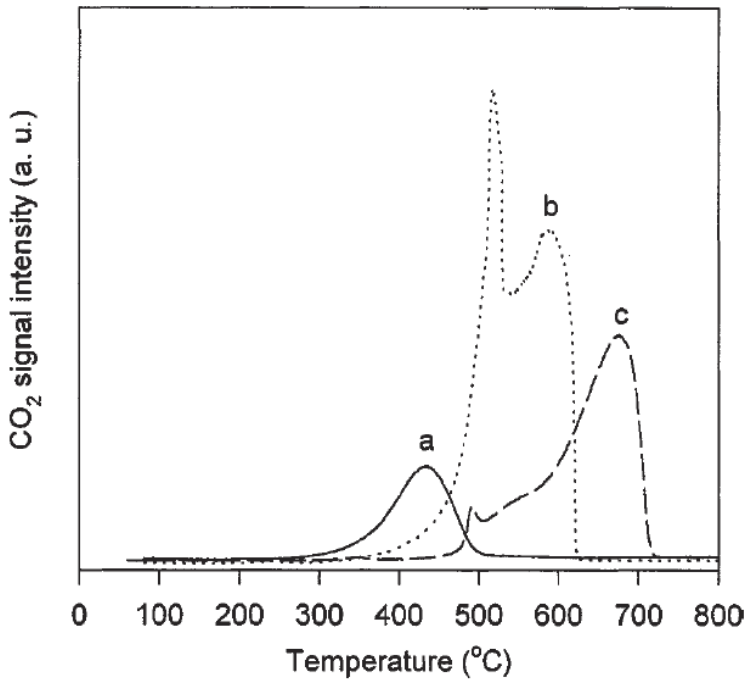

Figure 15: TPO profile of carbon deposited from CH_4 decomposition over: (a) Ni/MgO; (b) Ni/CeO_2; (c) Ni/CaO (Tang, et al. 1998)

NiO/MgO has been tested in the partial oxidation of methane at low temperature (Choudhary, et al. 1992). High conversion and selectivity were obtained at 1073K after calcining at 1173K. However, the catalyst performance was reduced drastically when the catalyst was calcined above 1323K due to the formation of an inactive solid solution. In addition, low MgO loading led to inactive catalysts. The addition of SrO or BaO instead of MgO did not produce active catalysts.

The effect of reduction on the activity of a NiO-CaO catalyst was investigated (Choudhary, et al. 1992). Methane conversion was increased when the NiO-CaO catalyst was reduced; but the selectivity to H_2 and CO was not significantly affected. With a calcium aluminate catalyst, the addition of a very small amount of Ni (0.1wt %) had little effect on the conversion or selectivities (Lemonidou et al. 1997). However, with slightly more Ni, 0.5 wt%, the product composition was comparable to equilibrium yields.

H-Y zeolites were studied as supports for nickel (1 and 5 wt%) (Vermeiren, et al. 1992) and compared to nickel supported on Al_2O_3, SiO_2-Al_2O_3, and SiO_2-ZrO_2 at 1053K. The Ni/Al_2O_3 catalyst had higher methane conversion and selectivities than the Ni/H-Y zeolite catalyst. 1wt % Ni on Al_2O_3 and SiO_2-ZrO_2 yielded results comparable with 5 wt% Ni on the same supports. However, 1 wt% Ni on SiO_2-Al_2O_3 and H-Y zeolite did not produce any hydrogen and the methane conversion was low (Table 3).

Table 3: Catalytic results of methane partial oxidation obtained at 1053K over a supported nickel catalyst (CH_4:O_2:N_2 = 2:1:7, W/F_0 = 6.72 kg.s/mole) (Vermeiren, et al. 1992)

Catalyst		Conversion	Selectivity		
Support	Ni	CH_4 (%)	CO (%)	CO_2 (%)	H_2 (%)
Al_2O_3	1	95.3	96.3	3.7	99.4
Al_2O_3	5	95.7	95.7	4.3	99.9
SiO_2-Al_2O_3	1	13	33.8	66.2	-
SiO_2-Al_2O_3	5	94.6	96.1	3.9	99.1
SiO_2-ZrO_2	1	95.6	96.1	3.9	99.6
SiO_2-ZrO_2	5	96.1	97.2	2.8	99.4
H-Y	1	25.9	52.4	47.8	-
H-Y	5	90	92.5	7.5	98.2

A Ni/TiO_2 catalyst was tested in the temperature range 573-1073K. For methane partial oxidation, the initial activity of the Ni/TiO_2 catalyst was high; however, it deactivated due to the formation of a $NiTiO_3$ solid solution (Yan, et al. 2003) and carbon deposition (Wu, et al. 2005) (Figure 16). In contrast, the performance for dry reforming was excellent for over 100 hrs on stream. The formation of $NiTiO_3$ made the catalyst more difficult to reduce, but it could be improved by adding Ce, which also improved the oxygen storage capacity and mobility, effectively reducing carbon formation (Zhang, et al. 2006).

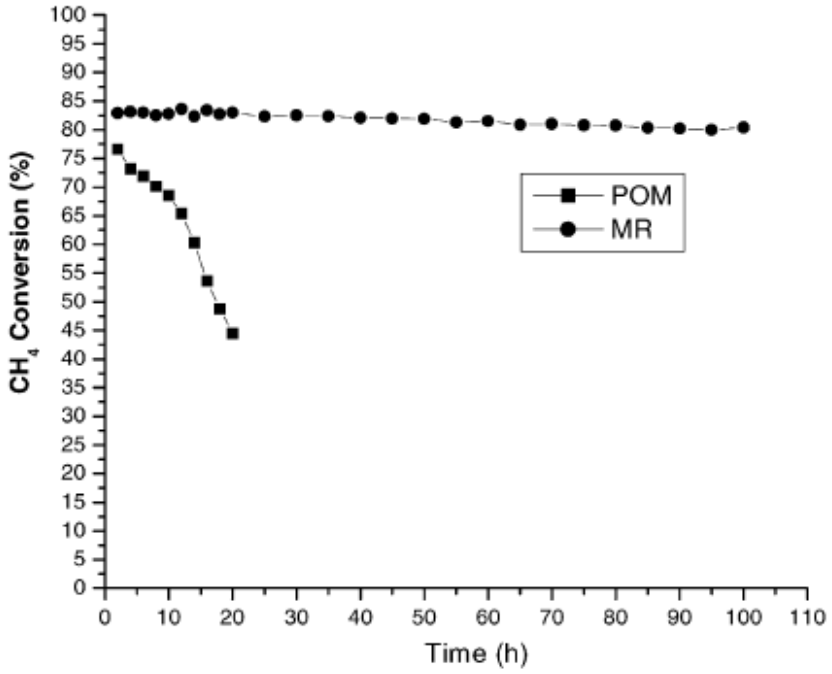

Figure 16: Activity vs. time for the POM and CO_2 reforming reactions over 8wt% Ni/TiO_2 (Yan, et al. 2003)

Adding noble metal to a 18.7 wt% Ni/Al_2O_3 catalyst lowered the reaction ignition temperature, with only 0.1 wt% addition lowering the ignition temperature from 1063 K to 878 K with Pd and 793 K with Pt (Choudhary, et al. 1992). Not only can noble metals lower the ignition temperature for the reforming reaction, but La can as well. Promoting with La_2O_3 reduces the ignition temperature because La can increase the ease of reduction or can inhibit the phase transition from NiO/Al_2O_3 to $NiAl_2O_4$ during high temperature calcination (Cao, et al. 1997). At La_2O_3 on NiO/Al_2O_3 loadings less than 2 wt%, the amount of carbon deposited was lower; however, at higher loadings carbon deposition increased. As further evidence, the effects of Na, Sr, Ce, and La modification of $Ni/\alpha\text{-}Al_2O_3$ and $Ni/\gamma\text{-}Al_2O_3$ on methane partial oxidation were studied and compared (Di, et al. 2006). The reduction temperature was decreased when the basic promoters were added, as shown in Figure 17. Based on thesedata, the addition of basic promoters can weaken the interaction between the active Ni component and Al_2O_3 support, and thus result in better performance since Ni is more easily reduced.

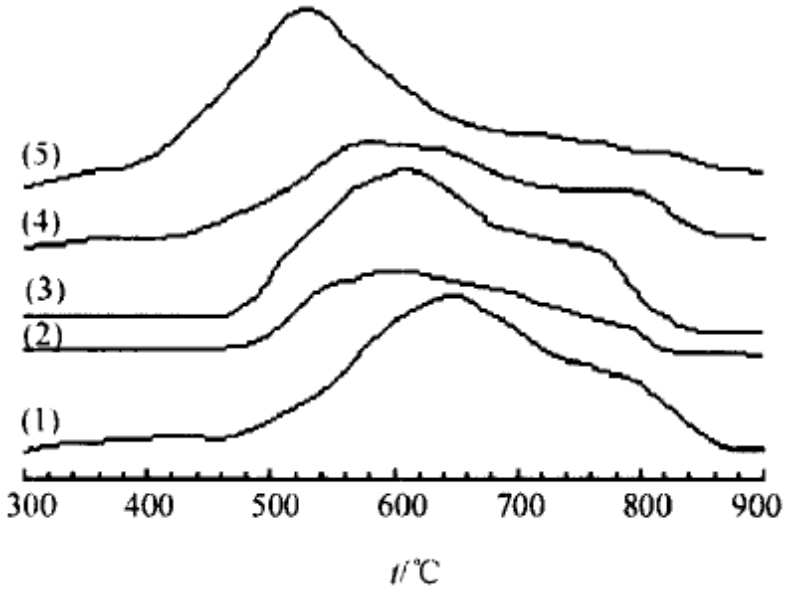

Figure 17: H_2-TPR spectra of catalysts samples; (1) Ni/γ-Al_2O_3; (2) Ni-Na/γ-Al_2O_3; (3) Ni-Sr/γ-Al_2O_3; (4) Ni-La/γ-Al_2O_3; (5) Ni-Ce/γ-Al_2O_3 (Di, et al. 2006)

NiO/Yb_2O_3, NiO/ZrO_2 and NiO/ThO_2 catalysts, i.e. using rare earths as supports, showed very high activity and selectivity for methane reforming reactions; but carbon deposition on them was also fast. However, the addition of cobalt to those catalysts reduced the ignition temperature, and inhibited carbon deposition (Table 4).

Table 4: Effect of adding cobalt to Ni-based catalysts for methane partial oxidation (CH_4/O_2 = 2 and GHSV = $5.2*10^5$ cm^3/g.hr) (Choudhary, et al. 1997)

Catalyst	Reaction start temp (℃)	Reaction temp (℃)	CH_4 conversion (%)	Selectivity (%)		Rate of carbon deposition ($mg/g_{cat}hr$)
				CO	H_2	
NiO/Yb_2O_3 (Ni:Yb=1:1)	545	700	86.1	96	95.2	16.7
$NiO/CoO/Yb_2O_3$ (Ni:Co:Yb=0.5:0.5:1)	470	700	79.8	93.3	91.7	2.5
NiO/ZrO_2 (Ni:Zr=1:1)	700	700	76.2	91.7	93.7	43.7
$NiO/CoO/ZrO_2$ (Ni:Co:Zr=1:1:1)	590	700	73.2	90.7	92.6	6.8
NiO/ThO_2 (Ni:Th=1:1)	450	500	68.9	87.6	83.2	831
$NiO/CoO/ThO_2$ (Ni:Co:Th=0.5:0.5:1)	420	500	63.7	86.2	79.8	1.2

2.2.4 Hydrotalcite-type catalysts

Using the precipitation catalyst preparation method with precursors containing metal ions bound in a stable crystal structure could result highly dispersed and stable metal particles on the surface, which may be resistant to sintering under more extreme conditions (Takehira, et al. 2004) (Fornasari, et al. 1995) (Shishido, et al. 2002). Hydrotalcite (HT)-like compounds, (a class of "layered" double hydroxides (LDHs)) containing exchangeable anions, is an excellent example of such a precursor (Cavani, et al. 1991). The hydrotalcite-type structure has (i) high surface area; (ii) basic properties; and (iii) small crystallite size oxide mixtures which are still stable after high temperature treatments, and are able to be reduced to thermally stable metal particles.

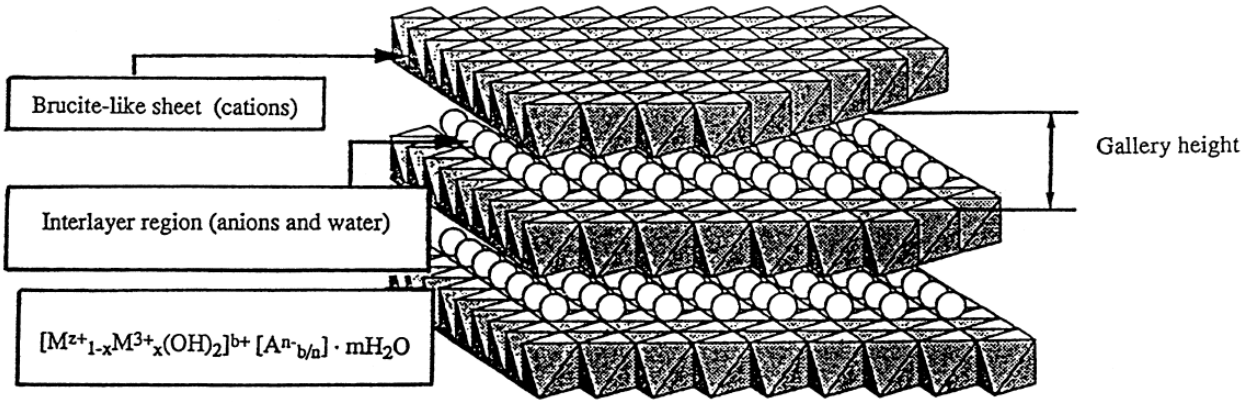

Figure 18: Schematic representation of the hydrotalcite-type anionic clay structure (Vaccari 1998)

Hydrotalcite-like compounds consist of brucite-like sheets separated by a layer of $Mg(OH)_2$, with the Mg^{2+} cations connected together to form this layer and layered double hydroxide structure [Figure 18] (Obalova, et al. 2004) (Cavani, et al. 1991). A hydrotalcite-type compound is prepared by mixing M^{2+} (ex. Mg^{2+}) and M^{3+} (ex. Al^{3+}) ions with basic OH ions from NaOH. A rapid precipitation of those ions produces the hydrotalcite structure. Synthetic hydrotalcite-type (HT) compounds are characterized by the formula:

$$[M^{2+}_{1-x}M^{3+}_{x}(OH)_2]^{x+}\left[A^{n-}_{x/n}\right]\cdot mH_2O \qquad \text{[Equation 30]}$$

where M donates metal cations and A donates anions. Distributed cations (Mg-Al) in the LDH structure give rise to small metal crystallites (mixed oxides) with a high surface area (typically 100-300 m^2/g) after calcination and reduction (Olsbye, et al. 2002). Also, the hydrotalcite-type precursor results in a more homogeneous, and reproducible, distribution of metal ions in the structure; and this preparation method is called the "solid phase crystallization (*spc*)" method. Many previous studies have investigated Ni/Mg/Al-LDH catalysts for reforming reactions (Kawabata, et al. 2005) (Takehira, et al. 2004). The Ni sites are highly dispersed inside the LDH structure and after reduction should lead to high catalytic performance.

Table 5: Characteristics of hydrotalcite-like compounds (Takehira, et al. 2004)

Catalyst	Atomic ratio	Ni loading	BET surface area	H_2 uptake	Ni dispersion	Particle size
	(Ni+Mg)/ Al	(wt%)	(m^2/g_{cat})	($\mu mol/g_{cat}$)	(%)	(nm)
spc-$Ni_{0.26}Mg_{0.74}Al$	1	16.7	124.6	253.5	17.8	7.8
spc-$Ni_{0.50}Mg_{2.50}Al$	3	15.8	178.6	265.1	19.7	7
spc-$Ni_{0.73}Mg_{4.27}Al$	5	17.8	125.1	203.5	13.4	8.2
imp-Ni/Mg_3Al	-	16.3	95.4	221.5	16	7.2

Among the different ratios of the Ni, Mg, and Al ($Ni_xMg_yAl_z$) listed in Table 5, $Ni_{0.5}Mg_{2.5}Al$ has the highest surface area. In addition, the structures of the catalysts, determined by XRD analysis, depend on the composition (Figure 19). After drying, HT and $Al(OH)_3$ peaks were observed. After high temperature calcination treatments (at 1123 K), the XRD peaks associated with the hydrotalcite structures disappear due to the collapse of the hydrotalcite structure. Instead, inactive $MgAl_2O_4$ spinel is present. The inactive $MgAl_2O_4$ compounds form when the interlayer water is removed from the layered structure at high calcination temperature (Takehira, et al. 2004).

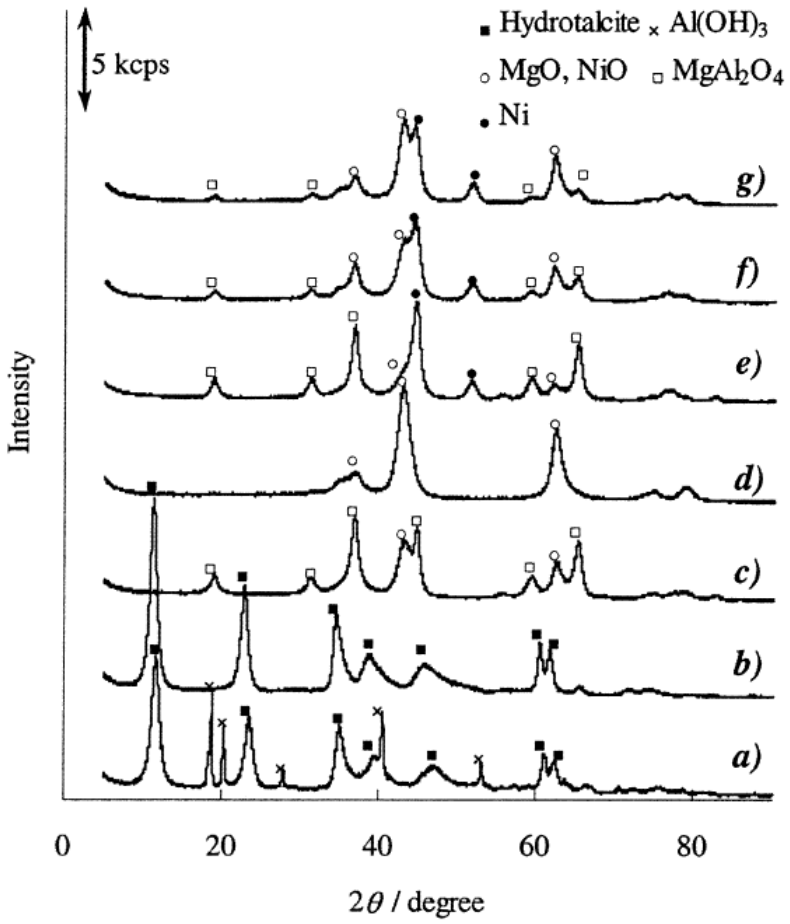

Figure 19: XRD patterns of the precursors of *spc*-Ni/MgAl catalysts; (a) *spc*-$Ni_{0.26}/Mg_{0.74}Al$ after drying, (b) $Ni_{0.5}/Mg_{2.5}Al$ after drying, (c) *spc*-$Ni_{0.26}/Mg_{0.74}Al$ after calcination, (d) $Ni_{0.5}/Mg_{2.5}Al$ after calcination, (e) *spc*-$Ni_{0.26}/Mg_{0.74}Al$ after reduction, (f) $Ni_{0.38}/Mg_{1.62}Al$ after reduction, (g) *spc*-$Ni_{0.5}/Mg_{2.5}Al$ after reduction (Takehira, et al. 2004)

In investigating the effects of the Mg/Al ratio, XRD analysis has also shown that when the Mg/Al ratio is increased above 2/1, the $Al(OH)_3$ peaks disappeared, and only hydrotalcite peaks are observed. At lower Mg/Al ratios (< 2), formation of the hydrotalcite structure is not favorable (Kawabata, et al. 2005). When the ratio of (Mg+Ni)/Al is 3/1 ($Ni_{0.5}Mg_{2.5}Al$ HT), the weakest line intensity of Mg(Ni)-Al HT is observed (Kawabata, et al. 2005). This suggests that the $Ni_{0.5}Mg_{2.5}Al$-HT catalyst has the smallest crystal size, and therefore the highest crystallite surface area. With a higher Mg/Al ratio, an increase in temperature is required for reduction since a large amount of Mg stabilizes a large amount of Ni^{2+} in the solid solutions. However, Al^{3+} incorporation into the MgO framework inhibits the crystal growth of MgO and the Mg-Ni-O

solid solution. This makes Ni reduction easier since the substitution of Al^{3+} in MgO affects the stability of Ni^{2+} in the solid solution (Takehira, et al. 2004).

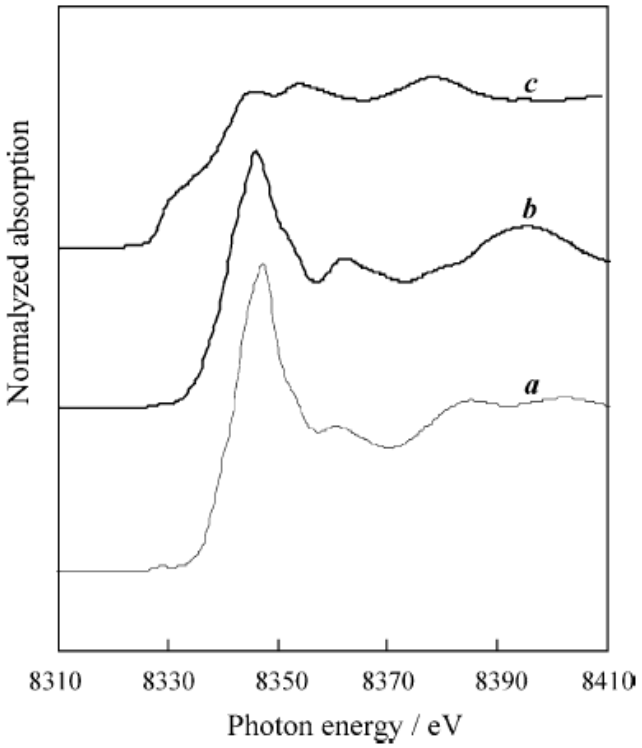

Figure 20: Normalized Ni K-edge XANES spectra of the catalyst; (a) $Ni_{0.5}Mg_{2.5}Al$-HT, (b) NiO, and (c) Ni foil (Kawabata, et al. 2005)

The coordination structure for the $Ni_{0.5}Mg_{2.5}Al$ catalyst was obtained by X-ray absorption near-edge structure (XANES) spectra. XANES can provide geometrical information about Ni sites and oxidation state changes. When the XANES spectra of a NiO and Ni foil are compared with that of $Ni_{0.5}Mg_{2.5}Al$ (Figure 20), the spectrum of the $Ni_{0.5}Mg_{2.5}Al$ resembles that of NiO. Both K-edge XANES spectra of $Ni_{0.5}Mg_{2.5}Al$ and NiO have a peak near 8333 eV, indicating that the Ni sites in those catalysts have octahedral structures (Colpas, et al. 1991). In addition, the lattice parameters for different ratios of Ni/Mg/Al mixture which were calcined at 1173 K are summarized in Table 6.

Table 6: The lattice parameters for different ratio of Ni/Mg/Al on the hydrotalcite-type catalysts (Basile, et al. 1998)

Atomic ratio	Identified crystallographic phases	Oxide crystal size (nm)	Spinel crystal size (nm)	Oxide lattice parameter a (nm)	Spinel lattice parameter a (nm)	Surface area after calcination at 1173K (m^2/g)
Ni/Mg/Al = 10/61/29	(Ni,Mg)O+$MgAl_2O_4$	14.5	18.5	0.4205(2)	0.8080(5)	53
Ni/Mg/Al = 34/37/29	(Ni,Mg)O+$MgAl_2O_4$	15.5	16	0.4195(2)	0.8056(5)	47
Ni/Mg/Al = 61/10/29	NiO+(Ni,Mg)Al_2O_4	12	19	0.4178(2)	0.8048(3)	39
Ni/Mg/Al = 71/0/29	NiO+$NiAl_2O_4$	14.5	16	0.4177(2)	0.8051(3)	27

Different amounts of Ni (Ni_x donates x mol% of Ni for the catalyst) on the catalysts lead to different crystallographic phases. Ni_{61} and Ni_{71} samples, which are Ni-rich, have segregated NiO and spinel $MgAl_2O_4$ or $NiAl_2O_4$ after calcination treatment. With lower Ni contents (Ni_{10}, Ni_{34}), however, the formation of NiO-MgO solid solutions and a spinel $MgAl_2O_4$ phase were observed. The surface areas for all the catalysts were quite low when the catalysts were calcined above 1173 K, due to a structural rearrangement associated with the segregation of spinel and solid oxide solutions. The low Ni-content catalysts (Ni_{10} and Ni_{34}) were difficult to reduce, which can be attributed to the segregation of NiO/MgO solid solutions in which the Ni^{2+} species were stabilized inside an inert MgO-type matrix. But the Ni-rich catalysts formed NiO crystallites during the high-temperature calcination (Basile, et al. 1998). The Ni-rich HT catalysts showed high methane conversion, but also rapid deactivation. This behavior was related to the easy reducibility of the large NiO crystallites. However, with the HT catalysts containing a small amount of Ni, no deactivation was observed even after 500 hrs of time-on-stream due to the formation of the stable NiO-MgO solid solution which gave rise to well dispersed Ni^0 particles.

2.3 Kinetic Studies

2.3.1 Steps in a catalytic reaction

Heterogeneous catalytic reactions are the combination of various reactions. Reactant gases should pass through a boundary layer in order to reach on the surface of the catalyst. In general, the sequence of individual steps is shown in Table 7 and Figure 21. As mentioned, those steps are classified as diffusion steps (step 1, 2, 6, and 7), and reaction steps (step 3, 4, and 5). In overall, when the diffusion steps are conducted very fast compared with the reaction steps, the effects of the transport limitation could be negligible.

Table 7: Steps in a catalytic reaction

Steps	
1	**External diffusion of reactant A**: Mass transfer of the reactants from bulk fluid to the external surface of the catalyst pellet
2	**Internal diffusion of reactant A**: Diffusion of the reactants from the pore mouth through the catalyst pores to the immediate vicinity of the internal catalytic surface
3	**Adsorption of reactant A**: Adsorption of reactants A onto the catalyst surface
4	**Reaction of A to B**: Reaction on the surface of the catalyst (A → B)
5	**Desorption of product B**: Desorption of the products B from the surface
6	**Internal diffusion of product B**: Diffusion of the products from the interior of the pellet to the pore mouth at the external surface
7	**External diffusion of product B**: Mass transfer of the products from the external pellet surface to the bulk fluid

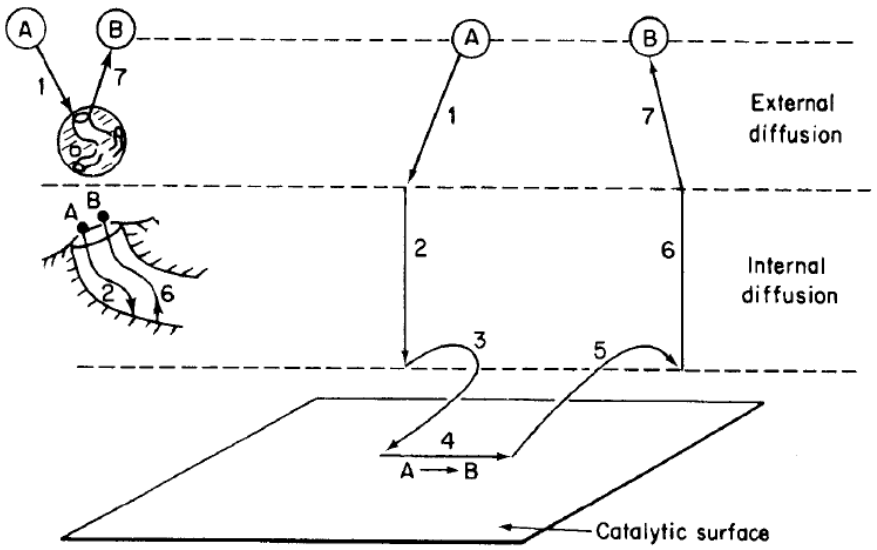

Figure 21: Steps in a heterogeneous catalytic reaction (Fogler 2006)

The overall rate of reaction is assumed to be equal to the rate of the slowest step in mechanism. In this chapter, how the overall reaction kinetics are determined depending on the different rate limiting steps.

2.3.2 External and internal diffusion

When gas reactants flow through the catalyst particle, boundary layer (or film) surrounds the catalyst surface; and the gas reactants should be passing through the gas film (i.e. diffusion) to reach to the catalyst surface in order to begin chemical reaction. The resistance by the diffusion of the reactant through the boundary layer can be varied by the flow rate of the fluid. Depending on the velocity of the fluid, the thickness of the boundary layer is affected, and shown in Figure 22.

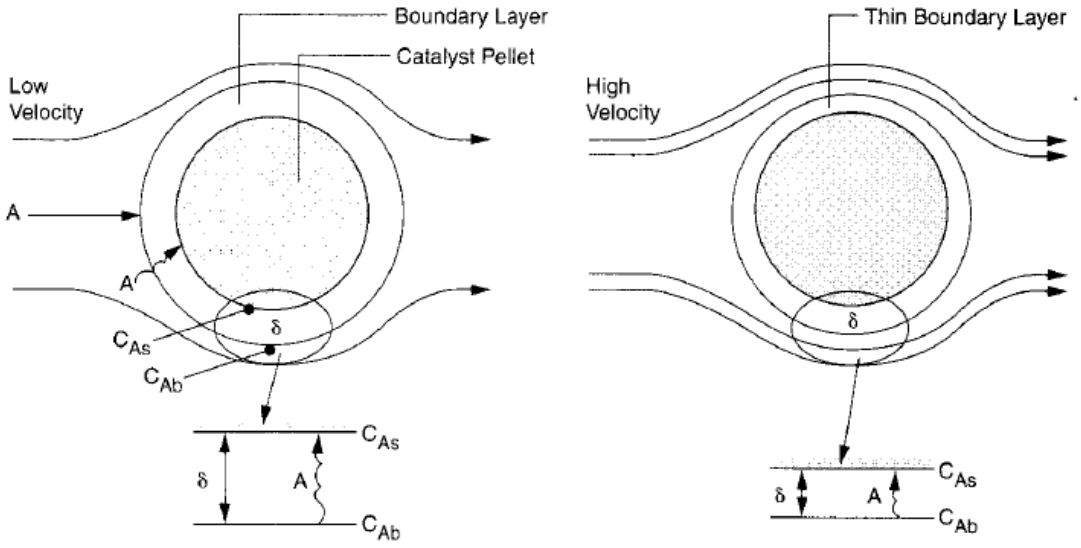

Figure 22: Diffusion through the external boundary layer (Fogler 2006)

At low velocity of the reactants passing over the pellet, a thick boundary layer is generated. Then it takes longer time for reactant A to travel to the surface than time for chemical reaction (A → B) on catalyst surface. Therefore, the diffusion step is limiting the overall rate of reaction since the supply of reactant A to the surface for the chemical reaction is slower. In addition, the large boundary layer thickness (δ) provides small mass transfer coefficient (k_C); then it leads to decrease the rate of reaction.

At high velocity of the fluid, however, the boundary layer thickness (δ) is decreased; then resistance by the diffusion across the boundary layer is decreased. Therefore, external mass transfer does not limit the rate of reaction since quick transportation of reactant A to the surface is available.

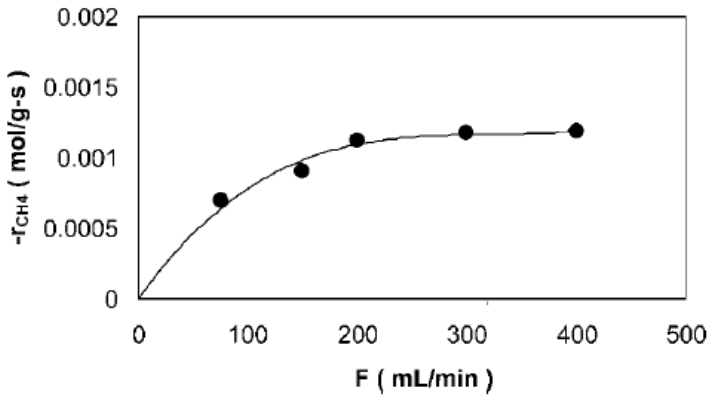

Figure 23: Effect of flow velocity on reforming rate over Ni-Co/Al-Mg-O catalyst at 750°C, 310kPa, and W/F = 0.002 (g_{cat}.s/mL) (Zhang, et al. 2009)

The effect of external mass transfer limitation can be studied experimentally with a fixed residence time through a variation of feed velocity (Zhang, et al. 2009) (Tsipouriari, et al. 2001) (Nandini, et al. 2006). With a constant contact time, a higher reactant flow rate decreases the boundary film thickness (δ); it indicates that limitation of external mass transfer is negligible.

2.3.3 Activation Energy

To begin a chemical reaction, the reactant gas molecules require energy to distort or stretch their bonds in order to form new bonds. It implies that the molecules in reactant gases should overcome an energy barrier, which is named as activation energy, to form new bonds. To estimate the activation energy, Arrhenius equation should be proposed (Eq. 31). The activation energy (E) can be found from a polt of lnk_A as a function of (1/T) (Figure 24). In general, the larger activation energy implies the more temperature-sensitive for the rate of reaction.

$$\ln k_A = \ln A - \frac{E}{R}\left(\frac{1}{T}\right) \qquad \text{[Equation 31]}$$

$$k(T) = k(T_0)e^{\frac{E}{R}\left(\frac{1}{T_0}-\frac{1}{T}\right)} \qquad \text{[Equation 32]}$$

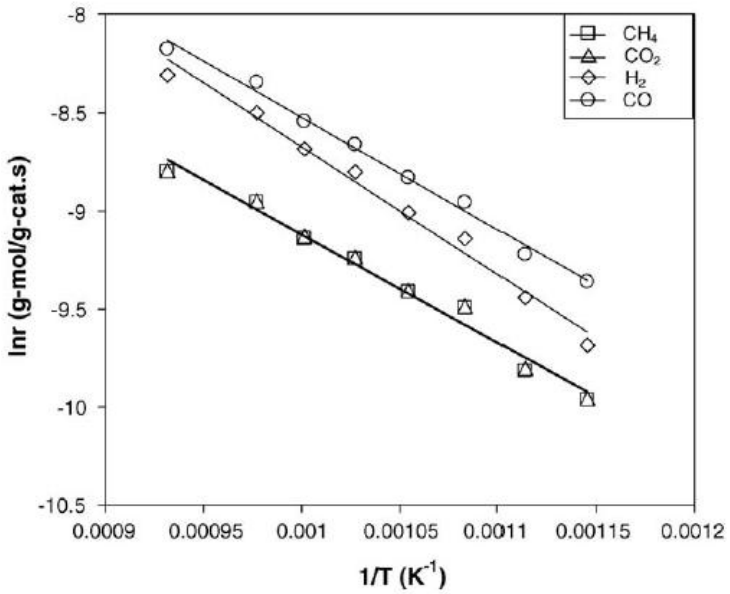

Figure 24: Arrhenius plots for CH_4 and CO_2 consumptions, and H2 and CO production (Nandini, et al. 2006)

In addition, the specific reaction rate at different temperature would be predicted by the following equations. Eq. 32 allows to obtain the specific reaction rate $k(T)$ at any other temperatures if we know $k(T_0)$ and E.

Table 8: Comparison of apparent activation energy (E, kJ/mol) over Ni catalysts (Nandini, et al. 2006)

Catalyst	E_{CH4}	E_{CO2}	E_{H2}	E_{CO}
13Ni-2K/10CeO_2-Al_2O_3 (873-1073K)	46.1	46.2	54.0	47.4
Ni/Al_2O_3 (773-973K)	50.9	56.1	N/A	80.5
Ni/Al_2O_3 (673-773K)	70.6	69.0	98.1	74.0
Ni/C (673-823K)	121.4	92.1	134.0	100.5
Ni/SiO_2 (673-823K)	96.3	79.6	113.0	83.7
Ni/SiO_2 (673-773K)	62.3	69.8	93.9	68.9
Ni/MgO (673-823K)	92.1	87.9	146.5	87.9
Ni/TiO_2 (673-823K)	108.9	87.9	134.0	96.3
Ni/CaO-Al_2O_3 (893-963K)	106.8	98.8	147.4	103.0

Many studies have been progressed to estimate the activation energy over Ni-based catalysts for CO_2 reforming of CH_4 process (Table 8). It indicates that the supports on Ni

crystallites influence the activation energy since the activation energy levels for CH_4 consumption vary on different supports. Activation energy for H_2 formation is always higher than the activation energy for CO formation. It implies that the reverse water-gas shift reaction occurs during the CO_2 reforming of CH_4 and it affects the apparent activation energies.

2.3.4 Effects of partial pressures on reforming rate

The kinetic behavior of the catalyst could be investigated from the functions of partial pressure of reactant gases (CH_4 and CO_2) and product gas (H_2) in order to obtain the intrinsic reforming rate. The effect of the CH_4 partial pressure at different temperatures

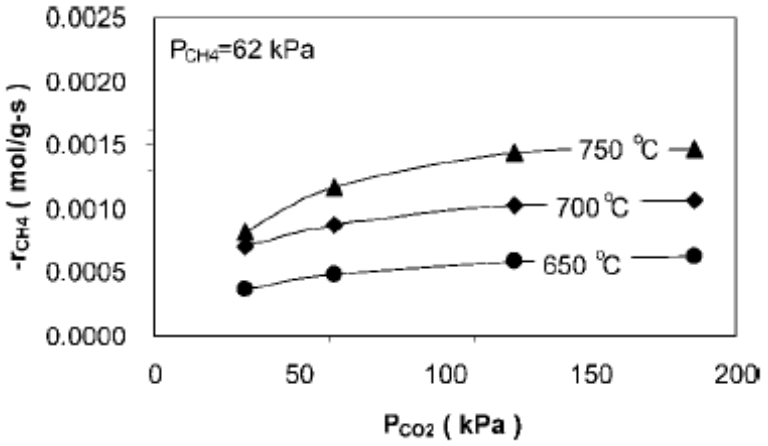

Figure 25: Effect of CO_2 partial pressure on the reforming rates of CO_2 reforming of CH_4 over Ni-Co/Al-Mg-O catalyst at 310 kPa and W/F = 0.002 gcat.s/mL (Zhang, et al. 2009)

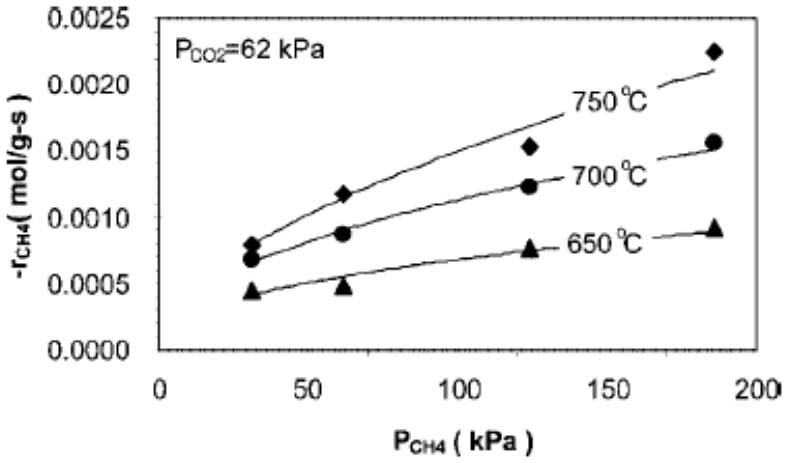

Figure 26: Effect of CH_4 partial pressure on the reforming rates of CO_2 reforming of CH_4 over Ni-Co/Al-Mg-O catalyst at 310 kPa and W/F = 0.002 g_{cat}.s/mL (Zhang, et al. 2009)

2.3.5 Reaction mechanism and kinetic model

CO_2 reforming of CH_4 reaction consists of three major steps; (a) dissociate CH_4 and CO_2, (b) adsorption of carbon, hydrogen, and oxygen species on active sites, (c) surface reaction to form product species, (d) desorption of product species, such as CO and H_2. The first reaction mechanism for CO_2 reforming of CH4 was introduced in 1967 by Bodrov and Apel'baum (Bodrov and Apel'baum 1967). The Bodrov's CO_2 reforming of CH_4 mechanism was used to describe steam reforming of CH_4. In 1994, a Langmuir-Hinshelwood model for CO_2 reforming of CH_4 was developed; and it proposed the CH4 dissociation step is the rate determining step (Zhang and Verykios 1994); and Wang and Au also proposed that CH_4 dissociation is the rate-limiting step as well in 1996 (Wang and Au 1996). However, several studies in 1997 proposed that the surface reaction between carbon and oxygen species is the rate-limiting step (Slagtern and Olsbye 1994) (Hu and Ruckenstein 1997) (Tsipouriari and Verykios 2001). In conclusion, the CH_4 dissociation step and the surface reaction step are generally accepted as rate-determining step for CO_2 reforming of CH_4 process.

Several mechanisms of CO_2 reforming of CH_4 have been proposed. In 1967, the first was introduced by Bodrov and Apel'baum (Lewis, et al. 1949).

$$CH_4 + S \rightarrow CH_2 \cdot S + H_2 \quad \text{[Equation 33]}$$

$$CO_2 + S \leftrightarrow CO + O \cdot S \quad \text{[Equation 34]}$$

$$O \cdot S + H_2 \leftrightarrow H_2O + S \quad \text{[Equation 35]}$$

$$CH_2 \cdot S + H_2O \leftrightarrow CO \cdot S + 2H_2 \quad \text{[Equation 36]}$$

$$CO \cdot S \leftrightarrow CO + S \quad \text{[Equation 37]}$$

S denotes active sites on the catalyst surface; → denotes a slower irreversible reaction (rate-determining step); and ↔ denotes a quasi-equilibrated reaction. Bodrov proposed three major steps. First, CH_4 is dissociated and adsorbed on active sites in the rate-determining step to yield CH_2 species (Eq. 33). From pulse tests of CH_4 and CO_2 over a Ni/Al_2O_3 catalyst, it was found that CH_4 dissociated on active Ni sites and CO_2 dissociated on the support or at the interface of the Ni and support (Ferreira-Aparicio, et al. 2000). Second, the dissociated CO_2 produces CO and oxygen species on the active sites (Eq. 34). The oxygen on the active sites reacts with H_2 produced by CH_4 dissociation producing H_2O (Eq. 35). Those steps (Eq. 34 and Eq. 35) are classified as the RWGS reaction. Finally, the H_2O produced from the RWGS reaction reacts with the CH_2 species producing H_2 and CO (Eq. 36 and Eq. 37) (Lewis, et al. 1949). It might explain the reason why CO_2 reforming of CH_4 process is classified as a slower reaction step than steam reforming of CH_4 process because direct addition of H_2O would increase the reaction rate than producing H_2O from the RWGS reaction (Bradford and Vannice 1999).

In 1993, the modification of the Bodrov's mechanism was introduced by Erdohelyi et al. (Erdohelyi, et al. 1993). First, Erdohelyi proposed that the various dissociated CH_4 species are presented on the catalyst surface; and it is depending on the catalyst's characterization. Therefore, Eq. 33 was modified to Eq. 38 and Eq. 39.

$$\mathrm{CH_4 + 2S \rightarrow CH_3 \cdot S + H \cdot S} \quad \text{[Equation 38]}$$

$$\mathrm{CH_3 \cdot S + (3 - x)S \leftrightarrow CH_x \cdot S + (3 - x)H \cdot S} \quad \text{[Equation 39]}$$

Second, Erdohelyi proposed the modification of the RWGS reaction (Eq. 34 and Eq. 35) to Eq. 40 and Eq. 41.

$$CO_2 + H \cdot S \leftrightarrow CO + HO \cdot S \quad \text{[Equation 40]}$$

$$2HO \cdot S \leftrightarrow H_2O + O \cdot S + S \quad \text{[Equation 41]}$$

There were many researches to investigate the CH_4 dissociation step. So far, the CH_4 dissociation step was assumed as an irreversible step. In 1996, Yong et al. also provided evidence that CH_4 dissociation step is a reversible step by the isotopic scrambling depending on conditions between CH_4 and CD_4 during CO_2 reforming of CH_4 process (Bradford and Vannice 1999). In addition, Osaki et al. proposed that the CH_4 dissociation step to produce CH_x and the surface reaction of CH_x are responsible for H_2 production (Osaki, et al. 1994). Solymosi et al. proposed that the adsorbed O species from the dissociation of CO_2 promote CH_4 dissociation (Solymosi, et al. 1991).

In 1999, a more recent study by Bradford and Vannice provides more detailed steps on supported Ni catalysts (Bradford and Vannice 1998) (Bradford and Vannice 1999).

$$CH_4 + S \leftrightarrow CH_x \cdot S + \left(\frac{4-x}{2}\right) H_2 \quad \text{[Equation 42]}$$

$$2[CO_2 + S \leftrightarrow CO_2 \cdot S] \quad \text{[Equation 43]}$$

$$H_2 + 2S \leftrightarrow 2H \cdot S \quad \text{[Equation 44]}$$

$$2[CO_2 \cdot S + H \cdot S \leftrightarrow CO \cdot S + OH \cdot S] \quad \text{[Equation 45]}$$

$$OH \cdot S + H \cdot S \leftrightarrow H_2O + 2S \quad \text{[Equation 46]}$$

$$CH_x \cdot S + OH \cdot S \leftrightarrow CH_xO \cdot S + H \cdot S \quad \text{[Equation 47]}$$

$$CH_xO \cdot S \rightarrow CO \cdot S + \left(\frac{x}{2}\right) H_2 \quad \text{[Equation 48]}$$

$$3[CO \cdot S \leftrightarrow CO + S] \quad \text{[Equation 49]}$$

As shown, CO_2 reforming of CH_4 goes through the following steps: (1) the reversible dissociation of CH_4 to yield CH_x species and H_2 (Eq. 42); (2) non-dissociative adsorption of CO_2 on the support (Eq. 43); (3) H-promoted CO_2 dissociation at the metal-support interfacial region (Eq. 45); (4) the reaction of CH_x species with OH species to yield CH_xO species at the metal-support interfacial region (Eq. 47); and (5) CH_xO decomposition at the metal-support interfacial region to yield CO and H_2 (Eq. 48 and Eq. 49).

Many studies were performed to express the rate of CO_2 reforming of CH_4 on various catalysts. The summary of the proposed rate models for CO_2 reforming of CH_4 is tabulated in Table 9.

Table 9: Proposed rate expressions for CO_2 reforming of CH_4

Model	Catalyst	Ref.
$r = \frac{kP_{CH_4}(P_{CO_2} + P_{H_2O})}{[1 + 24(P_{CO_2} + P_{H_2O}) + 8P_{H_2}]^2}$	Cu/SiO_2	(Qin and Lapszewicz 1994)
$r = \frac{kP_{CH_4}}{1 + a(P_{H_2O}/P_{H_2}) + bP_{CO}}$	Ni foil	(Mark and Maier 2003)
$r = \frac{kK_{CO_2}K_{CH_4}P_{CO_2}P_{CH_4}}{(1 + K_{CO_2}P_{CO_2} + K_{CH_4}P_{CH_4})^2}$	Rh/Al_2O_3	(Richardson and Paripatyadar 1990)
$r = \frac{k\sqrt{K_1K_2P_{CO_2}P_{CH_4}}}{(1 + \sqrt{K_1P_{CO_2}} + \sqrt{K_2P_{CH_4}})^2}$	Ni/Al_2O_3_ $Ni/CaO\text{-}Al_2O_3$ Ni/SiO_2	(HoriuchiT. et al. 1996)
$r = \frac{aP_{CH_4}P_{CO_2}^2}{(P_{CO_2} + bP_{CO_2}^2 + cP_{CH_4})^2}$	Ni/Al_2O_3 $Ni/CaO\text{-}Al_2O_3$	(Zhang and Verykios 1994)

Chapter 3. Experimental Details

3.1 Catalyst Preparation

The $Ni_{0.5}Mg_{2.5}Al$-HT and $Ni_{0.5}Ca_{2.5}Al$ were prepared using the co-precipitation method. The preparation procedure for all catalysts was identical, with either Mg or Ca nitrates used. The Ni/Al_2O_3 catalyst was prepared by wet-impregnation method.

For the preparation of the $Ni_{0.5}Mg_{2.5}Al$-HT catalyst, 30 mL of 1M Ni nitrate (nickel(II) nitrate hexahydrate, $Ni(NO_3)_2.6H_2O$, Puratronic®, 99.9985%) aqueous solution, 150 mL of 1M Mg nitrate (magnesium nitrate hexahydrate, Alpha-Aesar, ACS grade 98.0 ~ 102.0%) aqueous solution and 60 mL of 1M Al nitrate (aluminum nitrate nonahydrate, $Al(NO_3)_3.9H_2O$, Alpha-Aesar, ACS grade 98.0~102.0%) aqueous solution were prepared and mixed together. The mixed nitrate solution was added drop-wise into 240 mL of 0.50M Na_2CO_3 aqueous solution at room temperature with vigorous stirring (400 rpm). Simultaneously, 3.00 M NaOH aqueous solution was added drop-wise as well to maintain the pH at 10.0 ± 0.1. The resulting precipitate was aged in the mother liquor at 120°C for 12 hr. Then the aged precipitate was cooled to room temperature and was held at room temperature for 1 hr. Then, it was washed and filtered with distilled and de-ionized water until the residual Na^+ in the aged precipitate was removed (pH ~7). The washed precipitate was dried at 120°C for 12 hr.

The $Ni_{0.5}Ca_{2.5}Al$ catalyst was prepared using a mixture of 30 mL of 1M Ni nitrate, 150 mL of 1M Ca nitrate ($Ca(NO_3)_2.4H_2O$, Alpha-Aesar, ACS grade 98.0~102.0%) and 60 mL of 1M Al nitrate. The $Ni_{0.5}Al_{3.5}$ catalyst was prepared using a mixture of 30 mL of 1M Ni nitrate and 210 mL of Al nitrate. The rest of the procedure is identical to that above for the $Ni_{0.5}Mg_{2.5}Al$ catalyst.

For preparing the 10wt% Ni/Al_2O_3 catalyst, ~75 mL of distilled water was heated to 80℃ with 400 rpm of stirring. 3.019g of γ-Al_2O_3 powder (Alumina oxide, γ-phase, Alpha-Aesar, 99.97% (metal basis)) was poured into the distilled water. 1.663g of 1M Ni nitrate was added drop-wisely in order to provide 10wt% of Ni on g of Al_2O_3 support. With continuous 400 rpm of stirring, water was evaporated at 80℃. Then, it was stored in oven overnight at 120℃ for 12 hr.

The dried precipitate was crushed to powder form. Then, the powder precipitate was calcined at 820°C in air for 5 hr in order to produce an oxide-phase catalyst. The calcined catalysts were pelletized to attain a particle size of 354-500 μm. The pelletized oxide-phase catalyst was reduced in H_2 balanced with N_2 at 720℃ for 1 hr to produce active Ni metal.

3.2 Catalyst Characterization

3.2.1 Surface Area (BET)

The Langmuir isotherm theory, which is the simplest and most widely used for monolayer adsorption, can be applied to model multilayer adsorption. The model of Brunauer, Emmett, and Teller (BET) in 1938 was the first successful attempt to model multilayer adsorption. To apply BET theory to measure multilayer adsorption, several assumptions are required. The concept of BET is extended from that of the Langmuir isotherm, whose assumptions are listed below.

(i) The adsorbate is typically adsorbed in a monolayer
(ii) One species is adsorbed per site
(iii) ΔH_a (enthalpy of adsorption) is independent of θ (coverage)
(iv) Equilibrium exists between adsorption and desorption

Normally, physical adsorption occurs in forming multilayers. The total surface area of the solid can be determined when the isotherm is modeled. The BET measurement for multilayer

adsorption requires additional assumptions including the Langmuir isotherm assumptions. The additional assumptions are:

(i) Adsorbed species in the first layer serve as sites of adsorption for the second layer;

(ii) The rate of adsorption (r_a) on the i^{th} layer is equal to the rate of desorption of the (i+1) layer;

(iii) ΔH_{ads} is the same for second and succeeding layers and equal to the heat of condensation of the gas.

Based on the assumptions listed above, the coverage for multilayer adsorption, θ, can be derived as:

$$\theta = \frac{V}{V_m} = \frac{cx}{(1-x)[1+(c-1)x]} \qquad \text{[Equation 50]}$$

where $x = P/P_0$, P_0 = vapor pressure of the adsorbing gas at a given temperature, and V_m is the maximum volume of gas adsorbed in the monolayer.

$$c = c_0 exp\left[\frac{\Delta H_{a1} - \Delta H_c}{RT}\right] \qquad \text{[Equation 51]}$$

where ΔH_{a1} = heat of adsorption on the first layer, ΔH_c = heat of condensation of gas, and $c_0 = a_1b_1/a_2b_2$ (a_1, a_2, b_1, b_2 are the preexponentials for condensation to and evaporation from the first and second layers).

The values of c and V_m can be obtained by experimental data. Eq. 50 can be linearized and rearranged as

$$\frac{x}{V(1-x)} = \frac{1}{cV_m} + \frac{(c-1)x}{cV_m} \qquad \text{[Equation 52]}$$

Volume adsorbed versus P/P_0 experimental data are collected at the boiling point of the adsorbate, normally N_2 at 77K. These data are then rearranged to plot x/[V(1-x)] versus x and generate a straight line with intercept = $1/cV_m$ and slope = $(c-1)/cV_m$. To calculate the surface area of the solid, the following equation is used, relating the monolayer volume to the number of moles adsorbed.

$$S = n_m N_{AV} \alpha (m^2/g) \qquad \text{[Equation 53]}$$

where S = surface area (m^2/g), n_m = number of mole, N_{AV} = Avogadro's number and $\alpha = 1.62 * 10^{-20}$ m^2/molecule for N_2.

For this study, the BET measurements were conducted using a Micromeritics Gemini 3 2375 (USA). Nitrogen gas was used as the adsorbate. Around 100 mg of the pelletized catalysts were loaded and the surface area was measured at 77 K, which is the boiling point of nitrogen. 11 points within a P/P_0 range between 0.05 to 0.3 were collected and used to produce the BET plot and calculate the surface area.

3.2.2 X-ray diffraction patterns

About 95% of solid materials can be described as crystalline, which means the atoms are repetitively arranged in a regular pattern in three dimensions. Since each substance has a unique X-ray diffraction (XRD) pattern, XRD is widely used to characterize and identify catalysts.

An X-ray beam is scattered when it hits the atoms in a crystal. Since crystals consist of regular, repeated arrays of atoms, the X-ray beam diffracted by the atoms has a regular array of waves.

$$n\lambda = 2dsin\theta \qquad \text{[Equation 54]}$$

Where,

λ: Wavelength of the X-ray

d: Distance between two lattice planes

θ: Angle between the incoming x-ray and the normal to the reflecting lattice plane

n: Integer called the order of the reflection

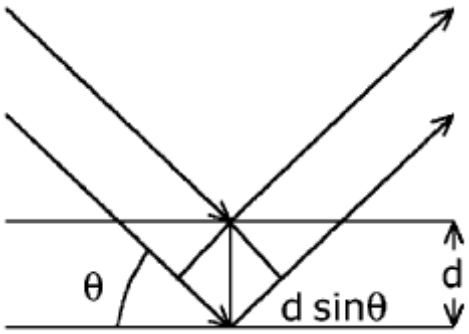

Figure 27: X-ray scattered by atoms in an ordered lattice interface

XRD patterns are generated using a stationary X-ray source (usually Cu Kα), and the scattered X-rays are detected by a movable detector. The detector scans the intensity of the diffracted radiation as a function of 2θ between the initial and the diffracted radiation. The 2θ angle value from XRD provides the corresponding lattice spacing which is characteristic of a certain crystal. The width of diffraction peaks provides information about the dimensions of the reflecting phases [Eq. 55]. The shape, intensity and position of the diffraction peaks can provide information about the crystaillinity.

$$< L >= \frac{K\lambda}{\beta cos\theta}$$ [Equation 55]

Where,

<L>: A measure for the dimension of the particle in the direction perpendicular to the reflecting plane

β: Peak width

λ: X-ray wavelength

K: A constant (~ 1)

θ: Angle between the beam and the normal on the reflecting plane

For this research, powder X-ray diffraction patterns were measured on a Rigaku D/Max-III C (USA) using standard Bragg-Brentano geometry with Ni-filtered Cu Kα radiation (λ_1 = 1.5406Å, λ_2 = 1.5444Å) and 40 kV/100 mA X-ray radiation. Spectra were collected for a 2θ range of 5 to 80° using a step size of 0.01 and a count time of 1s.

3.2.3 Temperature-programmed reduction

Temperature-programmed reduction (TPR) is used to characterize the interaction strength between the active phase and support. Depending on the strength, the amount of reducible metal oxide can be measured. The reduction of the nickel-supported catalyst is explained below:

$$NiO + H_{2(g)} \rightarrow Ni^0 + H_2O \qquad \text{[Equation 56]}$$

While H_2 diluted with inert gas (N_2 or He) is flowing through the reactor, the temperature of the sample is increased at a constant rate and the rate of H_2 consumption is measured. It provides the total amount of reducible metal oxide and the strength of the metal-oxygen bond.

In this study, around 100 mg of calcined catalyst was placed in a quartz tube. The temperature was ramped at 10℃/min from 25 to 900℃ in a 10% H_2/N_2 reducing gas mixture flowing at 30 mL/min. The product gas was delivered to a thermal conductivity detector (TCD) to measure the amount of H_2 consumption. The simplified diagram of the TPR equipment used in this study is shown in Figure 28.

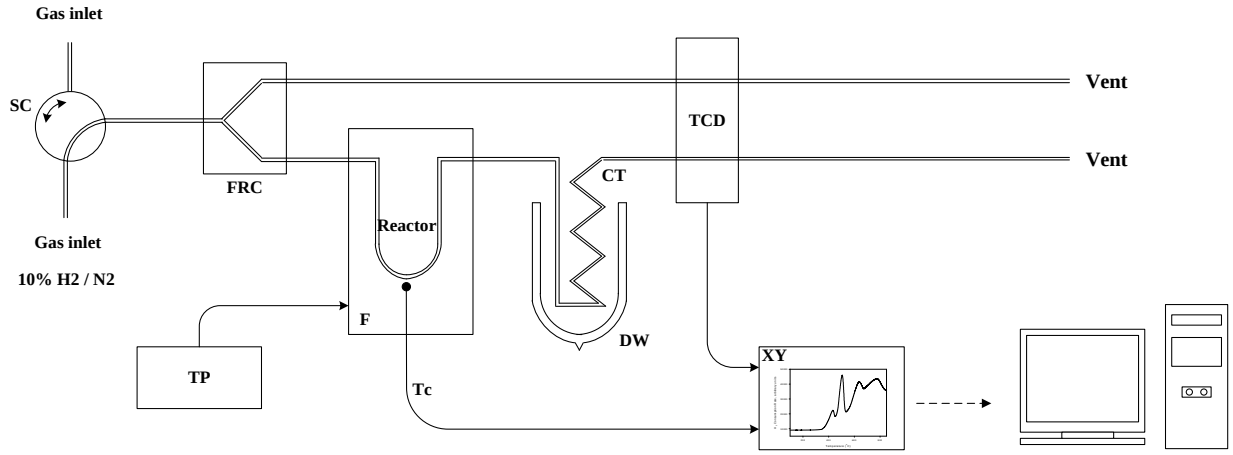

Figure 28: Simplified diagram of temperature-programmed reduction equipment

3.2.4 Temperature-programmed oxidation

Hydrocarbon-based reactions on solid catalysts can be accompanied by the formation of by-products, some of which can form a carbonaceous deposit on the surface and cause deactivation (Bond, et al. 1995). Temperature-programmed oxidation (TPO) was used to analyze residual carbon materials deposited during the reactions, by flowing an O_2/inert gas mixture while increasing the sample temperature. In addition, TPO is a useful method for quantifying the different carbon species present on a given sample. TPO provides a direct measurement of the amount of carbon gasified as a function of temperature. A 10% O_2/He mixture was used with flow rate of 30 mL/min.

3.2.5 Scanning Electron Microscopy

Scanning electron microscopy (SEM) can be used to evaluate the morphology of the catalysts. It allows taking images of the sample surface using a high-energy beam of electrons. For this research, a Leo FESEM 1530 (Germany) was used. The vacuum pressure was less than $1.5e^{-5}$ mbar.

3.3 Catalyst reaction tests

3.3.1 Description of operation

A fixed-bed reactor was designed by a former Ph.D student of Professor Eric Croiset's lab to examine catalyst performance. In this study, methane partial oxidation, methane dry reforming, and the combined reactions have been examined. As shown in Figure 29, all reacting feed gases (CH_4, CO_2, air, and N_2) are combined in a quartz tube and flow through the catalyst bed. A pressure gauge monitors the pressure inside the reactor. If the pressure is too high (20 psig) for any reason (e.g. carbon deposition plugging the reactor), the gas inside the reactor is released by a relief valve automatically and the reactor is shut down for safety reasons. A thermocouple, which is located at the top of the catalyst bed, controls the furnace, and is used to provide isothermal conditions during the reaction tests.

For each reaction test, 50 mg of the calcined catalyst, which had a particle size of 420 to 500 µm, were diluted with 400 mg of inert SiC (~ 500µm) The SiC was used to help prevent pressure increases due to coke formation and improve the thermal dispersion through the catalyst bed. The catalysts were reduced at 720℃ in 200 mL/min of 10% H_2/N_2 for 1 hr. After the reduction, the bed temperature was reduced to the desired reaction temperature, in 100% N_2,

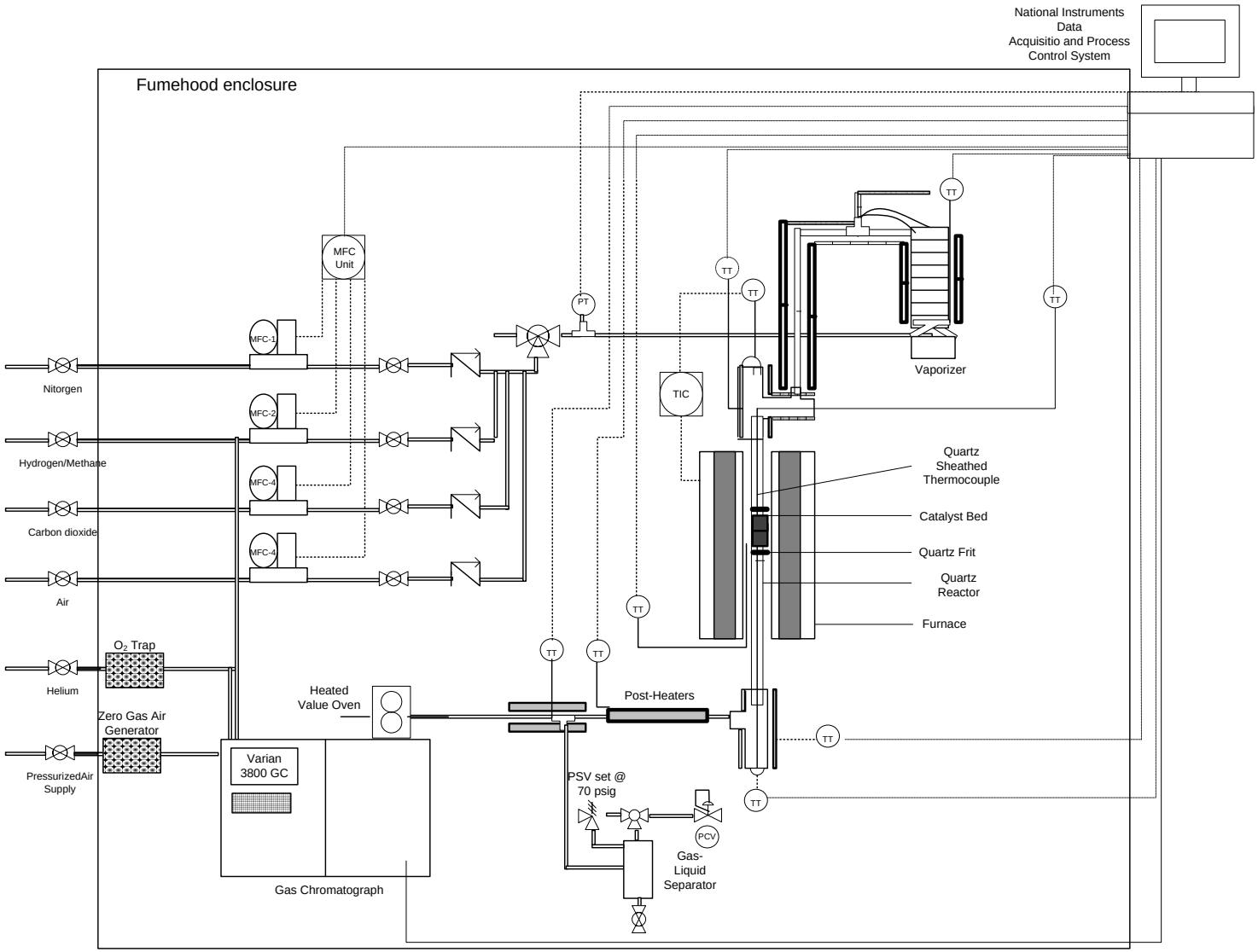

Figure 29: Fixed-bed reactor catalyst test station

The thermocouple located on top of the catalyst bed monitored and controlled the furnace heat duty. Therefore, all reactions could be conducted under isothermal conditions over the reaction period. The total gas flow rate was set to 200 mL/min. 80 mL/min of reactant gases and 120 mL/min of N_2 were flowed into the reactor. For each reforming reaction, the concentrations of the reactant gases were calculated based on the stoichiometry of the reaction. The product gases were collected and sampled using gas chromatography (GC) to analyze the components of the product gases.

3.3.2 Gas reactant feed delivery system

For this research, six gases were used and purchased from Praxair (purities listed); CH_4 (2.0), H_2 (5.0), N_2 (4.8), He (5.0), CO_2 (3.0), and air (extra dry). The feed gas flow rates were controlled by UNIT 1100 mass-flow controllers (MFCs). To ensure consistent flow from the MFCs, the gas pressure from the high-pressure gas cylinders was regulated at 40 psig by dual-stage regulators (Praxair). The gas feed was delivered to the reactor through ¼" stainless steel tubing and compression fittings (Swagelok®). A check valve was installed after each MFC to ensure that backflow was prevented. All compression fittings were leak-tested at a pressure of 50 psig to confirm no leaks. The MFCs were calibrated using a bubble-film flowmeter. The calibration data for MFCs are described in Appendix C.

3.3.3 Heating sections: Vaporizer, pre-, and post-reactor heater

The temperatures of six different heating sections (vaporizer, pre-reactor heater, three post-reactor heaters, and a GC sample line heater) were set to 473 K. Each section of tubing was wrapped in STH101 heating tape (500W, OMEGA Engineering Inc.) and controlled at 473 K by a LabView control program. Omega FGH051 heavy insulating tape was wrapped around the heating tapes to reduce heat loss.

3.3.4 Furnace

A Lindberg Blue 2000W furnace was used and controlled by a LabView control program. A quartz-sheathed micro K-type thermocouple located at the top of the catalyst bed controlled the heat duty of the furnace to maintain isothermal conditions for the catalyst bed.

3.3.5 Quartz-tube reactor

The catalyst was loaded in a quartz-tube reactor. The schematic diagram of the quartz-tube system is shown in Figure 30. The reactor consisted of a 10 mm I.D. quartz tube with a highly porous quartz frit which supported 50 mg (420 ~ 500 μm) of catalyst dispersed in 400 mg of SiC (inert). The quartz-tube was attached to stainless steel tubing at the reactor inlet and outlet by bored-through style ½" NPT * ½" Swagelok Ultra-Torr® vacuum fittings. The Ultra-Torr® fittings assembly included a finger-tightened knurled nut and a metal ferrule to compress a Viton O-ring.

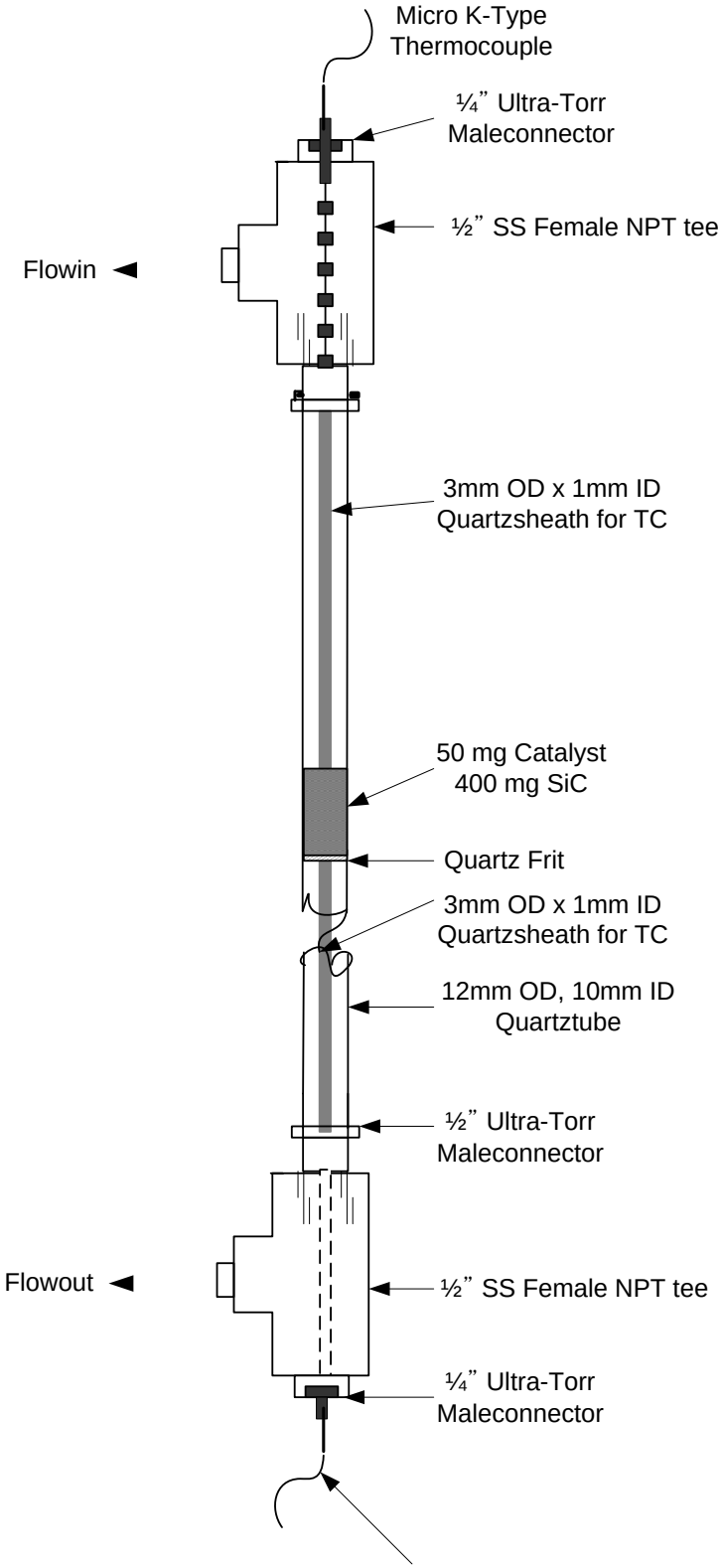

Figure 30: Quartz tube reactor

3.4 Evaluation of catalytic performance

A LabView software (National Instruments) was used to collect data and communicate with FieldPoint devices (National Instruments) to read data and control reactant flow rates, total reactor pressure, catalyst bed temperature, and temperatures of each controlled section. The product stream exiting the reactor passed through a series of heated sections (post-heaters) maintained at 473 K to ensure the products remained gaseous and continued to a Varian CP3800 GC (column oven temperature range: 35-225℃, time: 27 min, sample flow: 55 ml/min, front detector type: TCD, TCD temperature: 250℃, filament temperature: 300℃) for product composition analysis.

Based on the GC results, the methane conversion (X_{CH4}), yield of H_2 (Y_{H2}), yield of CO (Y_{CO}), and H_2/CO ratio were obtained.

$$X_{CH4} = \frac{n_{CH4,in} - n_{CH4,out}}{n_{CH4,in}} \quad \text{[Eq. A]}$$

$$Y_{H2} = \frac{n_{H2,out}}{2 \times n_{CH4,in}} \quad \text{[Eq. B]}$$

$$Y_{CO} = \frac{n_{CO,out}}{n_{CH4,in} + n_{CO2,in}} \quad \text{[Eq. C]}$$

$$H_2/CO\ ratio = \frac{n_{H2,out}}{n_{CO,out}} \quad \text{[Eq. D]}$$

$$C\ balance = \frac{weigthed\ \ sum\ of\ mole\ out\ of\ carbon\ containing\ species}{n_{CH4,in} + n_{CO2,in}} \quad \text{[Eq. E]}$$

Where $n_{CH4,in}$ and $n_{CH4,out}$ are the molar flow rates (mol/min) of methane entering and exiting the reactor, respectively; $n_{CO2,in}$ and $n_{CO2,out}$ are the molar flow rates (mol/min) of carbon dioxide entering and exiting the reactor, respectively; and $n_{H2,out}$ and $n_{CO,out}$ are the molar flow rates (mol/min) of hydrogen and carbon monoxide exiting the reactor, respectively.

For the kinetic study, equations below were used to investigate the activity of the catalyst for the CO_2 reforming of CH_4 reaction.

- CH_4 or CO_2 consumption rate: (i = CH_4 or CO_2)

$$-r_i'\left(\frac{mol}{g_{cat}\cdot sec}\right) = \frac{X_i \times F_i\left(\frac{mL}{min}\right)}{W_{catalyst}(g)} \times \frac{1}{1000}\left(\frac{L}{mL}\right) \times \frac{1}{60}\left(\frac{min}{sec}\right) \times 24.7\left(\frac{mol}{L}\right)$$ [Equation 57]

- H_2 or CO formation rate: (j = H_2 or CO)

$$r_j'\left(\frac{mol}{g_{cat}\cdot sec}\right) = \frac{n_j(mol/min)}{W_{cat}(g)} \times \frac{1}{60}\left(\frac{min}{sec}\right)$$

[Equation 58]

Chapter 4. Results and Discussions

4.1 Catalyst Performance

Three different catalysts ($Ni_{0.5}Mg_{2.5}Al$-HT, $Ni_{0.5}Ca_{2.5}Al$ and Ni/Al_2O_3) were investigated for the three different reactions (partial oxidation of CH_4, CO_2 reforming of CH_4, and oxidative CO_2 reforming of CH_4). To start to understand the effects of basic parameters on performance, thermodynamic equilibrium values were obtained, using commercial software Aspen Plus™ (See Appendix E). In addition, actual catalyst performances for those reactions, as determined from the fixed bed reactor experiments, are discussed.

4.1.1 Partial oxidation of CH_4

The overall reaction pathway for the partial oxidation of CH_4 is:

$$CH_4 + 0.5O_2 \leftrightarrow 2H_2 + CO \qquad \text{[Equation 59]}$$

The reaction (Eq. 59) shows the direct route to synthesis gas. It is known that the partial oxidation of CH_4 process is an exothermic reaction and the ASPEN Plus™ simulation shown in Table 10 can prove it. Therefore, the equilibrium CH_4 conversion should decrease when the reaction temperature increases, which is not observed in Figure 31. However, when the reaction temperature increases, the enthalpy difference ($\Delta H°$) shows smaller negative values; therefore, less exothermic nature occurs. As a result, when the reaction temperature increases, the CH_4 conversion and yields of H_2 can CO increase (Figure 31 and Table 10).

Table 10: Equilibrium values for partial oxidation of CH4 (simulated by ASPEN Plus™)

Temperature (℃)	ΔH_T (kJ/mol)	X_{CH4} (%)	Y_{H2} (%)	Y_{CO} (%)
200	-52.38	25.27	0.52	0.00
300	-51.14	26.77	3.47	0.10
400	-47.35	31.57	12.34	1.57
500	-38.69	42.81	29.28	12.67
600	-23.97	64.41	55.92	45.79
700	-12.63	85.71	81.71	79.41
800	-9.07	95.34	93.82	93.69
900	-8.98	98.39	97.80	97.92

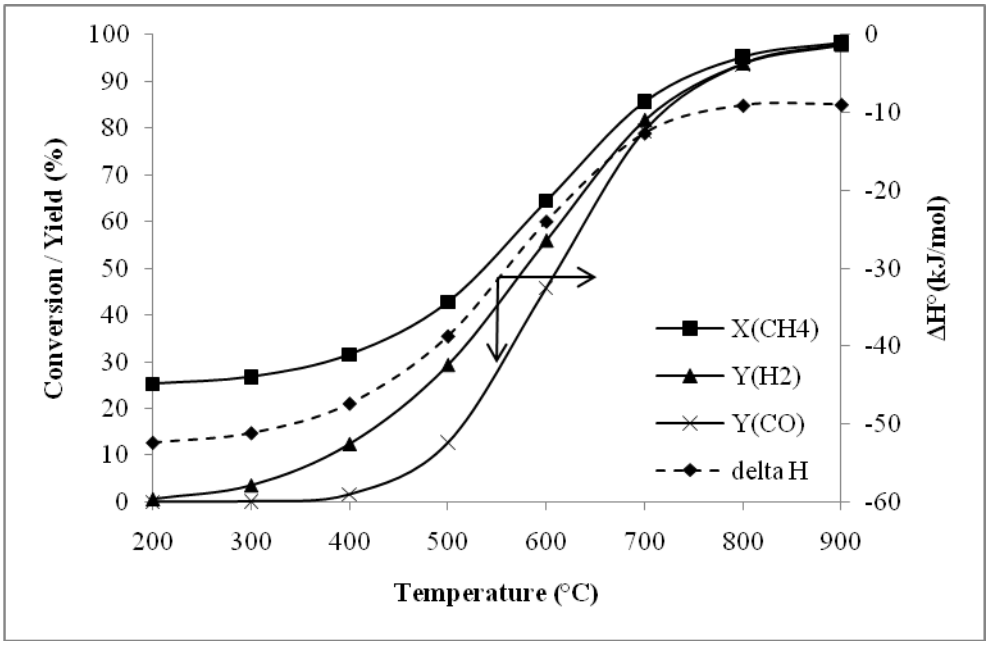

Figure 31: Thermodynamic equilibrium of partial oxidation of CH_4 at different temperatures at 1atm predicted by Aspen Plus™ (reactant gases: $CH_4/O_2/N_2$ = 0.26/0.13/0.60)

For the partial oxidation of CH_4, the equilibrium H_2 yield is always higher than the CO yield, but both yields are temperature dependent. At low temperatures (< 400℃), the CH_4 conversion was low (between 25 and 35%); and complete combustion of CH_4 is more favorable than partial oxidation, leading to product CO_2 instead of CO. Between 400 to 700℃, the CH_4 conversion increases up to ~85%, and partially oxidized CH_4 generated more CO, therefore, the yield of CO increased from ~5% to ~80%. When the reaction temperature is above 700℃, the H_2 and CO yields are pretty much close to the CH_4 conversion level (~ 95%). In addition, at 700℃,

the partial oxidation of CH4 process has an endothermic nature since the delta H value is 12.29 kJ/mol.

The effect of pressure on the equilibrium conversion and equibrium CO and H_2 yields were investigated and the results are shown in Figure 32. The equilibrium CH_4 conversion, and H_2 and CO yields decrease with increasing the reaction pressure. This is expected because CH_4 partial oxidation reaction leads to a higher number of moles in the product stream than in the reactant stream. For partial oxidation of CH_4, therefore, high reaction temperature and low pressure are required in order to obtain high equilibrium CH_4 conversions and high yields of H_2 and CO.

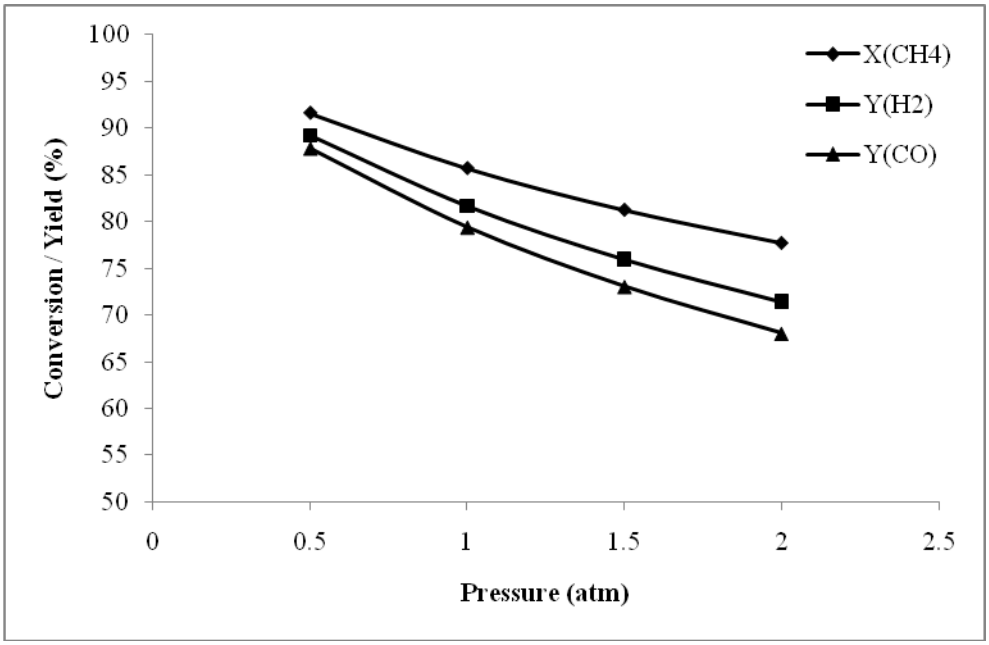

Figure 32: Thermodynamic equilibrium for the partial oxidation of CH_4 at different pressures at 700℃ predicted by Aspen Plus^{TM} (reactant gases: $CH_4/O_2/N_2$ = 0.26/0.13/0.60)

The major role of the catalyst is to reduce the energy barrier of the reaction and thereby accelerate the rate of reaction. Before the actual reaction occurs, all catalysts should be reduced in reducing gas (H_2/N_2 in our study) at slightly higher temperature (720℃ here) than the reaction temperature (here 700℃ maximum) in order to generate active Ni phases. In this research, all catalysts were reduced for 1 hr. After the reduction, the catalyst bed temperature decreased to the

desired reaction temperature in N_2 environment. When the bed temperature reaches the desired reaction temperature, reactant gases (CH_4, O_2 and N_2) flew into the reactor with appropriate ratios.

It is well known that the partial oxidation of CH4 process consists of two steps: (i) total combustion of CH_4, and (ii) reforming of CH_4 or H_2O. As shown in Figure 33, the temperature of the catalyst bed dramatically increased when the CH_4/O_2 (~ 2) mixture (60% diluted with N_2) was introduced into the catalyst bed. This confirms that the methane partial oxidation reaction produces a hot-spot in the catalyst bed due to the total combustion of CH4 at the initial period of reaction. When the hot-spot was generated, the furnace duty was decreased to lower the catalyst bed temperature to the set-point condition of 700℃. The variation of the temperature was stabled to 700℃ after 20 minutes of reactant injection. Since our GC collects data every 30 minutes, we can assume our experimental data presents isothermally reacted condition.

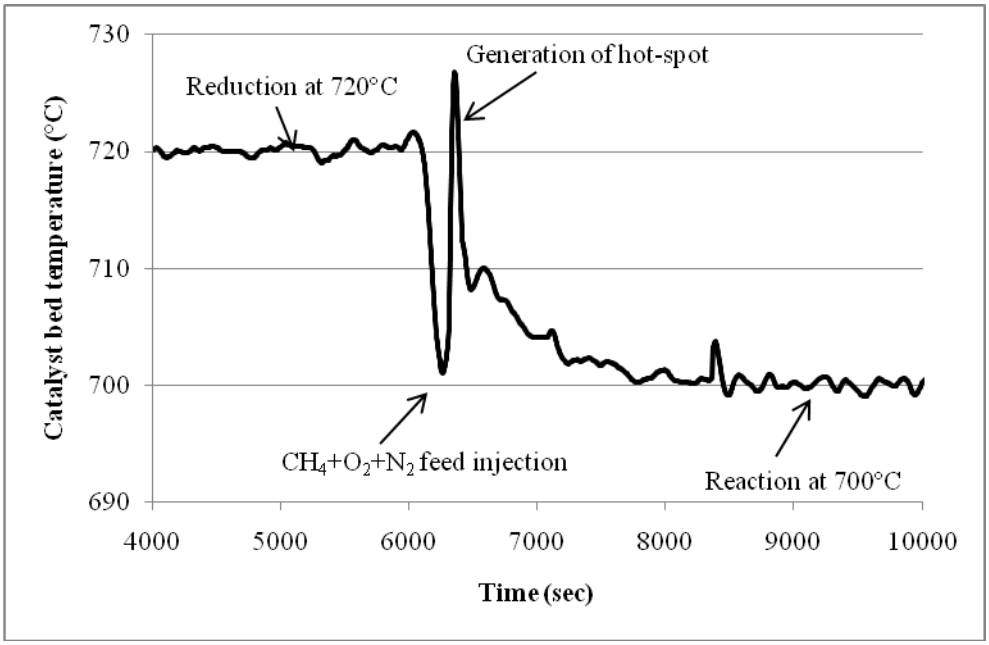

Figure 33: Temperature profile showing the exothermic nature of partial oxidation of CH_4 (50 mg of $Ni_{0.5}Mg_{2.5}Al$ catalyst, GHSV of 240,000 cm^3/g-hr)

The theoretical equilibrium calculations by ASPEN PLUS^{TM} (CH_4 conversion and yields of H_2 and CO) were compared to actual catalyst performances. During 20 hrs of partial oxidation of CH_4, all catalysts ($Ni_{0.5}Mg_{2.5}Al$-HT, $Ni_{0.5}Ca_{2.5}Al$, and Ni/Al_2O_3 catalysts) showed ~85% of CH_4 conversion; and had no significant deactivation (Figure 34). Those levels of reactivity were pretty closed to the equilibrium levels. However, only Ni/Al_2O_3 catalyst showed very small deactivation after 13 hrs of reaction (~80% of CH_4 conversion) confirming that Ni/Al_2O_3 catalyst showed deactivation, due to coke formation (as shown in the Catalyst Characterization section).

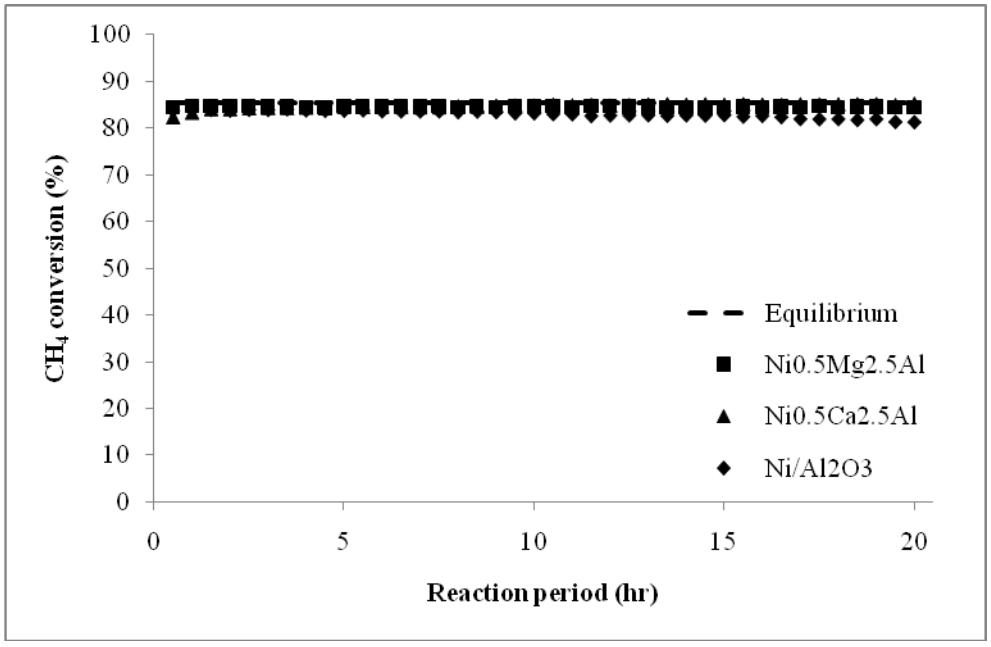

Figure 34: CH_4 conversion profile for partial oxidation of CH_4 on different catalysts (50 mg of catalyst, 1 hr of reduction at 720℃, 20 hr of reaction at 700℃, $CH_4/O_2/N_2$ = 0.26/0.13/0.6, GHSV of 240,000 cm^3/g-hr)

H_2 and CO yields are shown in Figure 35 and Figure 36. Similar to the CH_4 conversion, the yields were quite stable over 20 hrs time on stream, indicating no significant deactivation occurred. The $Ni_{0.5}Mg_{2.5}Al$-HT catalyst showed the highest yields of H_2 and CO among others; and Ni/Al_2O_3 catalyst showed the lowest reactivity. In addition, when slight deactivation was observed for Ni/Al_2O_3 after 13 hrs of reaction, the CO yield decreased more than the H_2 yield. It might imply that combustion of CH_4 might be more favorable than partial oxidation when the

catalyst began to be deactivated. In addition, the $Ni_{0.5}Mg_{2.5}Al$-HT catalyst showed the most stable yields over the reaction.

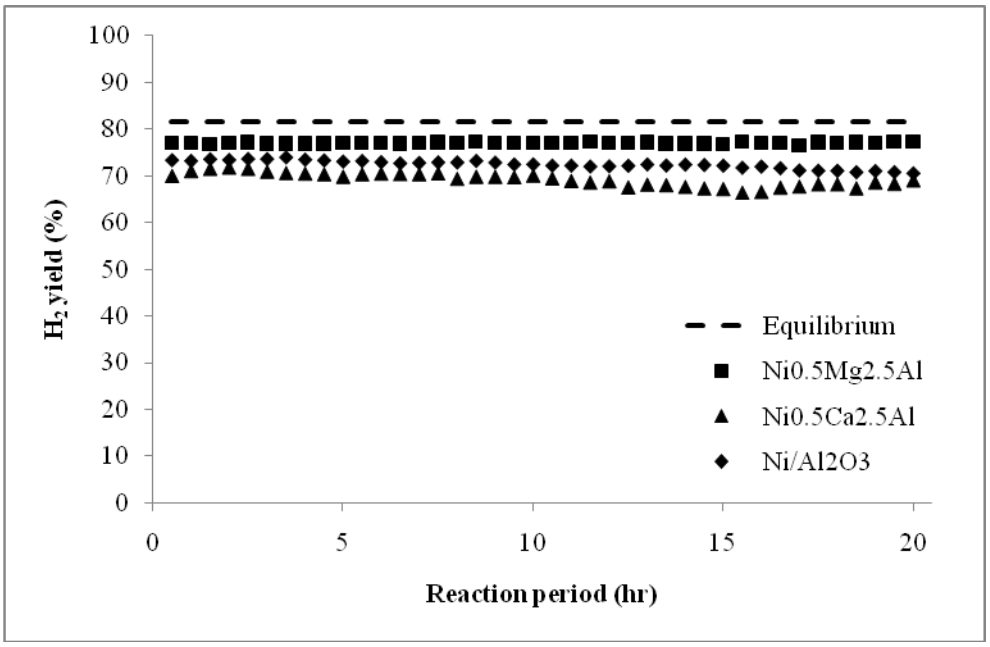

Figure 35: H_2 yield profile for partial oxidation of CH_4 on different catalysts (50 mg of catalyst, 1 hr of reduction at 720℃, 20 hr of reaction at 700℃, $CH_4/O_2/N_2$ = 0.26/0.13/0.6, GHSV of 240,000 cm^3/g-hr)

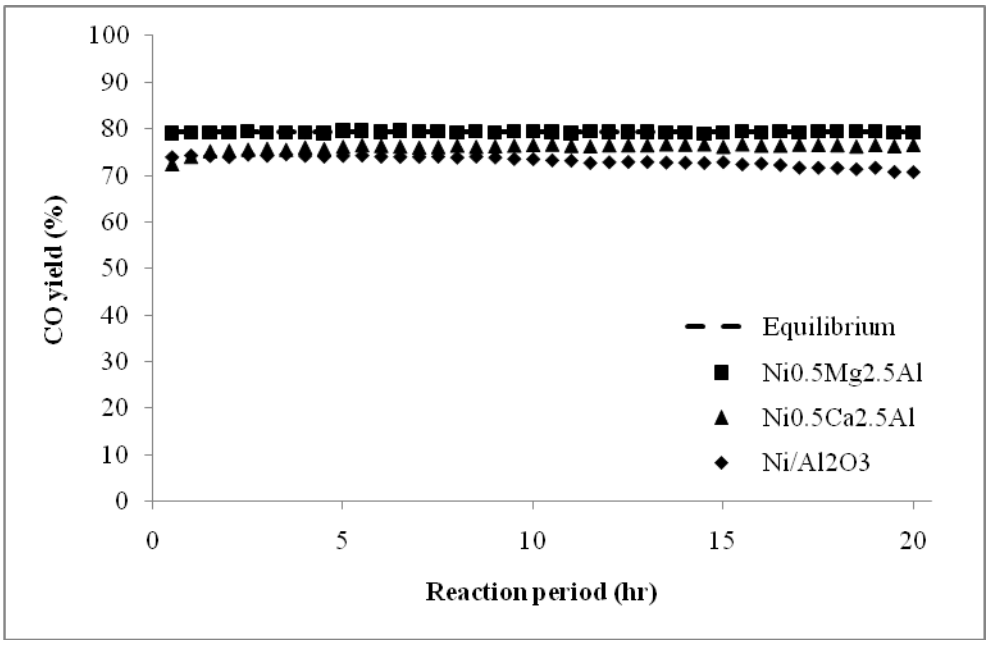

Figure 36: CO yield profile for partial oxidation of CH_4 on different catalysts (50 mg of catalyst, 1 hr of reduction at 720℃, 20 hr of reaction at 700℃, $CH_4/O_2/N_2$ = 0.26/0.13/0.6, GHSV of 240,000 cm^3/g-hr)

The synthesis gas ratios (H_2/CO ratio) obtained with each catalyst are shown in Figure 37 and show similar patterns. $Ni_{0.5}Mg_{2.5}Al$-HT and $Ni_{0.5}Ca_{2.5}Al$ catalysts resulted in a syngas ratio close to 2 which is closed to the theoretical level. This indicates that even though the selectivity of the product gases varied due to its dependence on the individual reactivities of the catalysts, the ratio of H_2/CO remained similar since H_2 and CO were produced in proportional relationship with the CH_4 conversion. In conclusion, for partial oxidation of CH_4, all catalysts ($Ni_{0.5}Mg_{2.5}Al$-HT, $Ni_{0.5}Ca_{2.5}Al$ and Ni/Al_2O_3) showed quite stable reactivity for 20 hrs of reaction and close to the equilibrium level.

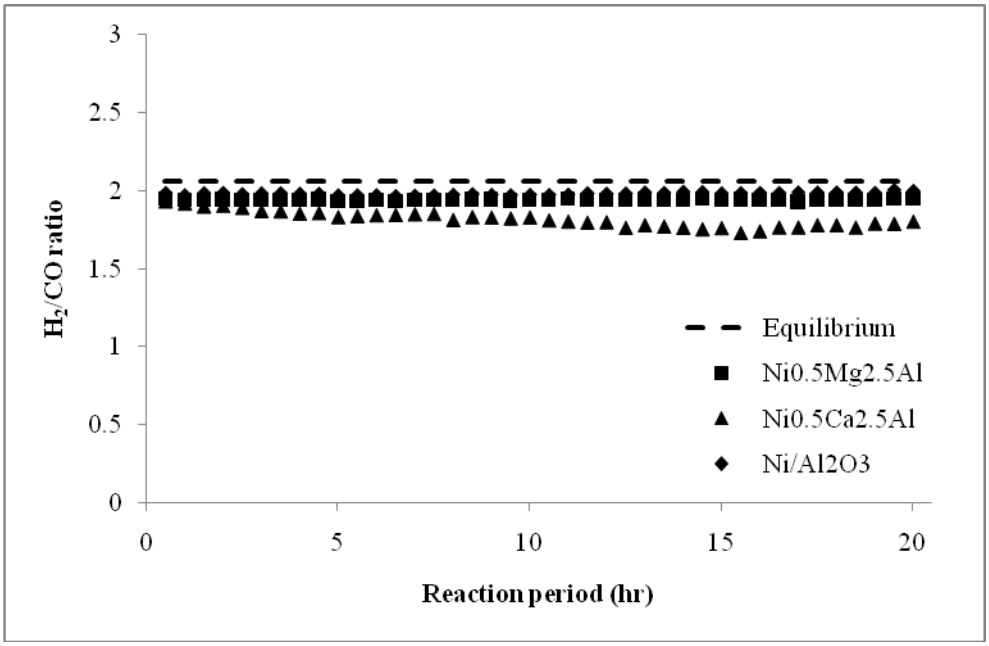

Figure 37: H_2/CO ratio profile for partial oxidation of CH_4 on different catalysts (50 mg of catalyst, 1 hr of reduction at 720℃, 20 hr of reaction at 700℃, $CH_4/O_2/N_2$ = 0.26/0.13/0.6, GHSV of 240,000 cm^3/g-hr)

4.1.2 CO_2 reforming of CH_4

Reducing CO_2 emission, by re-using CO_2, is one of the critical solutions in order to minimize greenhouse effect. Therefore, CO_2 reforming of methane has been receiving more and more attention, even though it is a highly endothermic reaction. In general, CO_2 reforming of CH_4 consists of two reactions (CO_2 reforming of CH_4 [Eq. 19] and reversible water-gas shift reaction [Eq. 20]) occurring simultaneously. The general reaction pathways are:

$$CH_4 + CO_2 \rightarrow 2H_2 + 2CO \quad \Delta H^{\circ}_{298K} = +260.5 kJ/mol \quad \text{[Equation 19]}$$

$$CO_2 + H_2 \leftrightarrow CO + H_2O \quad \Delta H^{\circ}_{298K} = +41.2 kJ/mol \quad \text{[Equation 20]}$$

Therefore, besides the main reaction [Eq. 19], the reversible water-gas-shift reaction (RWGS) [Eq. 20] affects the overall pathway. Because of the RWGS reaction, the theoretical syngas ratio (H_2/CO) is always less than 1 as shown in Figure 38. It confirms that the yield of H_2 is less than the yield of CO. At low temperature (below 400℃), the conversion of CH_4 is very

low (~10%) (Figure 38 and Table 11) compared with the conversion level for the partial oxidation of CH_4 which was ~30% (Figure 31). However, like the partial oxidation of CH_4, lower pressure is favorable to the CH_4 conversion, as seen in Figure 39 which, again, was predictable since the partial reforming reaction leads to a higher number of moles in the product stream than in the reactant stream.

Table 11: Equilibrium values for CO_2 reforming of CH_4 (simulated by ASPEN Plus^{TM})

Temperature (°C)	ΔH_T (kJ/mol)	X_{CH4} (%)	X_{CO2} (%)	Y_{H2} (%)	Y_{CO} (%)
200	0.06	0.05	0.14	0.02	0.10
300	0.75	0.81	1.62	0.41	1.22
400	4.71	5.42	9.09	3.59	7.26
500	16.80	21.37	30.26	16.94	25.82
600	35.79	52.71	63.70	47.22	58.21
700	49.01	81.72	88.35	78.41	85.04
800	52.94	94.23	96.95	92.87	95.60
900	53.02	98.05	99.13	97.51	98.60

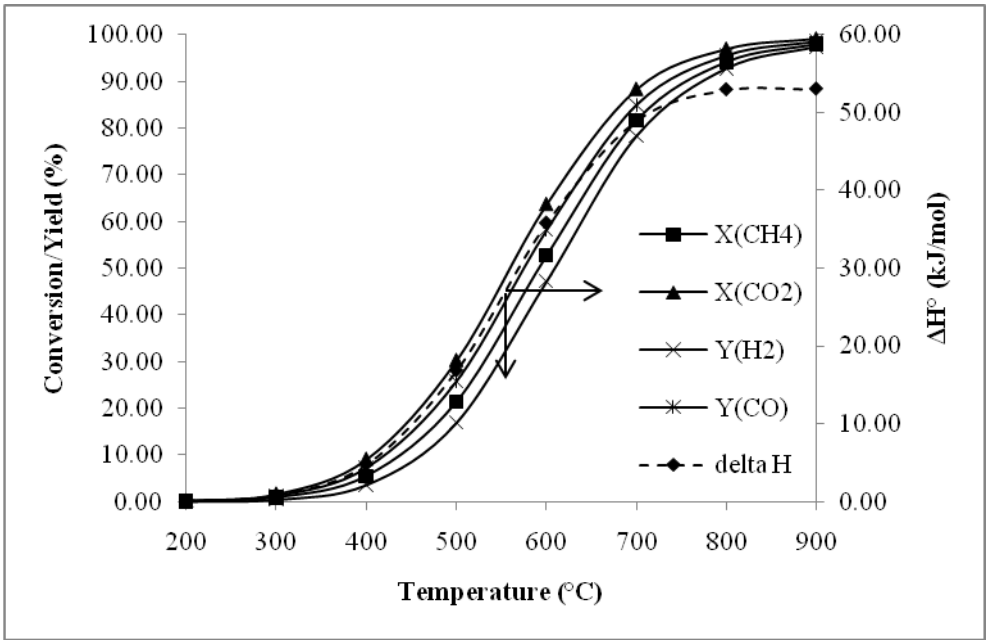

Figure 38: Thermodynamic equilibrium of CO_2 reforming of CH_4 at different temperatures at 1atm predicted by Aspen Plus^{TM} (reactant gases: $CH_4/CO_2/N_2$ = 0.2/0.2/0.6)

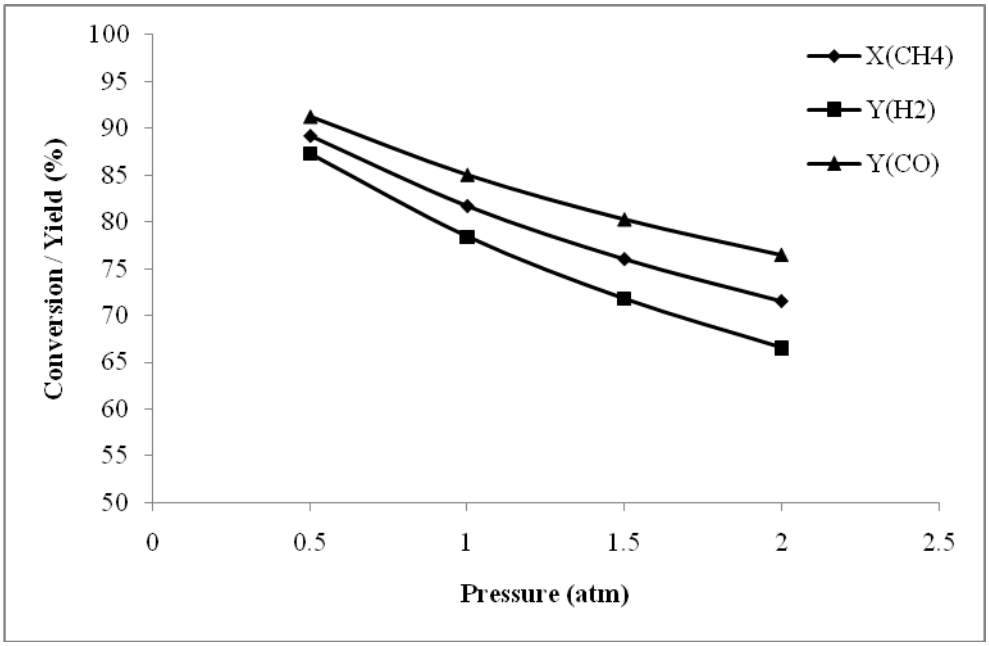

Figure 39: Thermodynamic equilibrium of CO_2 reforming of CH_4 at different pressures at 700℃ predicted by Aspen Plus^{TM} (reactant gases: $CH_4/CO_2/N_2$ = 0.2/0.2/0.6)

CO_2 reforming of CH_4 is an endothermic reaction; and even stronger endothermic nature at higher reaction temperature. To observe this phenomenon, the temperature change was recorded after the completion of the reduction step. Due to the endothermic nature of the reaction, the temperature of the catalyst bed decreased immediately (Figure 40) when reactant gases (CO_2 and CH_4) were injected through the catalyst bed. In order to maintain isothermal condition for the reaction, the furnace duty was controlled; and it increased the catalyst bed temperature to 700℃ within 15 minutes.

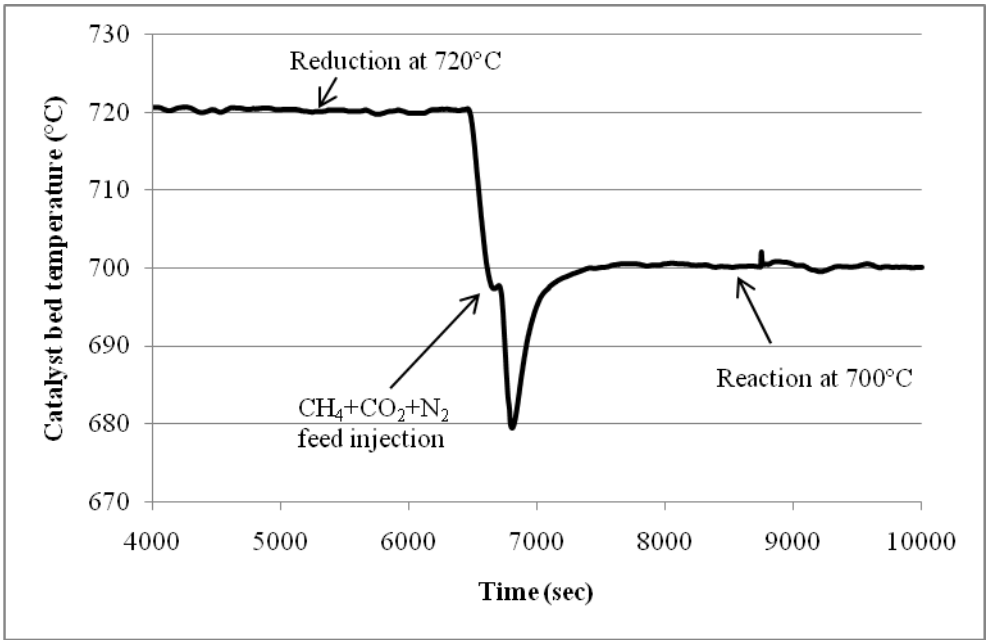

Figure 40: Temperature profile showing an endothermic nature of CO_2 reforming of CH_4 (50 mg of $Ni_{0.5}Mg_{2.5}Al$ catalyst, GHSV of 240,000 cm^3/g-hr)

CO_2 reforming of CH_4 is considered a severe condition for the catalyst where carbon deposition is more likely to occur than during partial oxidation because of the low oxygen content. It might lead to produce more coke by CH_4 dissociation or CO disproportionation on the catalyst's surface. Covering active Ni sites by coke will lower the catalyst's activity. Therefore, it is assumed that methane dry reforming is a good indicator of the carbon deposition resistance of a given catalyst.

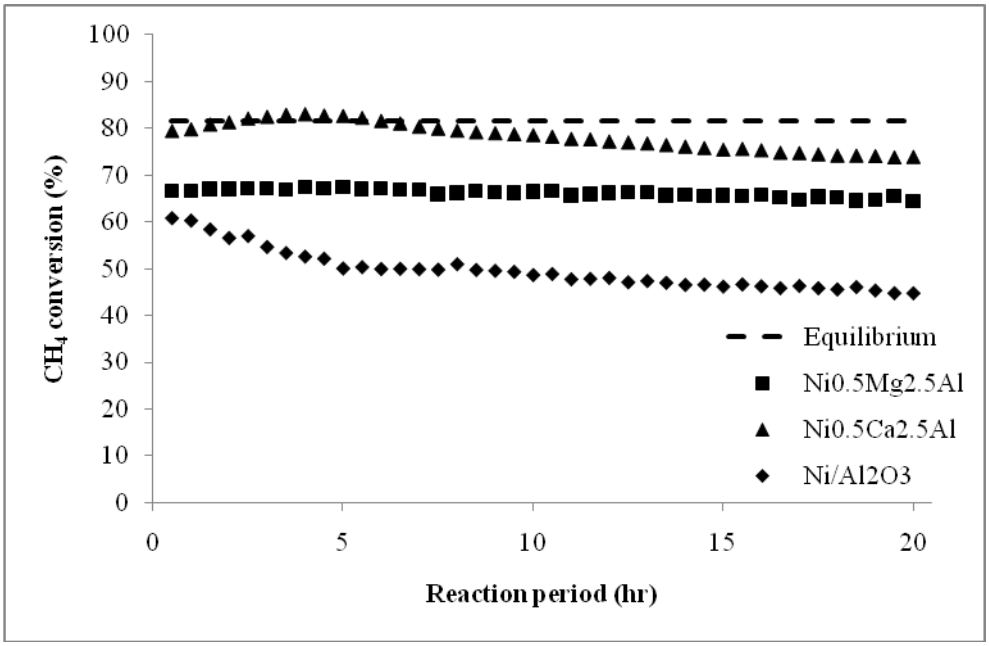

Figure 41: CH_4 conversion profile for CO_2 reforming of CH_4 on different catalysts (50 mg of catalyst, 1 hr of reduction at 720℃, 20 hr of reaction at 700℃, $CH_4/CO_2/N_2$ = 0.20/0.20/0.6, GHSV of 240,000 cm^3/g-hr)

The CH_4 conversions at 700°C for different catalysts, along with the equilibrium conversion are shown in Figure 41. At 700℃, the theoretical CH_4 conversion level is ~82%. The CH_4 conversion of the $Ni_{0.5}Ca_{2.5}Al$ catalyst increased slightly at the beginning and reaches the equilibrium CH_4 conversion (82%) within 4 hours time-on-stream. However, it slowly deactivated over time (from 82% to 75% after 20 hours). This was likely caused by carbon buildup on the surface; and it was confirmed by TPO (Figure 61). The Ni/Al_2O_3 catalyst showed continuous deactivation from an initial CH_4 conversion of 60%, down to 48% conversion after 20 hours. Note that Ni/Al_2O_3 also had the lowest initial CH_4 conversion. On the other hand, the $Ni_{0.5}Mg_{2.5}Al$-HT catalyst showed very stable conversion (68%). However, the conversion is lower than the equilibrium conversion, and lower than that conversion obtained with the Ca-containing catalyst. This indicates that the $Ni_{0.5}Mg_{2.5}Al$-HT catalyst has the highest resistance to deactivation. The trends in the H_2 and CO yields are similar to those of the CH_4 conversion (Figure 42 and Figure 43).

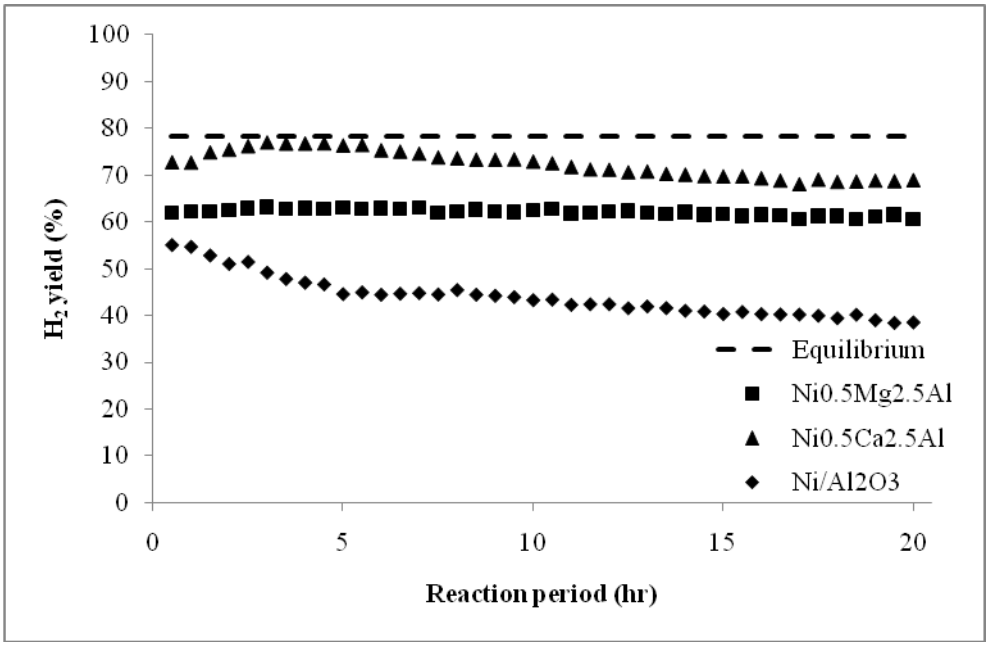

Figure 42: H_2 yield profile for CO_2 reforming of CH_4 on different catalysts (50 mg of catalyst, 1 hr of reduction at 720°C, 20 hr of reaction at 700°C, $CH_4/CO_2/N_2$ = 0.20/0.20/0.6, GHSV of 240,000 cm^3/g-hr)

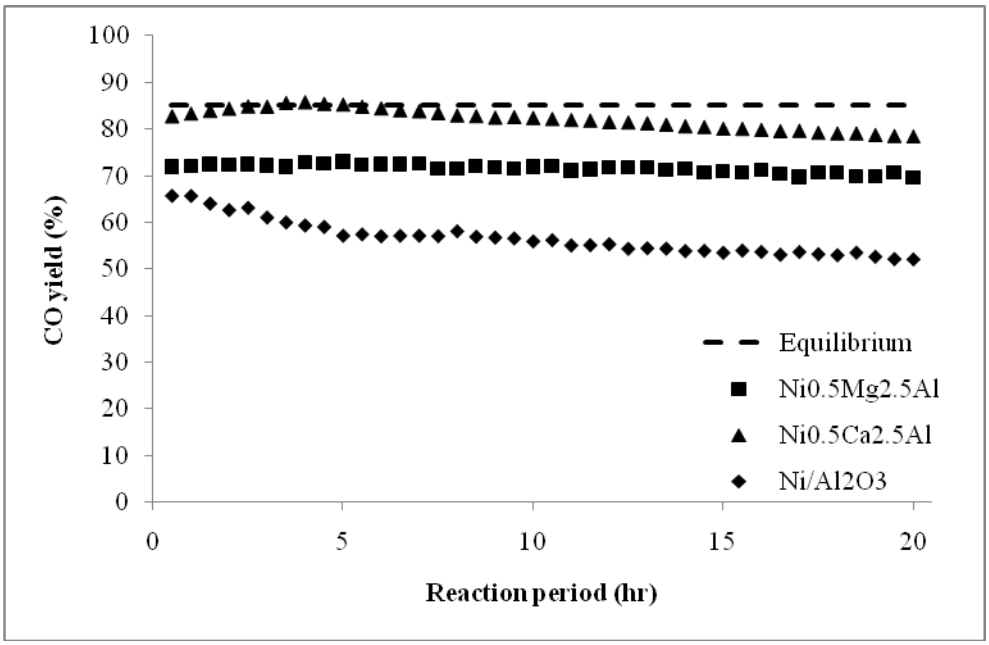

Figure 43: CO yield profile for CO_2 reforming of CH_4 on different catalysts (50 mg of catalyst, 1 hr of reduction at 720°C, 20 hr of reaction at 700°C, $CH_4/CO_2/N_2$ = 0.20/0.20/0.6, GHSV of 240,000 cm^3/g-hr)

The syngas ratios (H_2/CO ratios) are less than unity due to the reverse water-gas-shift reaction (Eq. 20). Even though there were differences in the yields of H_2 and CO between the catalysts, the syngas ratios were similar, and all catalysts started with a ratio of ~0.9, which is close to the equilibrium value. However, the Ni/Al_2O_3 catalyst showed a slight decreasing trend in the syngas ratio, since the decrease in the H_2 yield was greater than the CO yield (Figure 44). As a result, even though the CH_4 conversions were dependent on the catalyst, the synthesis gas ratios were similar for all catalysts and closed to the value at equilibrium. This indicates that the RWGS reaction rapidly reaches equilibrium.

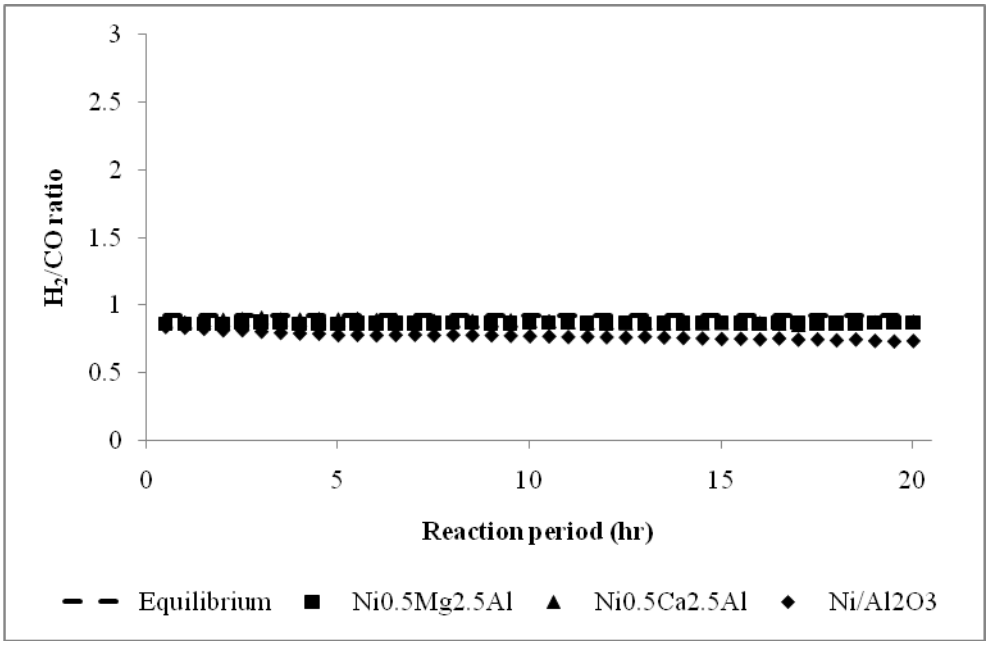

Figure 44: H_2/CO ratio profile for CO_2 reforming of CH_4 on different catalysts (50 mg of catalyst, 1 hr of reduction at 720℃, 20 hr of reaction at 700℃, $CH_4/CO_2/N_2$ = 0.20/0.20/0.6, GHSV of 240,000 cm^3/g-hr)

For 20 hrs of reaction, the effect of support against coke formation was investigated. During 20 hrs time-on-stream, the $Ni_{0.5}Mg_{2.5}Al$-HT catalyst showed excellent stability, contrary to the $Ni_{0.5}Ca_{2.5}Al$ catalyst that showed deactivation. However, even after 20 hrs, the activity of the Ca-based catalyst was higher than the Mg-based catalyst. It was, therefore, to conclude, after 20 hr time-on-stream, which of these two catalysts is the better one. Therefore, experiments with 100 hrs time-on-stream were carried out for these two catalysts. In this study, all pre-treatment

processes were identical with previous experiments. Figures 45 and 46 present the results for the $Ni_{0.5}Mg_{2.5}Al$-HT catalyst and $Ni_{0.5}Ca_{2.5}Al$, respectively.

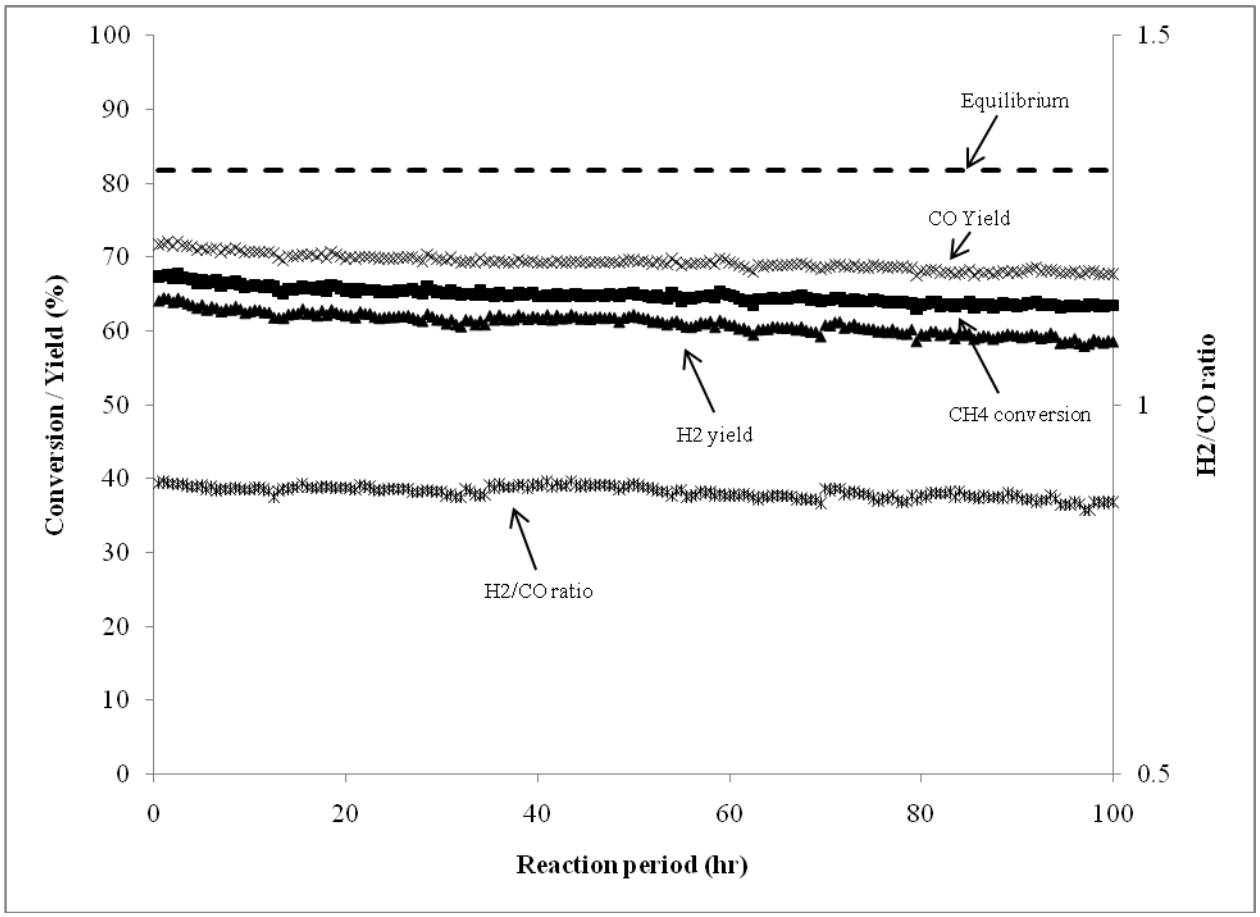

Figure 45: Long-term catalyst performance profile for CO_2 reforming of CH_4 on $Ni_{0.5}Mg_{2.5}Al$ catalyst (50 mg of catalyst, 1 hr of reduction at 720℃, 100 hr of reaction at 700℃, $CH_4/CO_2/N_2$ = 0.20/0.20/0.6, GHSV of 240,000 cm^3/g-hr)

For over 100 hrs of CH_4 dry reforming of, the $Ni_{0.5}Mg_{2.5}Al$-HT catalyst showed still very stable reactivity for CH_4 conversion, H_2 and CO yield, and the H_2/CO ratio (Figure 45). The CH_4 conversion decreased by about 4% over 100 hrs (from 67% to 63%). However, the $Ni_{0.5}Ca_{2.5}Al$ catalyst, the deactivation trend observed during the first 20 hrs, continued throughout 100 hrs (Figure 46). The CH_4 conversion decreased about 20% (from 78% to 62%); but the syngas ratio only slightly decreased over 100 hrs.

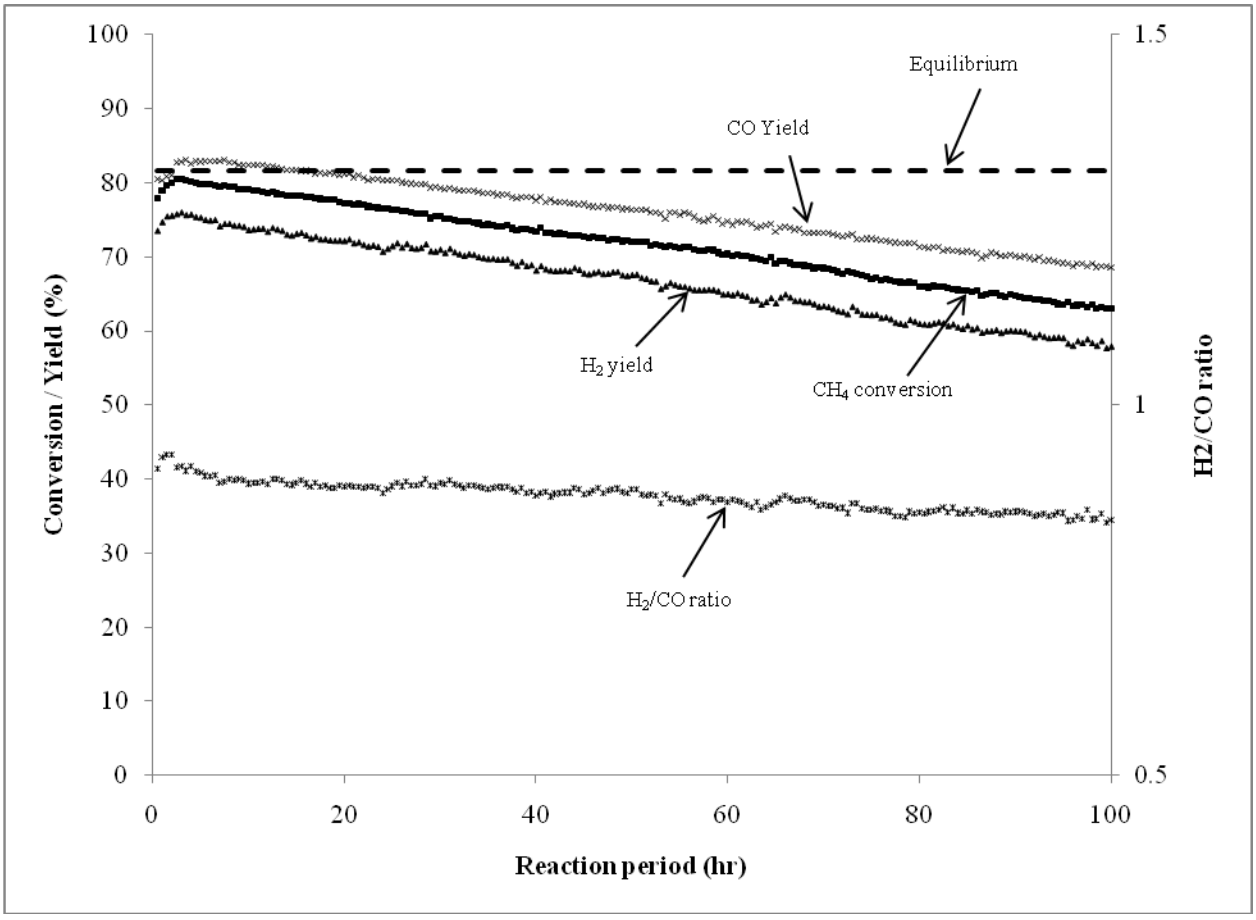

Figure 46: Long-term catalyst performance profile for CO_2 reforming of CH_4 on $Ni_{0.5}Ca_{2.5}Al$ catalyst (50mg of catalyst, 1 hr of reduction at 720℃, 100 hr of reaction at 700℃, $CH_4/CO_2/N_2$ = 0.20/0.20/0.6, GHSV of 240,000cm^3/g-hr)

From Figures 45 and 46, it is now clear that the $Ni_{0.5}Mg_{2.5}Al$-HT catalyst suffered considerably less deactivation than the $Ni_{0.5}Ca_{2.5}Al$ catalyst, indicating that the hydrotalcite-type catalyst, which has a layered structure, showed much higher resistance to coke formation. In conclusion, the $Ni_{0.5}Mg_{2.5}Al$ catalyst showed the highest stability, even though the activity remained lower than the equilibrium expectation. The $Ni_{0.5}Ca_{2.5}Al$ catalyst showed initially the highest activity, reaching equilibrium expectation after about 4 hours time-on-stream, but, unfortunately, past 4 hrs, its activity continuously decreased at a rate of 0.2%/hr. Finally, the Ni/Al_2O_3 catalyst showed the worst reactivity and stability for CH_4 dry reforming.

4.1.3 Oxidative CO_2 reforming of CH_4

CH_4 partial oxidation releases heat during reaction due to the total combustion of CH_4 with O_2 and its exothermic nature. Although the product syngas ratio of 2 (as obtained from CH_4 partial oxidation) is ideal for downstream methanol production, hot-spots developed in the catalyst bed could ultimately lead to catalyst sintering, and therefore catalyst deactivation. However, combining exothermic partial reforming with the endothermic CO_2 reforming can help greatly in minimizing hot spots. It can be confirmed by the comparison of the ΔH for partial oxidation, oxidative CO_2 reforming, and CO_2 reforming of CH_4 at 700℃ (-12.63 (Table 10) < 36.09 (Table 12) < 49.01 (Table 11), respectively). Also, as mentioned previously, dry reforming contributes to the utilization of CO_2; this makes such process all the more environmentally attractive. In addition, the combined process can generate various syngas ratios by adjusting the input reactant ratios. The chemical reaction for the combined reaction can be expressed as [Eq. 60]:

$$6\,CH_4 + x\,CO_2 + (3 - x/2)\,O_2 \rightleftharpoons 12\,H_2 + (6 + x)\,CO \quad \text{[Equation 60]}$$

In Equation 60, "*x*" represents the amount of CO_2 added. If *x* is equal to zero, then Equation 60 is equivalent to the partial oxidation reaction. If *x* is equal to 6, then Equation 60 is equivalent to the CO_2 reforming reaction. By varying *x*, it is clear that we can tailor the resulting H_2/CO ratio. By changing x between 0 and 6, the H_2/CO ratio can vary between 2 and 1. In the following, most of the experiments were performed for *x* = 4 for easy calculation.

Figure 47 shows the equilibrium conversion, and H_2 and CO yields for oxidative CO_2 reforming, based on a reactant mixture $CH_4/CO_2/O_2/N_2$ = 0.218/0.145/0.036/0.6 (i.e. stoichiometry corresponding to x = 4 in Equation 60), as calculated using Aspen Plus™. When x = 4, the oxidative CO_2 reforming has an exothermic nature at low temperature (< 500℃); however, it turns to an endothermic reaction at high temperature. Even though it shows the exothermic nature at low temperature, the ΔH decreases with increasing temperature. Therefore, the CH_4 conversion, H_2 and CO yields increase with increasing temperature (Figure 47 and Table 12).

Table 12: Equilibrium values for oxidative CO_2 reforming of CH_4 [$6CH_4+4CO_2+O_2 = 12H_2 + 10CO$] (simulated by ASPEN Plus^{TM})

Temperature (°C)	ΔHT (kJ/mol)	X(CH4) (%)	Y(H2) (%)	Y(CO) (%)
200	-14.33	8.46	0.26	0.00
300	-13.67	9.32	1.77	0.26
400	-10.47	13.21	6.69	3.69
500	0.57	27.21	20.44	20.81
600	19.00	55.87	49.51	54.69
700	32.05	82.77	79.22	83.60
800	35.99	94.50	93.08	95.12
900	36.09	98.12	97.56	98.43

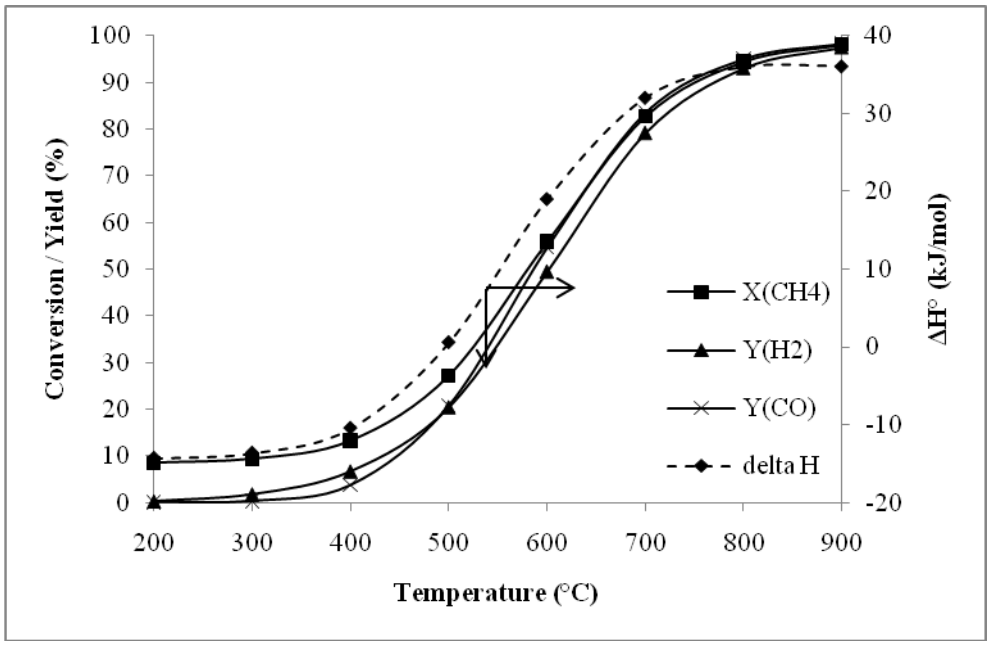

Figure 47: Thermodynamic equilibrium of oxidative CO_2 reforming of CH_4 at different temperatures at 1atm predicted by Aspen Plus^{TM} (reactant gases: $CH_4/CO_2/O_2/N_2$ = 0.218/0.145/0.036/0.6)

At low temperature (< 400°C), the CH_4 conversion level for oxidative CO_2 reforming of CH_4 (~15%) is in between that for partial oxidation of CH_4 (~30%) and that for CO_2 reforming of CH_4 (~5%). However, at high temperature (> 700°C), the CH_4 conversions for each reaction condition were pretty similar to ~80%. When the temperature is lower than 500°C, the H_2 yield is higher than the CO yield; and it is the same pattern as with CH_4 partial oxidation. However, at

higher temperature (> 500℃), the CO yield becomes higher than the H_2 yield; and it is the same pattern as with CO_2 reforming of CH_4. Again, as shown in Figure 48, and as expected from Le Chatelier principle, lower pressure leads to higher conversion.

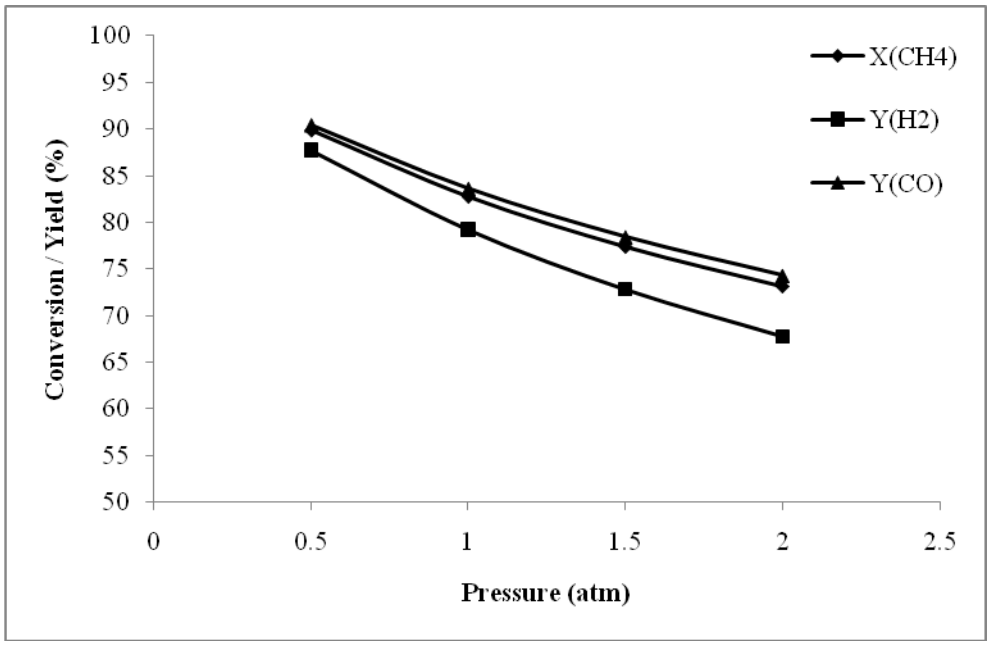

Figure 48: Thermodynamic equilibrium of oxidative CO_2 reforming of CH_4 at different pressures at 700℃ predicted by Aspen Plus™ (reactant gases: $CH_4/CO_2/O_2/N_2$ = 0.218/0.145/0.036/0.6)

To investigate the effect of combining exothermic and endothermic reactions, the temperature changes were recorded when the oxidative CO_2 reforming of CH_4 was begun (See Figure 49). For CO_2 reforming of CH_4, the temperature initially decreased by ~20℃ from 700℃ since the reaction was absorbing heat (due to the endothermic nature); but, for oxidative reforming of CH_4, the temperature initially decreased by only ~5℃. This shows that that coupling partial oxidation and CO_2 reforming of CH_4 decreases the heat requirement.

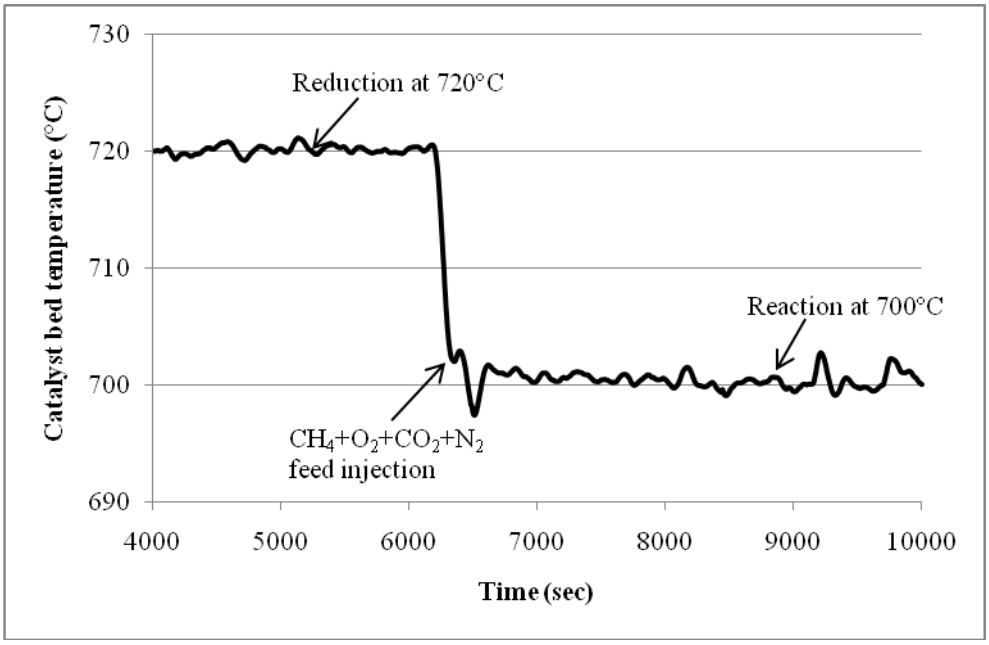

Figure 49: Temperature profile showing the endothermic nature of the combined partial oxidation and CO_2 reforming of CH_4 (50 mg of $Ni_{0.5}Mg_{2.5}Al$ catalyst, $CH_4/CO_2/O_2/N_2$ = 0.218/0.145/0.036/0.6, GHSV of 240,000 cm^3/g-hr)

The catalytic activities for the combined reactions are shown below. The addition of O_2 to the feed is expected to reduce carbon deposition on the catalytic surface and increase methane conversion. As seen in Figure 50, the $Ni_{0.5}Ca_{2.5}Al$ catalyst showed the highest initial CH_4 conversion (~82%, similar to the equilibrium conversion). However, the $Ni_{0.5}Ca_{2.5}Al$ catalyst deactivates immediately, but stabilizes at a level close to the CH_4 conversion for the $Ni_{0.5}Mg_{2.5}Al$-HT catalyst (~72%). The $Ni_{0.5}Mg_{2.5}Al$-HT catalyst had the most stable reactivity over 20 hrs of reaction. This again suggests that the hydrotalcite-type catalyst has the strongest resistance against sintering and/or coke formation. The Ni/Al_2O_3 catalyst had the lowest reactivity (~46%) and also began deactivating immediately.

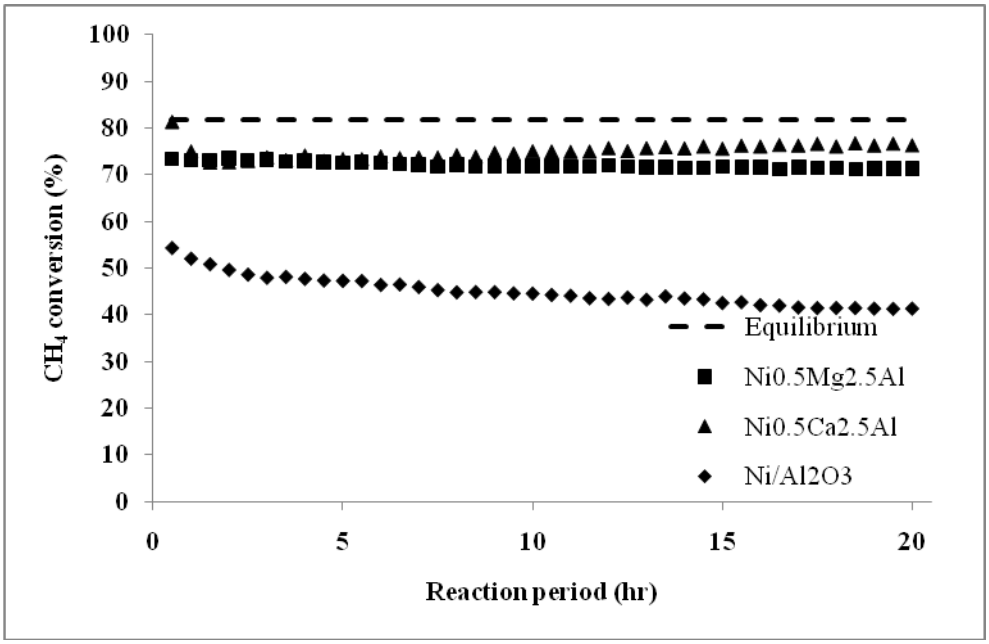

Figure 50: CH_4 conversion profile for oxidative CO_2 reforming of CH_4 on different catalysts (50 mg of catalyst, 1 hr of reduction at 720℃, 20 hr of reaction at 700℃, $CH_4/CO_2/O_2/N_2$ = 0.218/0.145/0.036/0.6, GHSV of 240,000 cm^3/g-hr)

The trends in the H_2 and CO yields for the combined reactions were similar to that of the CH_4 conversions (Figure 51 and Figure 52). The $Ni_{0.5}Ca_{2.5}Al$ catalyst had higher yields of H_2 and CO at early time-on-stream, but decreased with time. The $Ni_{0.5}Mg_{2.5}Al$-HT catalyst showed the most stable yields of H_2 and CO over 20 hrs of reaction without any deactivation.

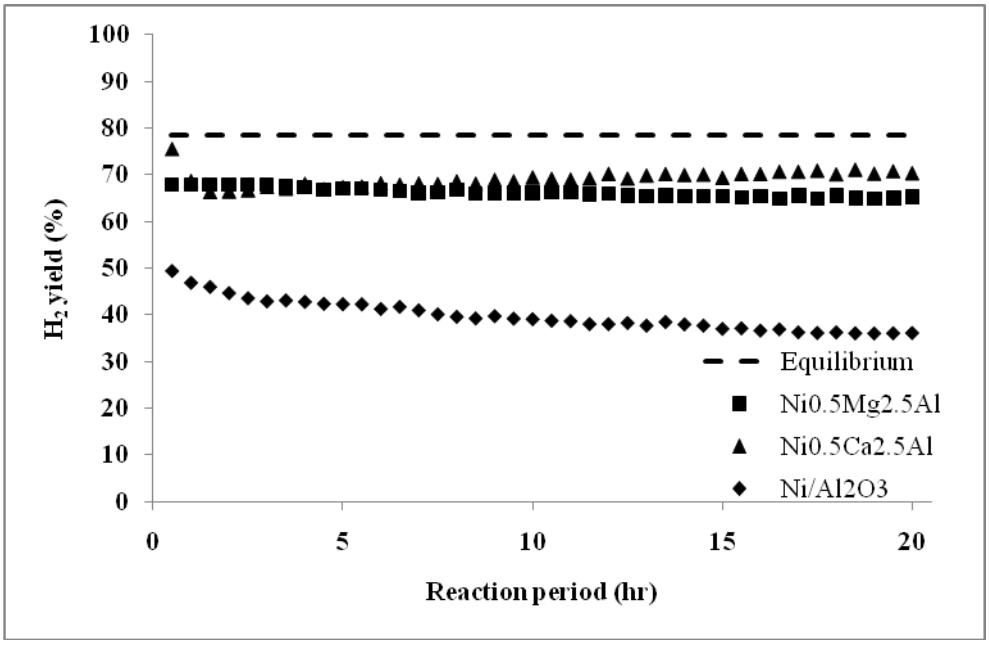

Figure 51: H_2 yield profile for oxidative CO_2 reforming of CH_4 on different catalysts (50 mg of catalyst, 1 hr of reduction at 720℃, 20 hr of reaction at 700℃, $CH_4/CO_2/O_2/N_2$ = 0.218/0.145/0.036/0.6, GHSV of 240,000 cm^3/g-hr)

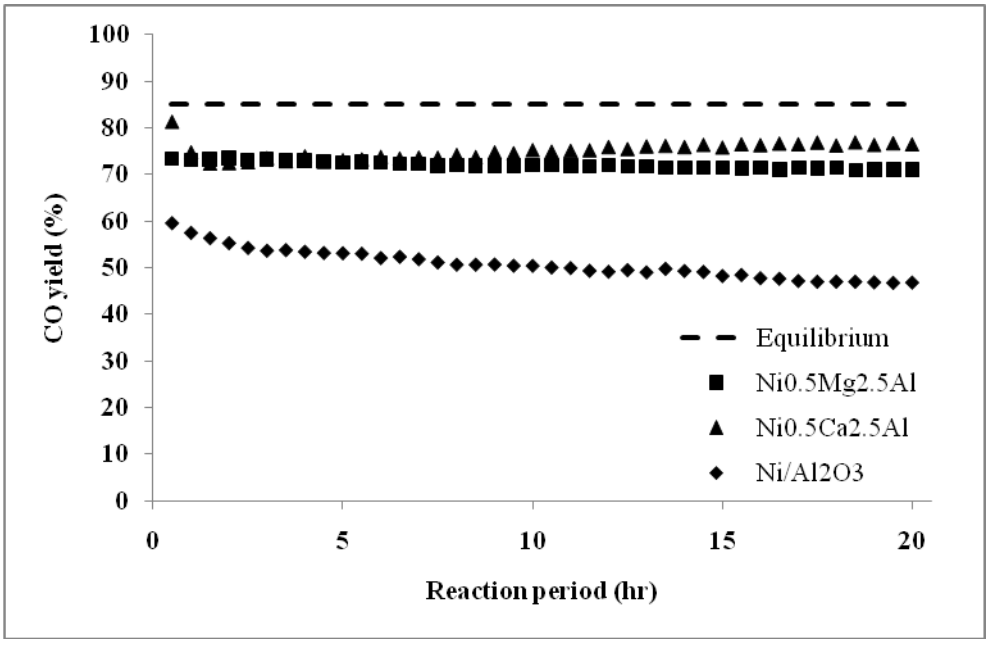

Figure 52: CO yield profile for oxidative CO_2 reforming of CH_4 on different catalysts (50 mg of catalyst, 1 hr of reduction at 720℃, 20 hr of reaction at 700℃, $CH_4/CO_2/O_2/N_2$ = 0.218/0.145/0.036/0.6, GHSV of 240,000 cm^3/g-hr)

For oxidative CO_2 reforming of CH_4, the reactivity of Ni/Al_2O_3 catalyst was quite low compared to that with the $Ni_{0.5}Mg_{2.5}Al$-HT and $Ni_{0.5}Ca_{2.5}Al$ catalysts. However, the synthesis gas ratios for those catalysts were pretty much identical, even though the syngas ratio for the Ni/Al_2O_3 was slightly lower than that of the other catalysts (Figure 53). This phenomenon also was observed from partial oxidation and CO_2 reforming of CH_4 reactions. It indicates that even though there are quantitative differences in the yields of H_2 and CO, the ratios of H_2/CO in product stream remains independent of the yields and conversion. Also, except for the Ni/Al_2O_3 catalyst, the H_2/CO ratio is very close to its equilibrium value. This again implies that the RWGS reaction reached equilibrium in the case of $Ni_{0.5}Mg_{2.5}Al$-HT and $Ni_{0.5}Ca_{2.5}Al$ catalysts.

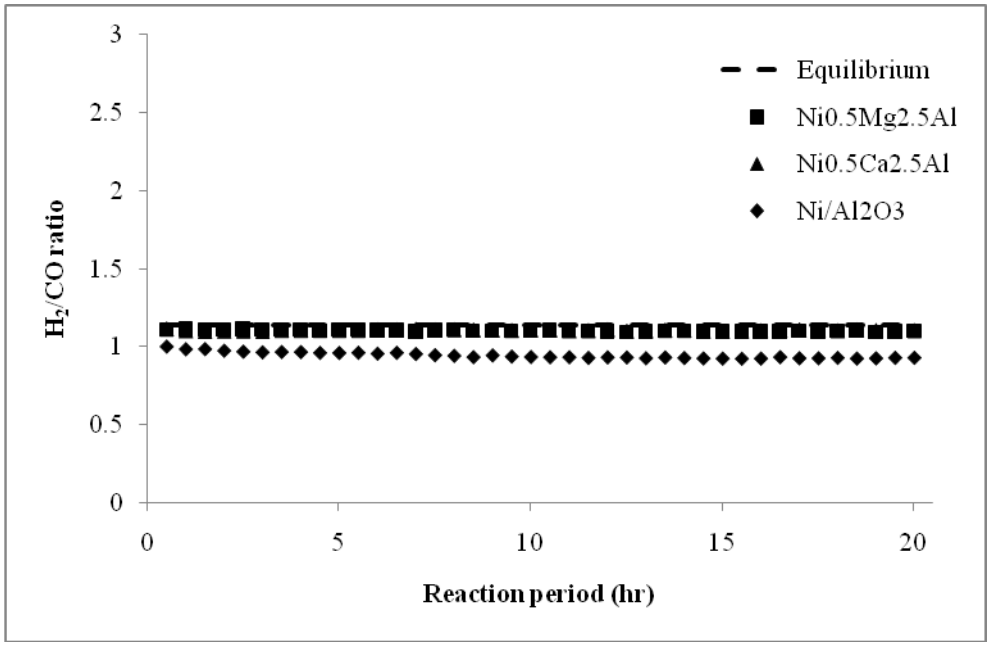

Figure 53: H_2/CO ratio profile for oxidative CO_2 reforming of CH_4 on different catalysts (50 mg of catalyst, 1 hr of reduction at 720℃, 20 hr of reaction at 700℃, $CH_4/CO_2/O_2/N_2$ = 0.218/0.145/0.036/0.6, GHSV of 240,000 cm^3/g-hr)

Overall, based on the reactivity tests for all three sets of reactions, the $Ni_{0.5}Mg_{2.5}Al$-HT catalyst showed the most stable reactivity over the test period (20 hrs and 100 hrs). In addition, the reactivity of the $Ni_{0.5}Mg_{2.5}Al$-HT catalyst, although lower than the equilibrium conversion, was still at a level greater than 70%. The $Ni_{0.5}Ca_{2.5}Al$ catalyst had the highest initial CH_4 conversion and H_2 and CO yields for all reactions. However, its reactivity began to degrade

shortly after the onset of the test. In long-term experiment test (for 100 hrs), the reactivity of the $Ni_{0.5}Ca_{2.5}Al$ catalyst became lower than the reactivity of $Ni_{0.5}Mg_{2.5}Al$-HT catalyst after ~70 hrs of CO_2 reforming of CH_4. The Ni/Al_2O_3 commercial catalyst had the lowest reactivity and worst stability among the three. Finally, as expected, the tests with oxidative CO_2 reforming of CH_4 showed performances in between those of partial oxidation and dry reforming. An important difference between oxidative CO_2 reforming and dry reforming for the $Ni_{0.5}Ca_{2.5}Al$ catalyst is that it became much more stable when adding oxygen; its activity decreased initially but stabilized at similar level as that for the $Ni_{0.5}Mg_{2.5}Al$-HT. Nonetheless, because of the superior stability of the $Ni_{0.5}Mg_{2.5}Al$-HT catalyst under dry reforming, the conclusion is that the $Ni_{0.5}Mg_{2.5}Al$-HT is the most promising catalyst here for oxidative CO_2 reforming of CH_4.

4.2 Catalyst Characterization

4.2.1 BET analysis

The chemical reactions occur on the catalyst surface. Therefore, the catalysts' surface areas might be related to their reactivities. Furthermore, it is expected that the different supports will result in different surface areas. After the calcination treatment at high temperature, the surface area of the catalyst might be reduced due to sintering effects. The support which has the strongest resistance against sintering is likely the best. However, it is not the only factor in determining catalyst reactivity.

To determine the specific surface area of the various catalysts (calcined and reduced catalysts), samples of about 100 mg with particle size in the range 354-500 μm were tested. As shown in Table 13, the Ni/Al_2O_3 catalyst had the highest surface area, followed by the $Ni_{0.5}Mg_{2.5}Al$ catalyst, and then by the $Ni_{0.5}Ca_{2.5}Al$ catalyst. After the calcined catalysts were reduced in 10% H_2/N_2 at 720℃ for 1 hr, the surface areas slightly increased (except for Ni/Al_2O_3 whose surface area did not change). This is caused by rearrangement of the catalyst structure when the surface oxygen, which is bonded with Ni (or NiO), is reduced by hydrogen; then the nickel oxide is turned to the active nickel metal (Eq. 61).

Table 13: Catalyst specific surface areas

Catalysts	After calcination (m^2/g)	After reduction (m^2/g)
Ni/Al_2O_3	191	191
$Ni_{0.5}Ca_{2.5}Al$	45	56
$Ni_{0.5}Mg_{2.5}Al$-HT	131	153

$$NiO + H_2 \rightarrow Ni^0 + H_2O \qquad \text{[Equation 61]}$$

In general, a catalyst, which has a higher surface area, has better reactivity since a higher surface area provides larger contact area for the reactant gas. Higher surface area, however, is not the only factor affecting catalyst reactivity. For example, as shown by the catalyst performance in section 4.1, the $Ni_{0.5}Ca_{2.5}Al$ catalyst initially had the highest reactivity, although it had the lowest surface area. This suggests that even though the $Ni_{0.5}Ca_{2.5}Al$ catalyst had the lowest overall surface area it may have had the highest amount of exposed active Ni.

4.2.2 Temperature-programmed reduction analysis

It is well known that nickel oxide, produced during the calcination step, needs to be reduced to active metal nickel (Eq. 61). The NiO species are typically reduced with hydrogen to form Ni metal particles, which are active to dissociate CH_4 in reforming reactions (Takenaka, et al. 2007). The reducibility of nickel-based catalysts during the reduction process is an important factor in determining the level of reactivity. The reducibility of the catalyst is affected by, and can be estimated by measuring, the interaction strength between the active phase and the support. The reduction temperature will, therefore, likely depend on the support. Therefore, a catalyst which is more reducible has weak interaction strengths between the active phase and the support; and it leads to a larger amount of active Ni for the reaction.

Reducibility of the catalyst can be measured using temperature-programmed reduction (TPR) tests. For each TPR test, samples with around 100 mg of calcined catalyst were reduced in a 10%/90% H_2/ N_2 mixture, with a flow rate of 30 mL/min. The temperature of the catalyst bed was increased from 25 to 900℃ with a 10℃/min ramp rate. While the temperature increased, a

thermal conductivity detector (TCD) measured the amount of hydrogen consumption. The TPR results for the $Ni_{0.5}Ca_{2.5}Al$ and $Ni_{0.5}Mg_{2.5}Al$ catalysts are shown in Figure 54.

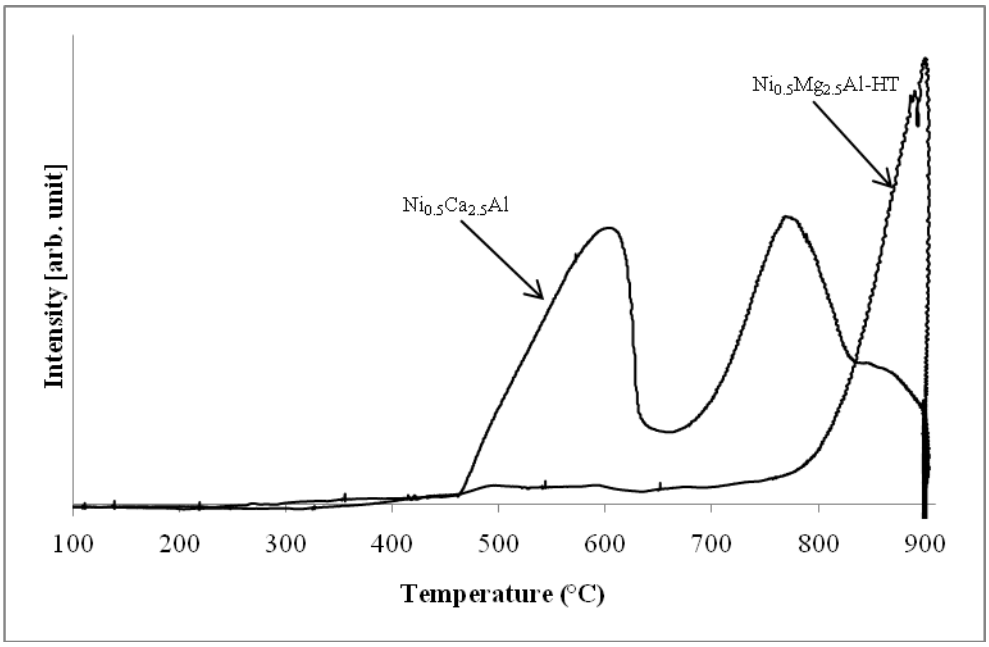

Figure 54: TPR results for the calcined $Ni_{0.5}Ca_{2.5}Al$ and $Ni_{0.5}Mg_{2.5}Al$-HT catalysts

The $Ni_{0.5}Mg_{2.5}Al$ catalyst required much higher temperature (~ 750℃). Therefore, it indicates that the $Ni_{0.5}Ca_{2.5}Al$ catalyst is easier to be reduced than the $Ni_{0.5}Mg_{2.5}Al$-HT catalyst. It also implies that the $Ni_{0.5}Mg_{2.5}Al$-HT catalyst has stronger interaction between Ni and support since the $Ni_{0.5}Mg_{2.5}Al$-HT catalyst requires the higher reduction temperature which required subtracting the oxygen bond from the active Ni and support.

In order to explain the reason why the $Ni_{0.5}Mg_{2.5}Al$-HT catalyst has stronger interaction strength between the active Ni and its support, the lattice size of MgO and CaO were compared with that of NiO in Table 14. It is known that MgO and CaO are face-centered cubic type oxides (Ruckenstein 1995). However, only MgO has lattice parameters and bond distances close to those of NiO. This suggests that NiO can be more easily substituted into the MgO lattice, producing a $MgAl_2O_4$ spinel phase (Morioka et al. ,2001; Takehira et al., 2004) which is considered as a solid solution.

Table 14: Crystal data for B1-type metal oxides (Ruckenstein 1995)

Compound	a (Å)	A-B (Å)
MgO	4.2112	2.11
CaO	4.8105	2.40
NiO	4.1946	2.10

Overall, the $Ni_{0.5}Mg_{2.5}$Al-HT catalyst is less reducible than the $Ni_{0.5}Ca_{2.5}$Al catalyst, indicating that the $Ni_{0.5}Mg_{2.5}$Al catalyst provides lesser active Ni metal sites and the interaction strength between the Ni metal and supports is stronger than on the $Ni_{0.5}Ca_{2.5}$Al catalyst. Clearly, the area under the TPR curve (Figure 54) is greater for $Ni_{0.5}Ca_{2.5}$Al than for $Ni_{0.5}Mg_{2.5}$Al-HT and therefore, it can be concluded that more Ni was reduced over the $Ni_{0.5}Ca_{2.5}$Al catalyst compared to the $Ni_{0.5}Mg_{2.5}$Al-HT catalyst.

4.2.3 X-ray diffraction analysis

The crystal structure of $Ni_{0.5}Mg_{2.5}$Al-HT was investigated using XRD, and all diffraction patterns were matched with JPCDS references. The XRD patterns of the $Ni_{0.5}Mg_{2.5}$Al confirmed that it contains a well-crystallized hydrotalcite-type phase, as seen in Figure 55. It implies that Ni^{2+} might be incorporated in the Mg^{2+} site positions and dispersed uniformly in the brucite layer of the HT structure. Especially, a set of three reflection peaks at 2θ values of 11.3, 22.7, and 34.5° (Kawabata, et al. 2005) indicates that the hydrotalcite-type structure possesses a layered structure, in which both Ni(II) and Al(III) substituted Mg(II) sites in the brucite-like sheet (Choudhary et al. 2003).

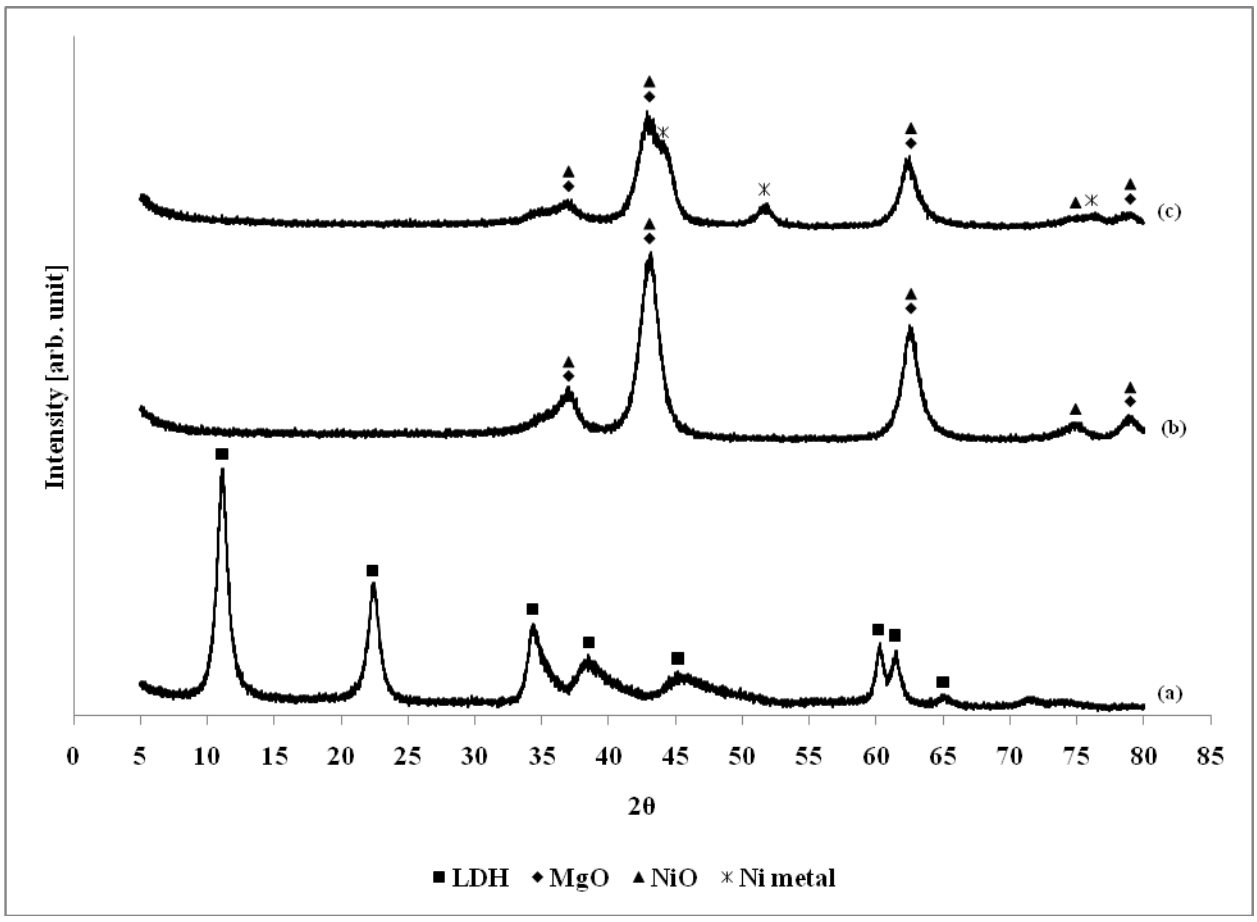

Figure 55: XRD patterns for the $Ni_{0.5}Mg_{2.5}Al$-HT catalyst: (a) fresh; (b) calcined at 820℃ in air for 5 hrs; (c) reduced at 720℃ in 10% H_2/N_2 for 1hr

After calcination at 820℃ in air for 5 hrs, the HT peaks disappeared and MgO (at 37.0°, 43.1°, 62.6°, and 79.0°) and NiO (at 37.0°, 43.1°, 62.6°, 74.9°, and 79.0°) peaks appeared and overlapped each other. But, active Ni metal peaks were not observed yet. After reduction at 720℃ in 10% H_2/N_2 for 1 hr, the NiO peaks were weakened and Ni metal peaks (at 44.1°, 51.7°, and 76.1°) were apparent. This indicates that during reduction, some of the NiO crystals transformed into active Ni phases.

Figure 56 shows the XRD patterns of the spent catalyst for partial oxidation, CO_2 reforming and oxidative CO_2 reforming of CH_4 at 700℃ after 20 hrs. After the reduction process, the active Ni phases were observed at 2θ = 44.1°, 53°, and 77°. It confirms that the reduction process in H_2/N_2 environment subtracts the oxygen content from the NiO phases; then the active

Ni phases were observed. Both Ni metal and NiO phases were observed after CH_4 partial oxidation and oxidative CO_2 reforming of CH_4 (Figure 56). The CH_4 partial oxidation and oxidative CO_2 reforming of CH_4, which contain oxygen in the feed, produced stronger Ni metal peaks than that of CO_2 reforming of CH_4 at 44.1°. Simultaneously, NiO peaks (at 63°) were stronger for partial oxidation and oxidative CO_2 reforming of CH_4 than CO_2 reforming of CH_4 process. This observation might be happened since oxygen in reactant gases can remove deposited carbon via oxidation; so, active Ni phases were maintained on the surface. In addition, it also oxide the active Ni to NiO again; then the NiO would be reduced to Ni metal again during the reaction. In addition, when oxygen fed for partial oxidation of CH_4 (b) and oxidative CO_2 reforming of CH_4 (d), stronger NiO peaks (and weaker Ni peaks) were observed (at 37° and 63°). It implies that the oxygen feed leads to oxidize the active Ni phases to NiO during the reaction. The re-generated NiO might be re-reduced by hydrogen generated during the reaction to provide the active Ni phases for the reforming reactions.

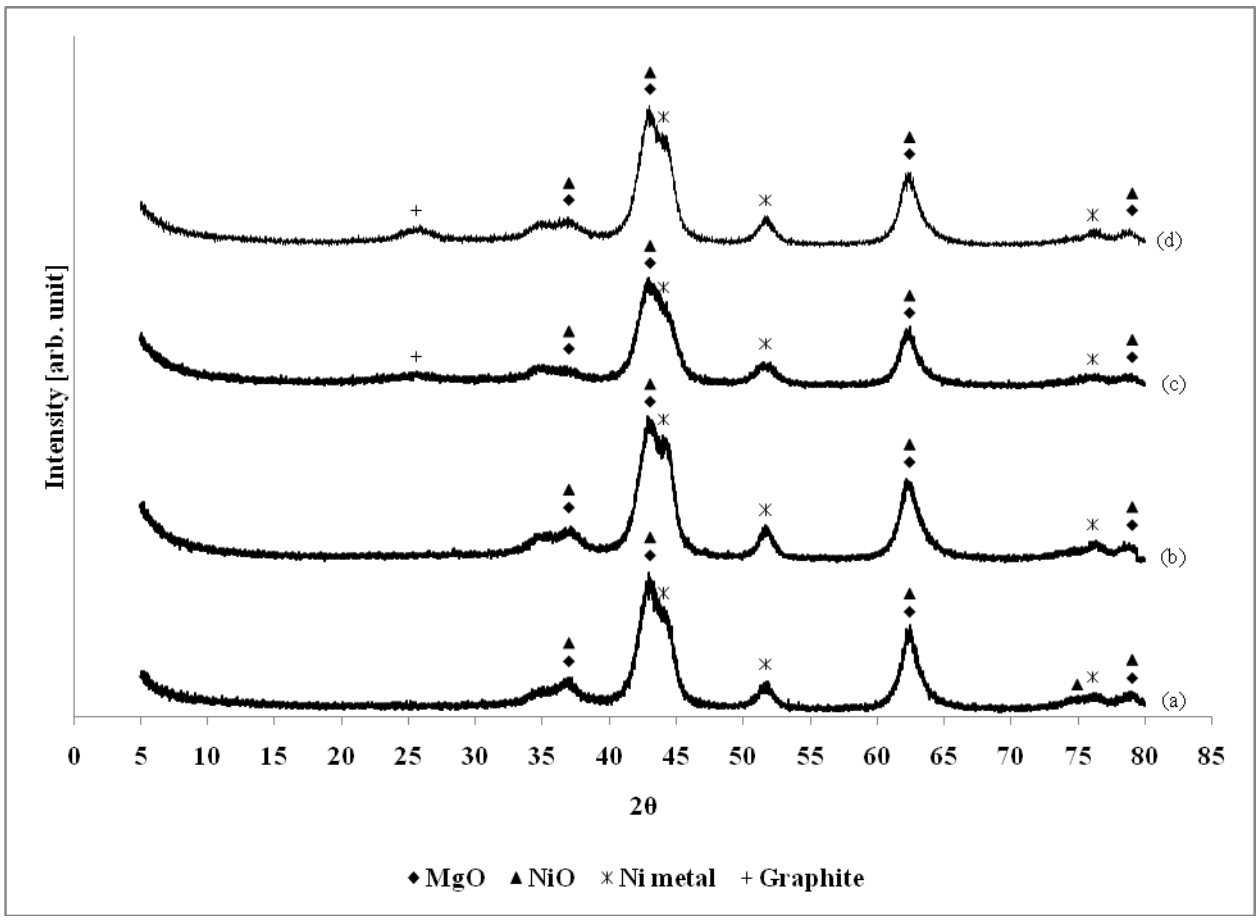

Figure 56: XRD patterns for the $Ni_{0.5}Mg_{2.5}Al$ catalyst: (a) after reduction; (b) after partial oxidation of CH_4; (c) after CO_2 reforming of CH_4; (d) after oxidative CO_2 reforming of CH_4; Reduction at 720°C, all other reactions at 700°C.

In addition, a weak graphite peak was observed (at 26.4°) after CO_2 reforming of CH_4 and oxidative CO_2 reforming of CH_4 tests, but not after CH_4 partial oxidation (Figure 56). The only source of carbon from CH_4 partial oxidation is methane. Therefore, the amount of carbon formation was minimized during partial oxidation.

As the reference, XRD patterns of Ni/Al_2O_3 catalyst were examined (Figure 57). After calcination at 820℃ in air, a $NiAl_2O_4$ solid solution formed. When the $NiAl_2O_4$ solid solution was reduced in 10% H_2/N_2 mixture for 1 hr at 720℃, those solid solution peaks weakened and active Ni metal peaks became apparent. After CO_2 reforming of CH_4 for 20 hrs at 700℃, the solid solution peaks were even weaker. A strong graphite peak was also observed. This peak is

much stronger than that on the $Ni_{0.5}Mg_{2.5}Al$ catalyst. It indicates that the amount of carbon deposited on Ni/Al_2O_3 is much larger than on the $Ni_{0.5}Mg_{2.5}Al$ catalyst. Conclusively, the $Ni_{0.5}Mg_{2.5}Al$ catalyst has much stronger resistance against the coke formation during the high temperature reaction (in particular CO_2 reforming).

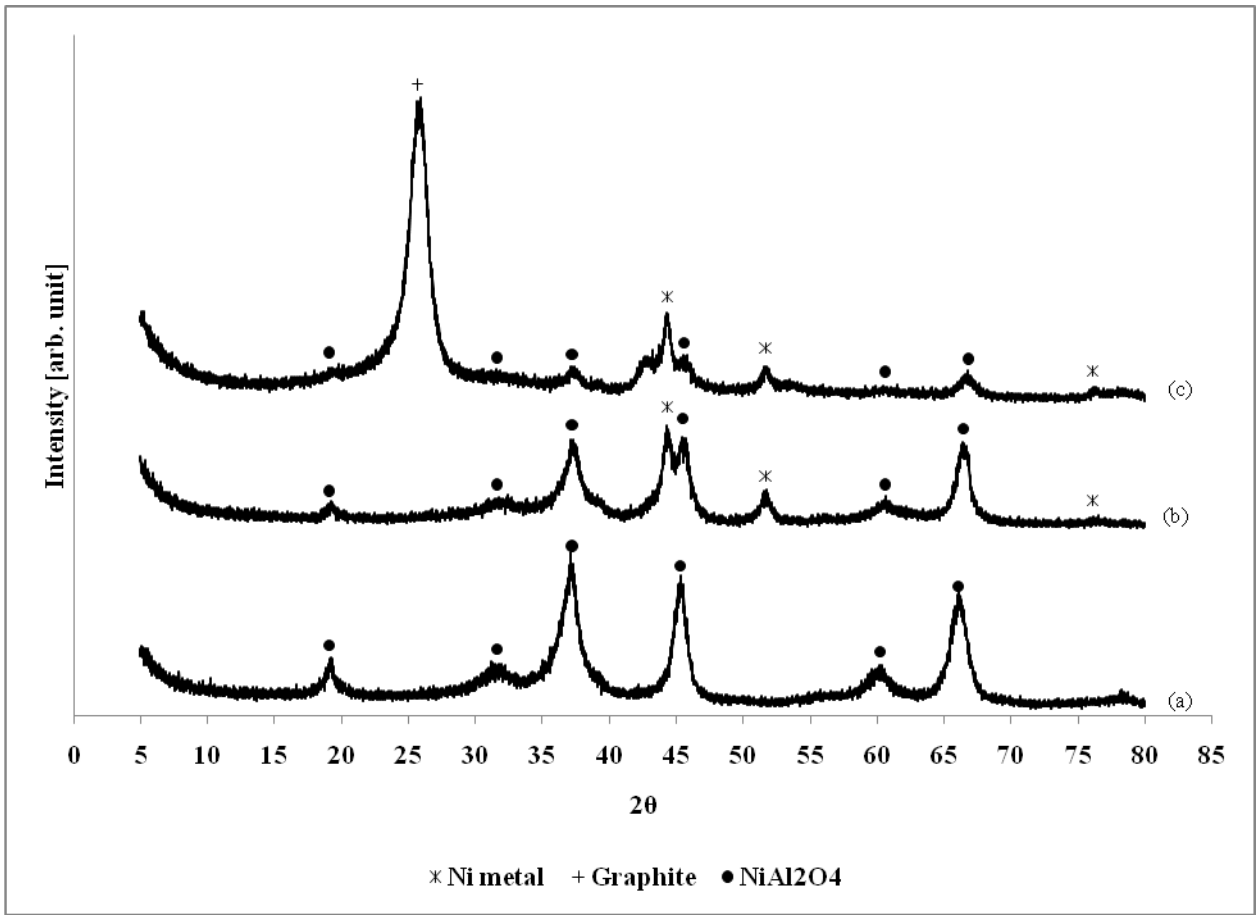

Figure 57: XRD patterns for the Ni/Al_2O_3 catalyst: (a) calcined at 820℃ in air for 5 hrs; (b) reduced at 720℃ in 10% H_2/N_2 for 1hr; (c) after CO_2 reforming of CH_4

4.2.4 SEM analysis

SEM analysis allows us visual investigation of the catalyst surface. Fresh and spent catalysts were coated with gold (for 2 min) before SEM pictures were taken. A SEM image of the fresh $Ni_{0.5}Mg_{2.5}Al$-HT (before calcination treatment) is shown in Figure 58. When the magnitude was increased 200,000x, clear hydrotalcite (or layered double hydroxide) shapes were

observed. The fresh HT structure clearly shows the "card house" structure (Kawabata, et al. 2005).

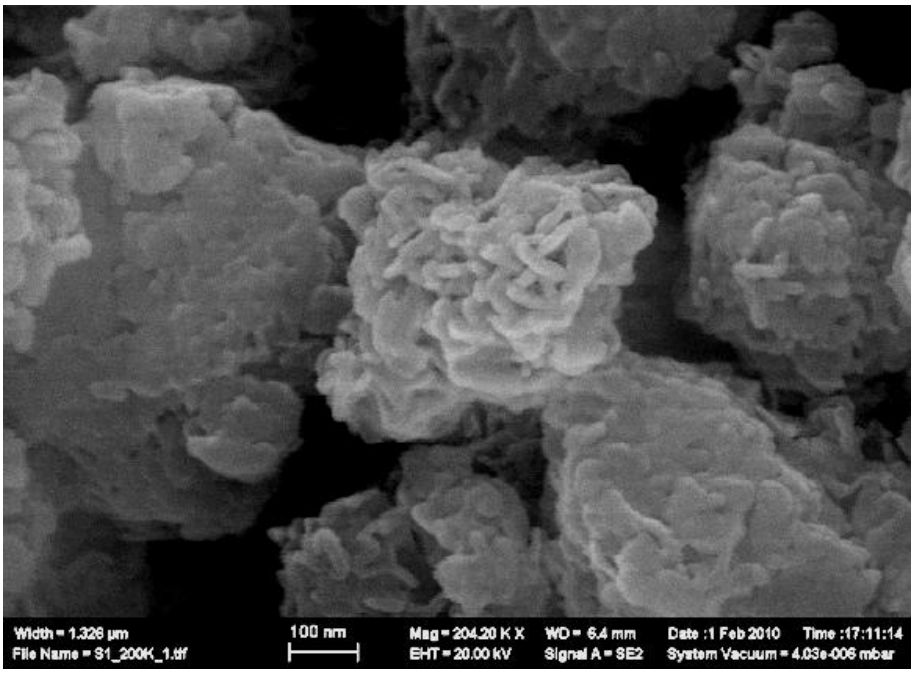

Figure 58: Fresh $Ni_{0.5}Mg_{2.5}Al$-hydrotalcite type catalyst (200,000x of magnification)

SEM images of spent $Ni_{0.5}Mg_{2.5}Al$-HT (Figure 59) and Ni/Al_2O_3 (Figure 60) catalysts after 20 hrs of CO_2 reforming of CH_4 at 700°C show significant differences in carbon deposition phenomena. To prevent any collapse of the conditions of the spent catalysts, the catalysts were not diluted with SiC inert material. It allows us to avoid the separation procedure between the spent catalyst and SiC because the carbon contained in SiC could make the reading of the SEM more difficult to interpret.

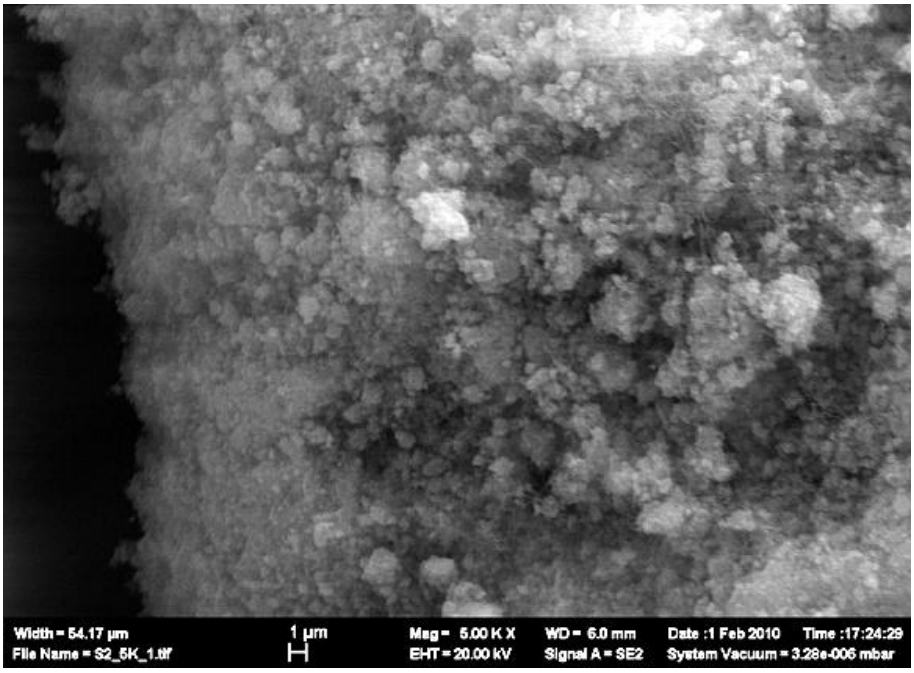

Figure 59: Spent $Ni_{0.5}Mg_{2.5}Al$-HT catalyst after 20 hrs of CO_2 reforming of CH_4 at 700℃ (5,000x of magnification)

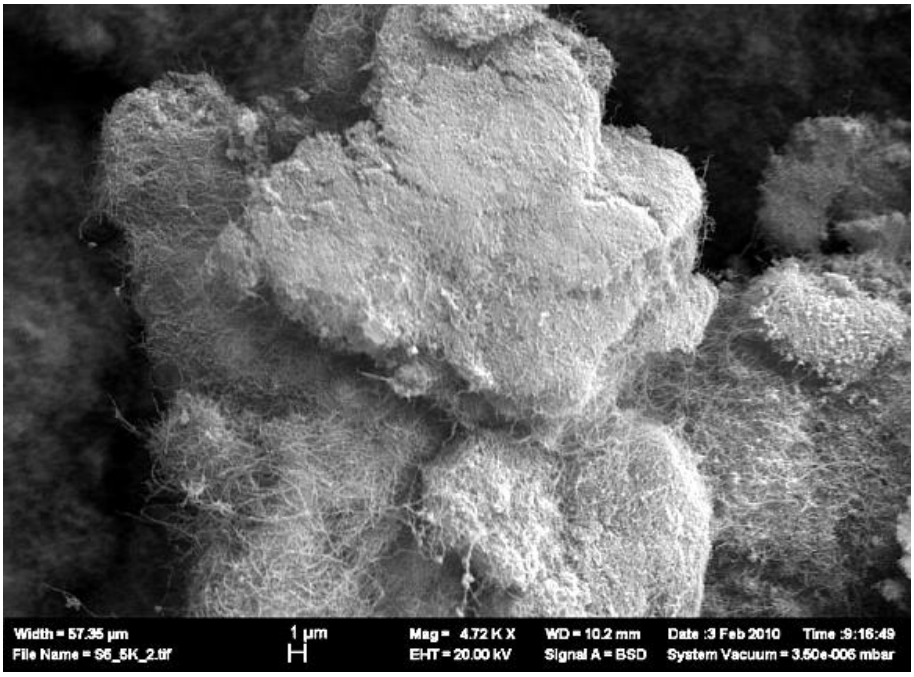

Figure 60: Spent Ni/Al_2O_3 catalyst after 20 hrs of CO_2 reforming of CH_4 at 700℃ (5,000 of magnification)

The $Ni_{0.5}Mg_{2.5}Al$-HT catalyst still contained a well-crystallized structure after 20 hrs of CO_2 reforming of CH_4 at 700℃. However, the Ni/Al_2O_3 catalyst produced a significant amount of carbon fibers, which covered the surface of the Ni/Al_2O_3 catalyst. Since the carbon fibers inhibit contact of reactants with the active Ni metal, this presumably led to the observed deactivation. From the image analysis, it is confirmed that less residual carbon is apparent on the $Ni_{0.5}Mg_{2.5}Al$-HT catalyst after reaction than on the Ni/Al_2O_2 catalyst.

4.2.5 Temperature-programmed oxidation analysis

The most critical disadvantage of using Ni-based catalysts is coke formation, which leads to catalyst deactivation. It is impossible to avoid carbon formation (or coke formation) on the nickel metal surface, unlike when using precious metals, such as Pt, Pd or Ru. It is well known that the carbon produced by methane dissociation or CO disproportionation reactions is deposited on the active nickel sites. This then leads to a decreased exposed active site surface area.

Temperature-programmed oxidation (TPO) allows us to estimate the amount of carbon deposited on the catalyst surface. Samples, containing around 50 mg of spent catalyst were loaded and air was flowing through the reactor. The temperature of the catalyst bed was increased from 25 to 900℃ at a rate of 10℃/min. The carbon deposited on the catalyst was oxidized and desorbed from the surface. Mass spectrometry (MS) was used to detect the carbon oxides formed, which in turn was used to determine the amount of carbon. The amount of carbon deposited on the catalysts can be estimated by calculating the area under the TPO curves (Figure 61). The amount of carbon deposited is shown in Table 15 and shows that the $Ni_{0.5}Mg_{2.5}Al$-HT catalyst had a stronger resistance to coke formation compared to the $Ni_{0.5}Ca_{2.5}Al$ catalyst.

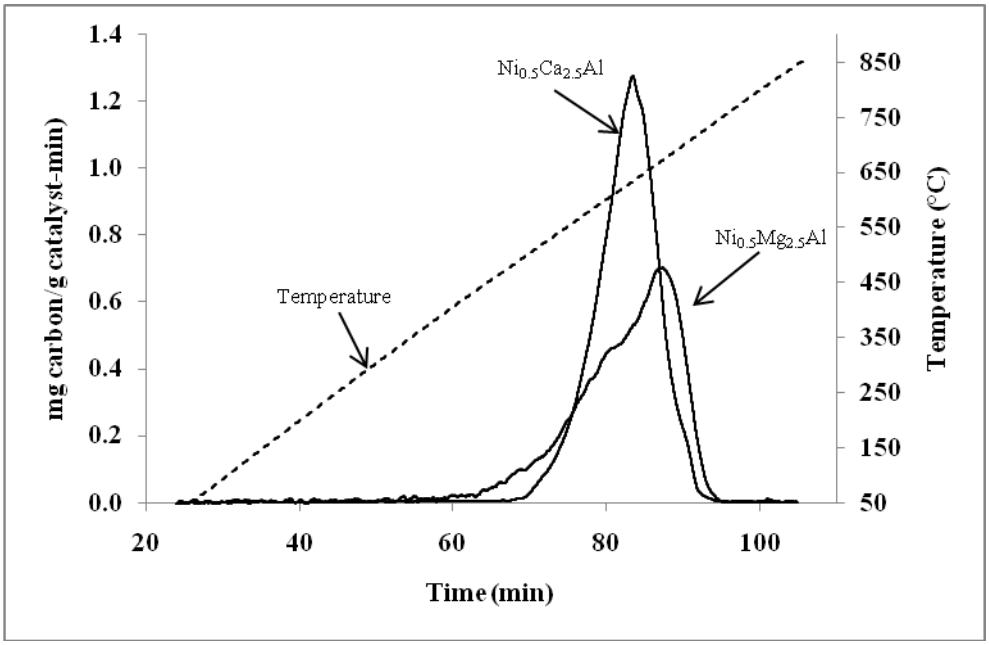

Figure 61: TPO results for $Ni_{0.5}Ca_{2.5}Al$ and $Ni_{0.5}Mg_{2.5}Al$-HT catalysts after CO_2 reforming of CH_4 at 700℃ for 20 hrs

Table 15: Amount of carbon deposition on $Ni_{0.5}Mg_{2.5}Al$ and $Ni_{0.5}Ca_{2.5}Al$ catalyst after 20hr, CO_2 reforming at 700°C

(per 1 g of spent catalyst)	$Ni_{0.5}Mg_{2.5}Al$-HT	$Ni_{0.5}Ca_{2.5}Al$
Carbon deposited (g)	0.98	1.19

The resistance to coke formation is related to the formation of the solid solution. As mentioned previously, XRD analysis demonstrated that the $Ni_{0.5}Mg_{2.5}Al$ catalyst produced a Ni-Mg-O solid solution. Because of the dissolution of NiO in the MgO, it is difficult to reduce the NiO to Ni. Small amounts of Ni segregate as small particles on the surface of the catalyst, resulting in less carbon deposition on surface. On the other hand, the $Ni_{0.5}Ca_{2.5}Al$ catalyst, which does not produce a solid solution, is more easily reduced and sintered. On the $Ni_{0.5}Mg_{2.5}Al$ catalyst, less carbon deposition occurred during CO_2 reforming of CH_4 reaction; and it might happen because the $Ni_{0.5}Mg_{2.5}Al$ catalyst possesses stronger interactions between the active Ni and support (difficult to reduce), and highly dispersed active Ni metal particles on surface due to the hydrotalcite-type structure.

4.3 Kinetic Study of CO_2 Reforming of CH_4 over $Ni_{0.5}Mg_{2.5}$Al-HT Catalyst

Because the $Ni_{0.5}Mg_{2.5}$Al-HT catalyst has shown the most promises, this catalyst has been chosen for further kinetics characterization, specifically kinetics for CO_2 reforming.

4.3.1 Mass transfer limitation and Activation energy barrier

Reliable kinetic data could be obtained when mass transfer limitation is negligible. There are two types of possible mass transfer limitations; (i) external diffusion and (ii) internal diffusion limitation. The external diffusion could be investigated by changing a flow rate of reactant gas over the catalyst bed with a constant residence time, or to more precise at constant GHSV. A higher flow rate of gas through the catalyst bed, that is higher superficial velocity, leads to thinner boundary layer thickness on the surface. It decreases the required time for the reactant gas to reach to the surface of the catalyst for the reaction. However, if the boundary layer is sufficiently thick that the transport rate of the gaseous species through this layer is slower than the rate of chemical reaction on the surface, then the external diffusion would govern the overall rate of reaction. The internal diffusion also can be studied by changing the particle size with a constant flow rate. If the species transport rate through the pores of the particle is slower than the rate of reaction on surface, then internal diffusion controls the overall rate of reaction. In conclusion, we should choose experimental conditions where the mass transfer effects, such as external and internal diffusion, are negligible, whenever possible.

For this study, the effect of feed flow rate and catalyst particle size on the reaction rate was determined experimentally with a feed mixture composed of $CH_4/CO_2/N_2$ (=20/20/60 vol%) at 700℃. For external diffusion tests, a constant W/F = 0.015 g.s/mL ratio was applied in order the contacting time constant. The effect of the flow rate at constant contact time is shown in Figure 62.

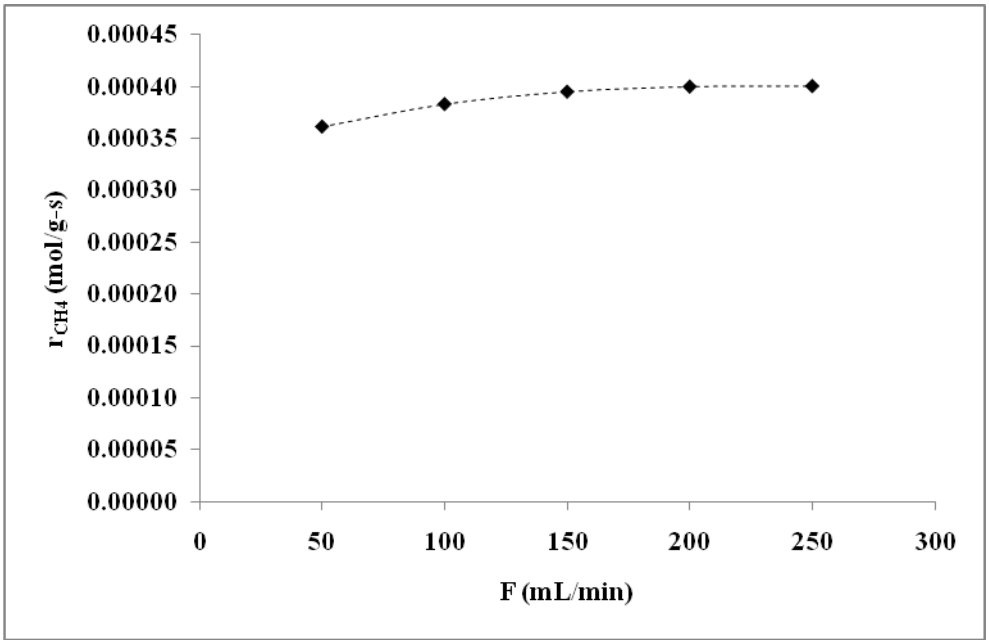

Figure 62: Effect of volumetric feed flow rate on the rate of CH_4 consumption during CO_2 reforming of CH_4 over the $Ni_{0.5}Mg_{2.5}Al$-HT catalyst (354-500µm) at constant W/F = 0.015 g.s/mL and 700℃.

It can be seen that the rate of CH_4 consumption (Eq. 57) increased until the flow rate was 200 mL/min. It indicates that up to the flow rate of 200 mL/min, external mass transfer had some influence on the overall reaction rate. However, when the flow rate exceeded 200 mL/min, the rate of CH_4 consumption remained constant. Therefore, experiments with a flow rate of 200 mL/min are adequate to obtain reaction data that are not masked by external transport limitation.

To investigate the possible effect of internal diffusion limitation, three different particle sizes were tested; (i) 251-354µm (average = 303µm); (ii) 354-500 µm (average = 427µm); and (iii) 500-710µm (average = 605µm). From the external diffusion limitation test, a flow rate of 200 mL/min (with GHSV = 240,000 cm^3/g.hr) was employed. The reaction temperature was 700℃. The effect of the particle size on the rate of CH_4 consumption is shown in Figure 63. It can be seen that the rate of CH_4 consumption is independent of the average diameter of the particles. This indicates that particle size between 250 and - 700 µm are small enough that the reaction is not affected by internal diffusion limitation at 700°C.

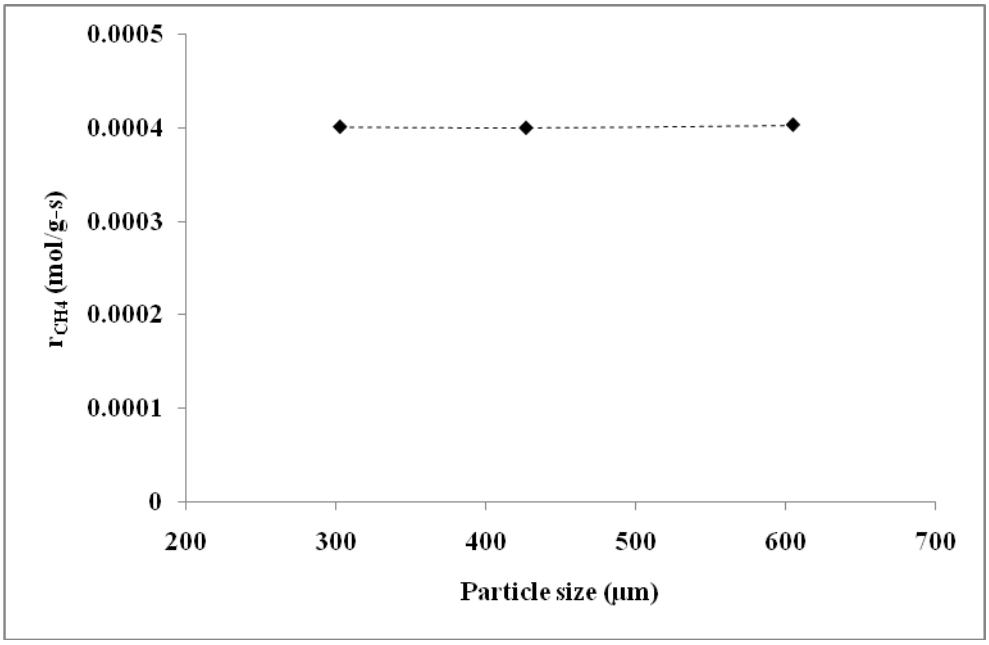

Figure 63: Effect of catalyst particle size on the rate of CH_4 consumption during CO_2 reforming of CH_4 over the $Ni_{0.5}Mg_{2.5}Al$-HT catalyst at constant F = 200 mL/min and 700°C

In conclusion, it has been decided to use the following operating conduction to carry out the kinetic tests:

- Particle size: 354-500 µm (average = 427µm)
- Amount of catalysis: 50mg of catalyst with 400mg of SiC
- Gas flow rate: 200 mL/min (with GHSV = 240,000 cm^3/g.hr)

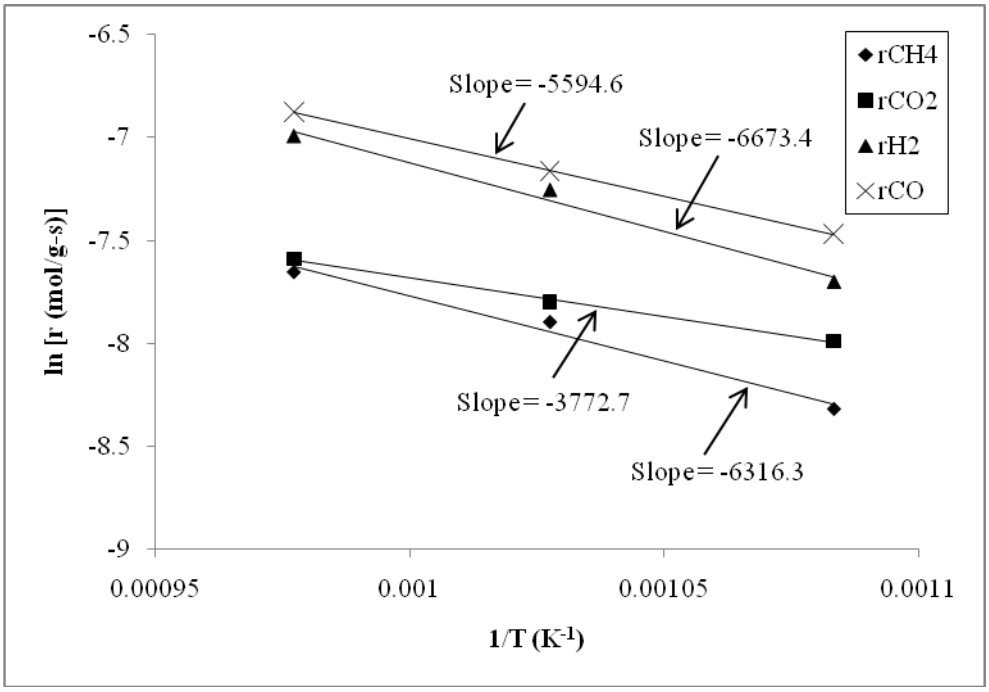

Figure 64: Arrhenius plot for CH_4 consumption rate at GHSV = 240,000 cm^3/g-hr. r_{CH4} and r_{CO2}: rate of consumption (Eq. 57); r_{H2} and r_{CO}: rate of formation (Eq. 58). Feed composition: $CH_4/CO_2/N_2$ (=20/20/60 vol%)

The temperature sensitivity of the CH_4 consumption rate over the $Ni_{0.5}Mg_{2.5}Al$-HT catalyst was investigated in the temperature range of 650-750℃. From this study, an Arrhenius plot could be obtained as shown in Figure 64. The Arrhenius plot allows obtaining the activation energy of CH_4 consumption, CO_2 consumption, H_2 formation and CO formation using the following equations. The activation energy of each species reaction rate is summarized in Table 13.

$$k_A(T) = Ae^{-E/RT} \qquad \text{[Equation 62]}$$

$$\ln k_A = \ln A - \frac{E}{R}\left(\frac{1}{T}\right) \qquad \text{[Equation 63]}$$

Table 16: Apparent activation energy (E, kJ/mol) over Ni-based catalysts

	E_{CH4}	E_{CO2}	E_{H2}	E_{CO}	Reference
$Ni_{0.5}Mg_{2.5}Al$-HT (923-1023K)	52.5	31.4	55.5	46.5	This work
Ni-Co/Al-Mg-O (923-1023K)	69.4	25.9	85.1	61.8	(Zhang, et al. 2009)
Ni/Al_2O_3 (773-973K)	50.9	56.1	-	80.5	(Wang and Lu 1999)
$Ni/CaO-Al_2O_3$ (893-963K)	106.8	98.8	147.4	103	(Lemonidou and Vasalosl 2002)

It is apparent that the support of Ni crystallites significantly influences the activation energy by altering the rate-controlling step in the reaction sequence. Since the activation energy barrier of CH_4 consumption step is greater than that of CO_2 consumption step, it can be assumed that the CH_4 dissociation step could be the rate determining step in this study. The lower activation energy barrier for CO_2 consumption might be caused due to the presence of strong Lewis base of MgO which can facilitate the activation of CO_2 (Zhang, et al. 2009). In addition, the apparent activation energy barrier for H_2 formation step is greater than that for the CO formation step. This indicates that the reverse water gas-shift (RWGS) reaction occurred during the CO_2 reforming of CH_4 process.

4.3.2 Effect of CH_4, CO_2 and H_2 partial pressures on the rate of CO_2 reforming of CH_4

The influence of the partial pressure of CH_4, CO_2, and H_2 on the rate of CH_4 consumption during CO_2 reforming of CH_4 was studied over the $Ni_{0.5}Mg_{2.5}Al$-HT catalyst at atmospheric pressure in the temperature rate 650-750℃. The experimental conditions for carrying the kinetic study are shown in Table 17. Note that the experiments shown in Table 17 were repeated at three different temperatures: at 650, 700 and 750°C.

Table 17: Experimental conditions and results for kinetic study

Temp 600°C	Partial pressure (atm)			Conversions of CH_4 and CO_2 (%) / Rate of CH_4 and CO_2 consumption (mol/g/s)				Yields of H_2 and CO (%) / Rate of H_2 and CO formation (mol/g/s)			
Test #	P_{CH4}	P_{CO2}	P_{H2}	X_{CH4}	r_{CH4}	X_{CO2}	r_{CO2}	Y_{H2}	r_{H2}	Y_{CO}	r_{CO}
1	0.5	1	0	83.6	0.000226	62.9	0.000340	81.2	0.000443	69.4	0.000568
2	1	1	0	64.1	0.000346	76.5	0.000413	60.5	0.000660	67.1	0.000733
3	2	1	0	40.6	0.000438	84.2	0.000455	36.4	0.000794	50.5	0.000826
4	1	0.5	0	35.7	0.000193	84.5	0.000228	37.4	0.000408	50.3	0.000412
5	1	1	0	45.2	0.000281	62.8	0.000339	41.5	0.000453	34.8	0.000570
6	1	2	0	53.4	0.000288	46.0	0.000497	40.7	0.000444	45.0	0.000737
7	1	1	0.5	50.8	0.000137	79.7	0.000215	N/A	N/A	62.6	0.000342
8	1	1	1	32.7	0.000088	79.7	0.000215	N/A	N/A	54.1	0.000295
9	1	1	2	17.9	0.000062	81.4	0.000220	N/A	N/A	47.6	0.000260

Temp 700°C	Partial pressure (atm)			Conversions of CH_4 and CO_2 (%) / Rate of CH_4 and CO_2 consumption (mol/g/s)				Yields of H_2 and CO (%) / Rate of H_2 and CO formation (mol/g/s)			
Test #	P_{CH4}	P_{CO2}	P_{H2}	X_{CH4}	r_{CH4}	X_{CO2}	r_{CO2}	Y_{H2}	r_{H2}	Y_{CO}	r_{CO}
1	0.5	1	0	95.0	0.000256	68.3	0.000369	87.6	0.000478	76.2	0.000623
2	1	1	0	71.0	0.000383	75.9	0.000410	71.6	0.000781	78.6	0.000861
3	2	1	0	46.0	0.000497	89.1	0.000481	38.8	0.000848	55.0	0.000896
4	1	0.5	0	38.2	0.000206	88.2	0.000238	40.2	0.000438	53.3	0.000436
5	1	1	0	69.0	0.000372	75.9	0.000410	71.6	0.000781	78.6	0.000861
6	1	2	0	71.0	0.000383	54.8	0.000592	53.2	0.000581	55.1	0.000903
7	1	1	0.5	65.1	0.000176	87.3	0.000236	N/A	N/A	72.8	0.000397
8	1	1	1	52.9	0.000143	86.8	0.000234	N/A	N/A	66.6	0.000363
9	1	1	2	43.4	0.000117	87.2	0.000235	N/A	N/A	62.2	0.000340

Temp 750°C	Partial pressure (atm)			Conversions of CH_4 and CO_2 (%) / Rate of CH_4 and CO_2 consumption (mol/g/s)				Yields of H_2 and CO (%) / Rate of H_2 and CO formation (mol/g/s)			
Test #	P_{CH4}	P_{CO2}	P_{H2}	X_{CH4}	r_{CH4}	X_{CO2}	r_{CO2}	Y_{H2}	r_{H2}	Y_{CO}	r_{CO}
1	0.5	1	0	96.7	0.000261	73.0	0.000197	90.5	0.000494	78.7	0.000644
2	1	1	0	82.6	0.000446	93.5	0.000252	80.4	0.000878	85.2	0.000929
3	2	1	0	45.0	0.000485	93.0	0.000251	41.0	0.000894	56.4	0.000924
4	1	0.5	0	39.0	0.000211	91.7	0.000247	41.6	0.000451	53.7	0.000440
5	1	1	0	88.0	0.000475	93.7	0.000506	80.7	0.000881	57.0	0.000933
6	1	2	0	90.0	0.000486	70.2	0.000758	77.7	0.000849	73.8	0.001208
7	1	1	0.5	76.9	0.000208	92.2	0.000249	N/A	N/A	82.4	0.000450
8	1	1	1	69.8	0.000188	91.6	0.000247	N/A	N/A	79.0	0.000431
9	1	1	2	63.4	0.000171	91.4	0.000247	N/A	N/A	75.7	0.000413

Runs A-1 to A-3 represent cases where a constant CO_2 partial pressure of 20.26 kPa was applied when CH_4 partial pressure was varied from 10.13 to 40.52 kPa balanced with N_2 (i.e. effect of CH_4 partial pressure). For runs B-1 to B-3, a constant CH_4 partial pressure of 20.26 kPa was applied when CO_2 partial pressure was varied from 10.13 to 40.52 kPa balanced with N_2 (i.e. effect of CO_2 partial pressure). Finally, in runs C-1 to C-3, the partial pressure of both CH_4 and CO_2 was kept constant at 10.13 kPa, while the partial pressure of H_2 was changed between 5.07 and 15.20 kPa (i.e. effect of H_2 partial pressure). For each test, the $Ni_{0.5}Mg_{2.5}$Al-HT catalyst was reduced in 10% H_2/N_2 gas with 200 mL/min at 720℃ for 1 hr. A total pressure was maintained at 101.3 kPa; and the GHSV was also remained constant at 240,000 cm^3/g-s.

To investigate the effects of the partial pressure on reaction rates, the logarithm graphs ($\ln(r_{CH4})$ vs. $\ln(_{CO2})$) have been prepared since the basic reaction rate of CO_2 reforming of CH_4 reaction could be expressed as $r_{CH4} = k(P_{CH4})^a(P_{CO2})^b(P_{H2})^c$. Therefore, it could be expressed as $\ln(r_{CH4}) = \ln k + a\ln(P_{CH4}) + b\ln(P_{CO2}) + c\ln(P_{H2})$. As seen in Figure 65, the CH_4 consumption rate was strongly affected by the partial pressure of CH_4 (while keeping the CO_2 partial pressure constant. However, as the CH_4 partial pressure increases, the slope for $\ln(r_{CH4})$ decreases, probably indicative of a non negligible CH_4 adsorption equilibrium constant. Referring to Figure 66, the CH_4 consumption rate also was affected strongly by the partial pressure of CO_2 in the range 10.13 to 20.26 kPa. However, the CH_4 consumption rate was quite independent of CO_2 partial pressure in range of 20.26 to 40.52 kPa and this was observed at all three temperatures. The fact that the rate of CH_4 consumption remains constant at sufficiently high value of P_{CO2} is likely due to a saturation of sites occupied by CO_2. In other word, the CO_2 adsorption equilibrium constant has probably a large value (larger than that for CH_4 absorption). Also, at lower temperature (650℃), the effect of CO_2 partial pressure on CH_4 consumption rate was less significant in comparison with that at higher temperature (750℃) since the slope for 650℃ (= 0.54) is lower than that for 750℃ (=1.17).

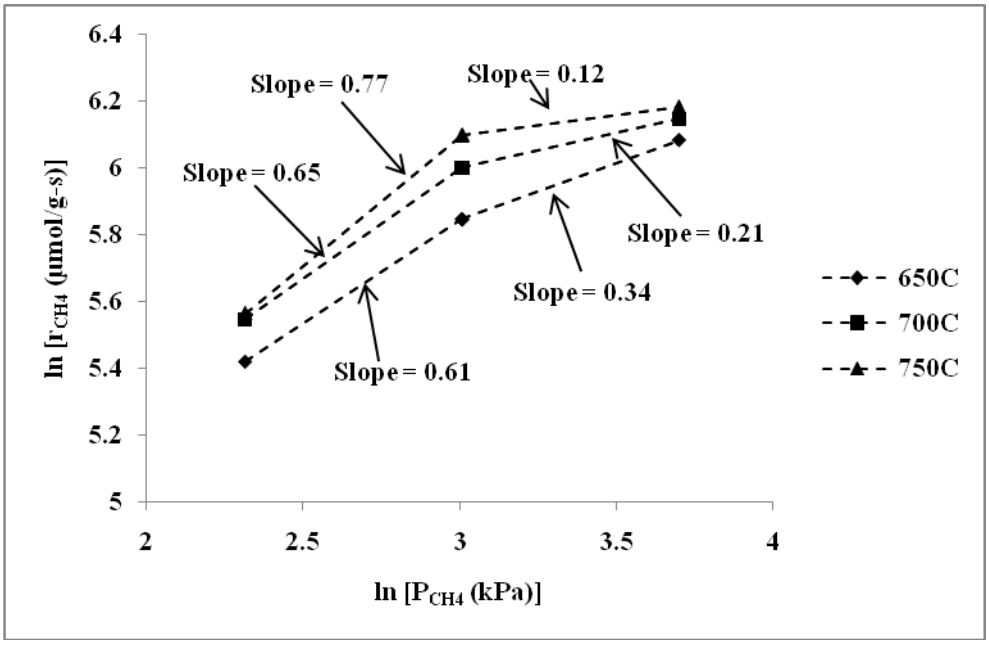

Figure 65: CH_4 consumption rate as a function of P_{CH4} at constant P_{CO2} = 20.26 kPa

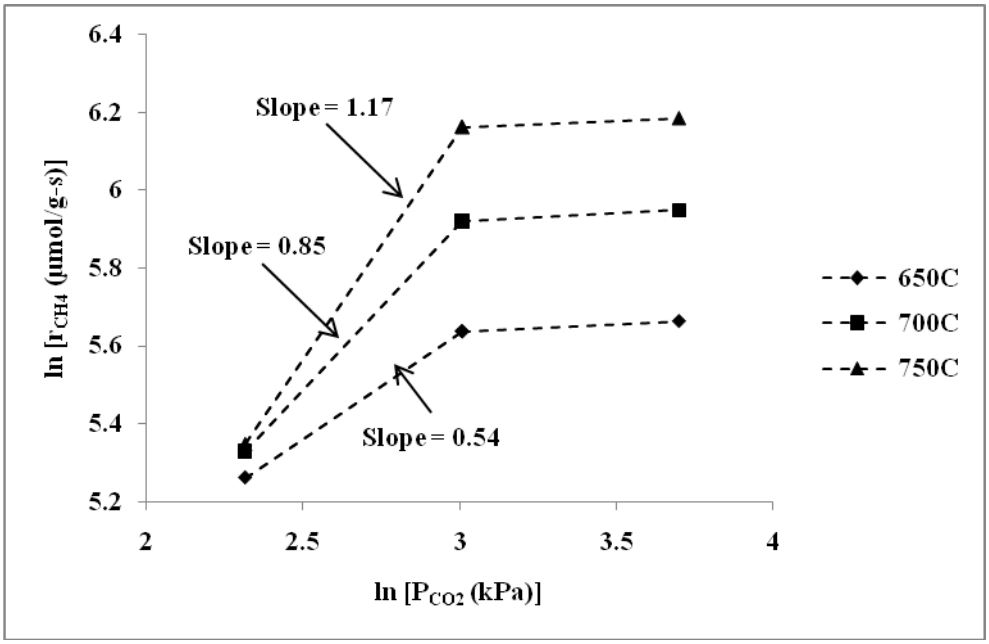

Figure 66: CH_4 consumption rate as a function of $P(CO_2)$ at constant $P(CH_4)$ = 20.26 kPa

From the comparison between Figure 65 and Figure 66, the CH_4 or CO_2 adsorption preference on the catalyst surface can be known. At low CO_2 and CH_4 partial pressures (< 20.26 kPa), the CH_4 consumption rates is more sensitive on CO_2 partial pressure than on CH_4 partial

pressure since the slopes in Figure 66 are higher than that in Figure 65 except 650℃. It indicates that CO_2 adsorption on the $Ni_{0.5}Mg_{2.5}Al$-HT catalyst is stronger than that of CH_4. However, at high CO_2 and CH_4 partial pressures (> 20.26 kPa), the CH_4 partial pressure affects more to the CH_4 consumption rates than the CO_2 partial pressure. It can be attributed to stronger adsorption of CH_4 to the surface of the catalyst than that of CO_2 at higher partial pressures.

Figure 67 shows the rates of CH_4 consumption at different temperatures and at various partial pressures of H_2 while keeping constant CH_4 and CO_2 partial pressures at 10.13 kPa. Clearly, increasing H_2 partial pressure decreases the rate of CH_4 consumption, which is to be expected since H_2 is a product of the CO_2 reforming reaction. The slopes observed in Figure 67 remains constant in the range of H_2 partial pressure considered here. It can be observed that different partial pressures of H_2 have relatively little effect on the reforming rates compared to various CH_4 or CO_2 partial pressures at high temperature. However, at low reaction temperature (650℃), the partial pressure of H_2 affects on the reforming rate of CH_4 consumption.

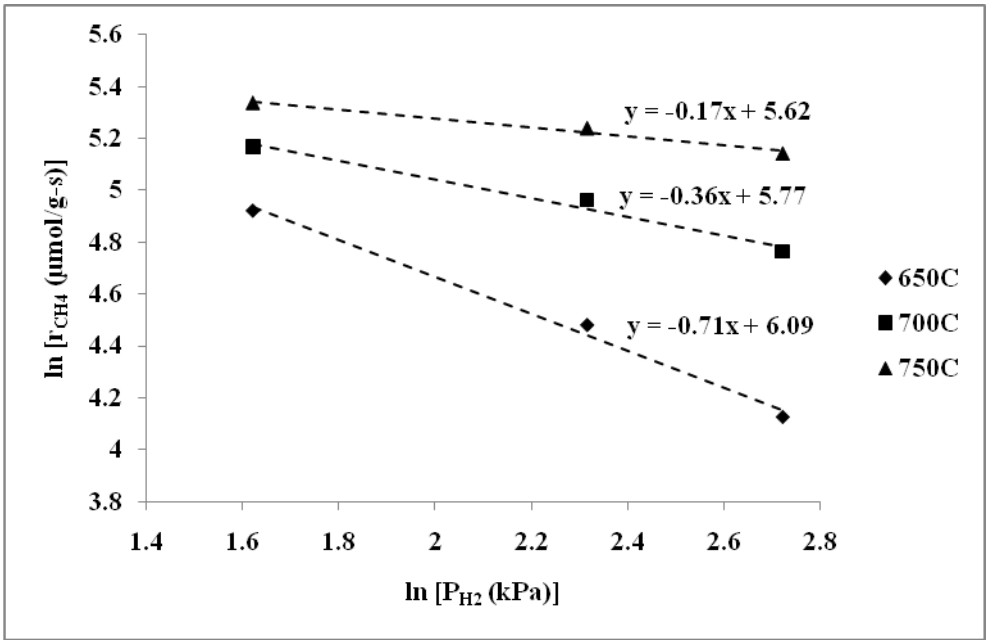

Figure 67: CH_4 consumption rate as a function of P_{H2} at constant P_{CO2} and P_{CH4} = 10.13 kPa in temperature range of 650 to 750℃.

Figures 68 and 69 represents the the H_2 and CO formation as well as CH_4 and CO_2 consumption rates at 700 ℃ over the $Ni_{0.5}Mg_{2.5}Al$-HT catalyst as a function of the CH_4 and CO_2 partial pressures, respectively. When the CH_4 partial pressure increased from 10.13 to 50.42 kPa with a constant CO_2 partial pressure (20.23 kPa), the CO_2 consumption rate increased, amd H_2 and CO formation rates also increased (Figure 68). When the CO_2 partial pressure increased from 10.13 to 50.42 kPa with a constant CH_4 partial pressure (20.23 kPa), the CO_2 consumption rate and the CO formation rate increased (Figure 69). However, the H_2 formation rate increased first as CO_2 partial pressure increased up to 20.26 kPa; then decreased with further increase in CO_2 partial pressure. When the CO_2 partial pressure is 20.26 kPa with a constant CH_4 partial pressure of 20.26 kPa, it satisfies the stoichiometric ratio of CO_2 reforming of CH_4 ($CH_4 + CO_2 \leftrightarrow 2H_2 + 2CO$). The stoichiometry of the CO_2 reforming reaction would indicate that the rate of formation of CO and H_2 should be the same (and also should the rate of consumption of CO_2 and CH_4). This was effectively observed in Figure 69 for P_{CO2} less than 20.26 kPa (i.e. $\ln(P_{CO2})$ less than 3). However, the results were much different for P_{CO2} greater than 20.26 kPa. This is because of the occurrence of the reverse water-gas shift (RWGS) reaction ($CO_2 + H_2 \leftrightarrow CO + H_2O$, Eq. 20), where H_2 reacts with excess CO_2. This observation agrees with other catalysts, such as Ni/CaO-Al_2O_3 (Lemonidou and Vasalosl 2002), Ni/La_2O_3 (Tsipouriari and Verykios 2001), and Ni/Al_2O_3 (Takano, et al. 1994).

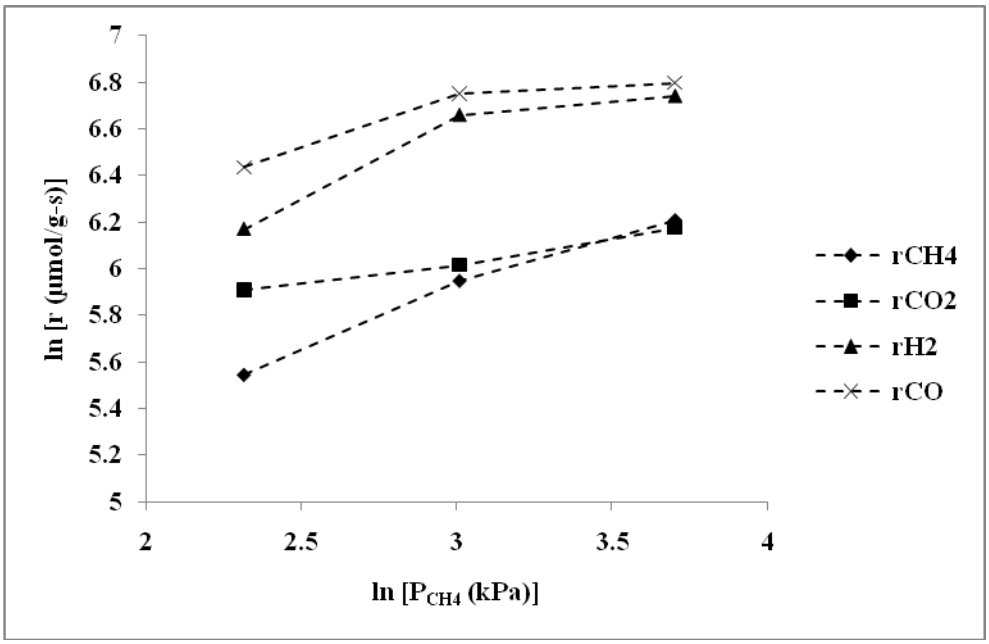

Figure 68: Reaction rates at 700℃ as a function of P_{CH4}, P_{CO2} = 20.26 kPa

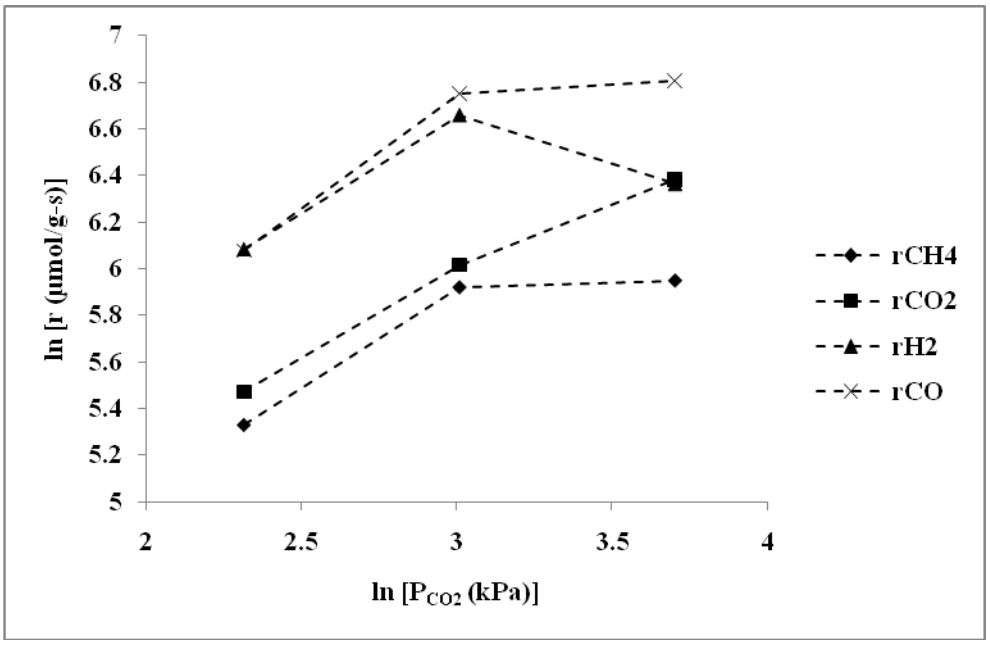

Figure 69: Reaction rates at 700℃ as a function of P_{CO2}, P_{CH4} = 20.26 kPa

Figure 70 shows the effect of reactant CH_4 (when CO_2 partial pressure was set constant) and CO_2 (when CH_4 partial pressure was set constant) partial pressures on the rate of formation of CO at different temperatures. It can be seen that the rate of CO formation increased more with the increase in CO_2 partial pressure than the increase in CH_4 partial pressure. This observation can be ascribed to the influence of reverse water-gas shift (RWGS) reaction (Eq. 20). In Figure 4.3.2-5, the CH_4 consumption rate was limited when high CO_2 partial pressure applied due to the limited availability of CH_4. However, the formation of CO still can be enhanced (in Figure 70) through the RWGS reaction between H_2 and excess CO_2.

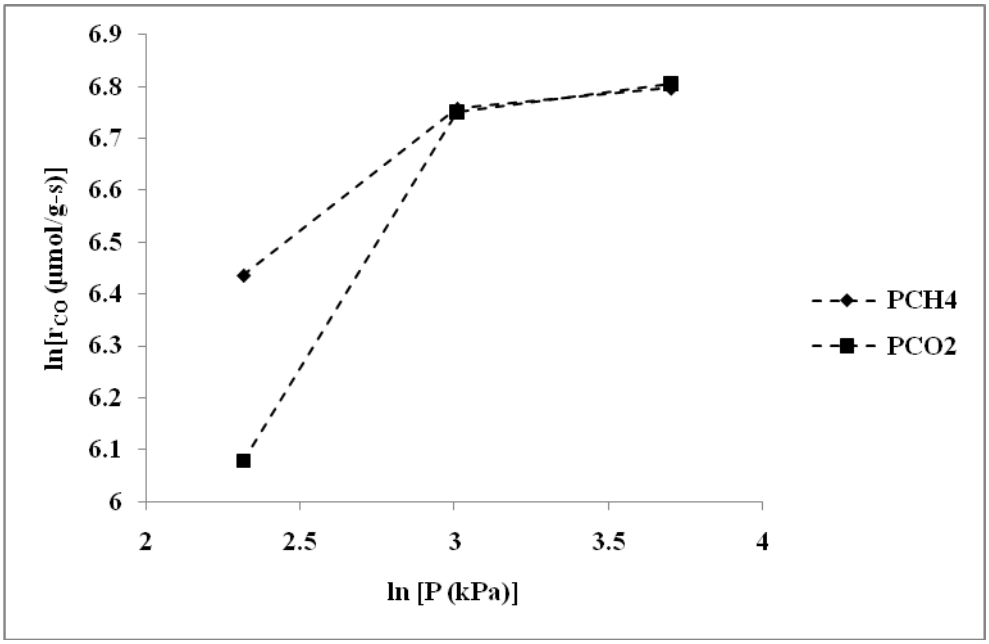

Figure 70: Effect of CH_4 (with constant CO partial pressure) and CO_2 (with constant CH_4 partial pressure) partial pressures on the formation rates of CO at 700℃

Chapter 5. Conclusions

Three major reactions (CH_4 partial oxidation, CO_2 reforming of CH_4 and oxidative CO_2 reforming of CH_4) to produce synthesis gas were evaluated at 700℃ for 20 hrs. In addition, for CO_2 reforming of CH_4, a long-term experiment (for 100 hrs) was conducted to further investigate the resistance to coke formation of the catalysts. Three catalysts, a $Ni_{0.5}Mg_{2.5}Al$ HT, a $Ni_{0.5}Ca_{2.5}Al$ and a Ni/Al_2O_3 catalyst, were tested. The $Ni_{0.5}Mg_{2.5}Al$-HT catalyst was the most promising catalyst since it showed very stable reactivity in any reforming reactions for 20hrs and produced less amount of coke due to the basic property and stronger interaction strength between the active metal and support (especially, for CO_2 reforming of CH_4, the $Ni_{0.5}Mg_{2.5}Al$-HT showed very stable and high reactivity than any other catalysts for 100 hrs). The CH_4 conversion, H_2 and CO yields, and the H_2/CO ratio were calculated to compare catalytic performance. In addition, the CH_4 consumption rate was calculated to explain the kinetic experiments.

Partial oxidation of CH_4 offers the greatest potential for a fast, efficient, and economical conversion of CH_4 to synthesis gas, due to its high conversion (~85%), high yields of H_2 (~82%) and CO (~80%), and suitable H_2/CO ratio (~2.1) for methanol production compared to other reactions. However, due to the exothermic nature of the reaction, hot-spots would be generated. For 20 hrs of reaction, the $Ni_{0.5}Mg_{2.5}Al$-HT, $Ni_{0.5}Ca_{2.5}Al$ and Ni/Al_2O_3 catalysts had similar levels of activity which were close to the equilibrium levels, and showed no deactivation. From XRD result, after 20 hrs of reaction, still active Ni phases were observed and no graphite was observed. It also confirmed that partial oxidation of CH_4 process produced less amount of carbon than other processes.

CO_2 reforming of CH_4 is an environmentally friendly process since CO_2 is consumed as a feedstock. However, it is an endothermic reaction that consumed much energy to maintain high conversions. The catalysts tended to deactivate due to coke deposition on the catalyst surface. The $Ni_{0.5}Mg_{2.5}Al$-HT catalyst had high and stable reactivity (~69% methane conversion) for over 20 hrs while the $Ni_{0.5}Ca_{2.5}Al$ and Ni/Al_2O_3 catalysts deactivated with time-on-stream due to coke formation. However, the $Ni_{0.5}Ca_{2.5}Al$ catalyst showed initially higher CH_4 conversion activity than the $Ni_{0.5}Mg_{2.5}Al$-HT catalyst since the $Ni_{0.5}Ca_{2.5}Al$ catalyst is a more reducible catalyst than

the $Ni_{0.5}Mg_{2.5}$Al-HT catalyst. For longer-term reaction tests, the $Ni_{0.5}Mg_{2.5}$Al catalyst showed no deactivation and high activity, while the $Ni_{0.5}Ca_{2.5}$Al catalyst showed continuous deactivation over 100 hrs due to coke formation on the catalyst surface. It was confirmed from TPO result that the $Ni_{0.5}Mg_{2.5}$Al-HT catalyst produced less amount of coke (0.98 g of carbon/g of spent catalyst) than the $Ni_{0.5}Ca_{2.5}$Al catalyst (1.29 g of carbon/g of spent catalyst) during 20 hrs of reaction at 700℃. From XRD result, for $Ni_{0.5}Mg_{2.5}$Al-HT catalyst, after 20 hrs of reaction, graphite phase was observed and active Ni phases were disappeared; this indicated that coke produced during the reaction covered the active Ni sites.

Oxidative CO_2 reforming of CH_4 appears promising for synthesis gas production. The coupling of the exothermic partial oxidation with endothermic CO_2 reforming of CH_4 can facilitate heat transfer between the reactions. Therefore, less heat was required to maintain the reaction temperature during the initial period of the reaction. The addition of O_2 allows maintaining high reactivities for catalysts during the CO_2 reforming of CH_4 process. The addition of O_2 reduces coke deposition on the catalysts since the oxygen can combust the surface carbon. Therefore, the catalyst activity levels for the three catalysts were closer than in the CO_2 reforming of CH_4 reaction (~72%). The $Ni_{0.5}Ca_{2.5}$Al catalyst showed the highest activity at the beginning of the reaction (~81%), but deactivated quickly due to coke deposition. The $Ni_{0.5}Mg_{2.5}$Al catalyst showed the most stable reactivity over 20 hrs of reaction.

Only the Mg-containing sample ($Ni_{0.5}Mg_{2.5}$Al-HT catalyst) results in a hydrotalcite-type (HT) layered structure since the atomic size and structure of Mg and Ni are similar; it was confirmed from XRD result. In addition, due to the strong Ni to support interaction (therefore, less reducible catalyst), the $Ni_{0.5}Mg_{2.5}$Al-HT catalyst showed excellent stability for the CO_2 reforming of CH_4 reaction, even in the absence of oxygen in feed gas. The HT structure seemed to stabilize the catalyst in terms of decreased coke formation, allowing conversions and product yields to remain constant. As a conclusion, the $Ni_{0.5}Mg_{2.5}$Al catalyst is the most promising catalyst since it had high reactivity and was more stable than the other catalysts tested.

For the kinetic studies, the CO_2 reforming of CH_4 reaction was examined over the $Ni_{0.5}Mg_{2.5}$Al-HT catalyst. The flow rate of 200 mL/min which was used for the reaction tests was

a suitable condition since the reaction was in the kinetically control region. Internal mass transfer limitation was negligible for the catalyst particle size in the range 354-500μm. The activation energy (or energy barrier) of CH_4 consumption (20.0 kJ/mol) was greater than that of CO_2 consumption (18.0 kJ/mol). It implies that the CH_4 dissociation step was the rate-limiting step for the CO_2 reforming of CH_4 process over the $Ni_{0.5}Mg_{2.5}Al$-HT at 700℃.

Changing the CH_4 partial pressure (while keeping the CO_2 partial pressure constant) affected the CH_4 consumption rate (or CH_4 reforming rate). However, the varying the CO_2 partial pressures (while keeping the CH_4 partial pressure constant) did not affect the CH_4 reforming rate when higher CO_2 partial pressures were applied. Also, at lower temperature (650℃), the effect of CO_2 partial pressure on CH_4 consumption rate was less significant in comparison with those at higher temperature (750℃). In addition, when higher partial pressures of the product gas (H_2) were used, the CH_4 reforming rate decreased.

**** Recommendations**

- For the Aspen Plus™ simulation, using different reactors to estimate the equilibrium levels and compare with Gibbs reactor could be interesting.
- Different calcination and reduction conditions (ex. temperature or period) could affect the reactivity of the catalysts.
- For the oxidative CO_2 reforming, various oxygen amount could explain the role of oxygen phase during the reaction, especially how to affect the carbon deposition on the catalyst surface.
- Deriving the kinetic rate expression and simulation confirmation should be needed to verify the kinetic behavior of the catalyst.

References

Amin N.A.S., Yaw T.C. "Thermodynamic equilibrium analysis of combined carbon dioxide reforming with partial oxidation of methane to syngas." "International Journal of Hydrogen Energy" 32 (2007): 1789 – 1798.

Ashcroft A.T., Cheetham A.K., Green M.L.H., Vernon P.D.F. "Partial oxidation of methane to synthesis gas using carbon dioxide." "Nature" 352, (1991): 225-226.

Bartholomew C.H., Farrauto R.J. "Fundametals of industrial catalytic processes." 2nd. Hoboken, NJ: John Wiles & Sons, 2006.

Basile F., et al. "Ni/Mg/Al Anionic Clay Derived Catalysts for the Catalytic Partial Oxidation of Methane." "Journal of Catalysis" 173 (1998): 247–256.

Beebe T.P., Goodman D.W., Kay B.D. "Kinetics of the activated dissociative adsorption of methane on the low index planes of nickel single crystal surfaces." "J. Chem. Phys." 87 (1987): 2305-2315.

Bodrov I.M., Apel'baum L.O. "Reaction kinetics of methane and carbon dioxide on a nickel surface." "Kinet. Catal." 8 (1967): 326.

Bond G.C., Dias C.R., Portela M.F. "Characterization of Carbonaceous Deposits by Temperature-Programmed Oxidation." "Journal of Catalysis" 156 (1995): 295-297.

Bradford M.C.J., Vannice M.A. "CO2 Reforming of CH4." "Catalysis Reviews" 41 (1999): 1-42.

Bradford M.C.J., Vannice M.A. "CO2 Reforming of CH4 over Supported Pt Catalysts." "Journal of Catalysis" 173 (1998): 157–171.

Cao L., Chen Y., Li W. "Effect of La2O3 added to NiO/Al2O3 catalyst on partial oxidation of methane to syngas." "Studies in Surface Science and Catalysis" 107 (1997): 467-471.

Cavani F., Trifiro F., Vaccari A. "Hydrotalcite-type anionic clays: Preparation, Properties and Applications." "Catalysis Today" 11 (1991): 173-301.

Choudhary V.R., Chaudhari P.A., Narkhede V.S. "Solvent-free liquid phase oxidation of benzyl alcohol to benzaldehyde by molecular oxygen using non-noble transition metal containing hydrotalcite-like solid catalysts." "Catalysis Communications" 4 (2003): 171-175.

Choudhary V.R., Mamman A.S., Sansare S.D. “Selective Oxidation of Methane to CO and H2 over Ni/MgO at Low Temperatures.” “Angew. Chem. Int. Ed. Engl.” 31 (1992): 1189-1190.

Choudhary V.R., Rajput A.M., Prabhakar B. “Low temperature oxidative conversion of methane to syngas over NiO-CaO catalyst.” “Catalysis Letters” 15 (1992): 363-370.

Choudhary V.R., Rane V.H., Rajput A.M. “Beneficial effects of cobalt addition to Ni-catalysts for oxidative conversion of methane to syngas.” “Applied Catalysis A: General” 162 (1997): 235-238.

Colpas G.J., et al. “X-ray spectroscopic studies of nickel complexes, with application to the structure of nickel sites in hydrogenases.” “Inorganic Chemistry” 30 (1991): 920-928.

Cui Y., Zhang H., Xu H., Li W. “Kinetic study of the catlytic reforming of CH4 with CO2 to syngas over Ni/a-Al2O3 catalyst: The effect of temperature on the reforming mechanism.” “Applied Catalysis A: General” 318 (2007): 79-88.

Di M., Dajiang M., Xuan L., Maochu G., Yaoqiang C. “Partial oxidation of methane to syngas over monolithic Ni/γ-Al2O3 catalyst–-effects of rare earths and other basic promoters.” “Journal of Rare Earths” 24 (2006): 451-455.

Edwards J.H., Maitra A.M. “The chemistry of methane reforming with carbon dioxide and its current and potential applications.” “Fuel Processing Technology” 42 (1995): 269-289.

Enger B.C., Lodeng R., Holmen A. “A review of catalytic partial oxidation of methane to synthesis gas with emphasis on reaction mechanisms over transition metal catalysts.” “Applied Catalysis A: General” 346 (2008): 1-27.

Erdohelyi A., Cserenyi J., Solymosi F. “Activation of CH4 and Its Reaction with CO2 over Supported Rh Catalysts.” “Journal of Catalysis” 141 (1993): 287-299.

Ferreira-Aparicio P., Fernandez-Garcia M., Guerrero-Ruiz A., Rodríguez-Ramos I. “Evaluation of the Role of the Metal–Support Interfacial Centers in the Dry Reforming of Methane on Alumina-Supported Rhodium Catalysts.” “Journal of Catalysis” 190 (2000): 296-308.

FoglerScott H. “Elements of Chemical Reaction Engineering.” Fourth Edition. Upper Saddle River, NJ: Pearson Education, Inc., 2006.

Fornasari G., Gazzano M., Matteuzzi D., Trifiro F., Vaccari A. “Structure and reactivity of high-surface-area Ni/Mg/Al mixed oxides.” “Applied Clay Science” 10 (1995): 69-82.

Fraenkel D., Levitan R., Levy M. “A solar thermochemical pipe based on the CO2---CH4 (1:1) system.” “International Journal of Hydrogen Energy” 11 (1986): 267-277.

Goula M.A., Lemonidou A.A., Grünert W., Baerns M. “Methane partial oxidation to synthesis gas using nickel on calcium aluminate catalysts.” “Catalysis Today” 32 (1996): 149-156.

Horiuchi T., Sakuma K., Fukui T., Kubo Y., Osaki T., Mori T. “Suppression of carbon deposition in the CO2-reforming of CH4 by adding basic metal oxides to a Ni/Al2O3 catalyst.” “Applied Catalysis A: General” 144 (1996): 111-120.

Hu Y.H., Ruckenstein E. “Temperature-Programmed Desorption of CO Adsorbed on NiO/MgO.” “Journal of Catalysis” 163 (1996): 306-311.

Hu Y.H., Ruckenstein E. “Transient Response Analysis via a Broadened Pulse Combined with a Step Change or an Isotopic Pulse. Application to CO_2 Reforming of Methane over NiO/SiO_2.” “J. Phys. Chem. B” 101 (1997): 7563-7565.

Jin R., et al. “Mechanism for catalytic partial oxidation of methane to syngas over a Ni/Al_2O_3 catalyst.” “Applied Catalysis A: General” 201 (2000): 71-80.

Kawabata T., Shinozuka Y., Ohishi Y., Shishido T., Takaki K., Takehira K. “Nickel containing Mg-Al hydrotalcite-type anionic clay catalyst for the oxidation of alcohols with molecular oxygen.” “Journal of Molecular Catalysis A: Chemical” 236 (2005): 206-215.

Kuijpers E.G.M., Breedijk A.K., van der Wal W.J.J., Geus J.W. “Chemisorption of methane on Ni/SiO_2 catalysts and reactivity of the chemisorption products toward hydrogen.” “Journal of Catalysis” 81 (1983): 429-439.

Lemonidou A.A., Stambouli A.E., Tjatjopoulos G.J., Vasalos I.A. “Partial oxidation of methane to synthesis gas over unpromoted and (0.1-0.5 wt%) Ni-promoted calcium aluminate catalysts.” “Catalysis Letters” 43 (1997): 235-240.

Lemonidou A.A., Vasalosl. A. “Carbon dioxide reforming of methane over 5 wt.% Ni/CaO-Al_2O_3 catalyst.” “Applied Catalysis A: General” 228 (2002): 227-235.

Lewis W.K., Gilliland E.R., Reed W.A. “Reaction of Methane with Copper Oxide in a Fluidized Bed.” “Ind. Eng. Chem.” 41 (1949): 1227–1237.

Li H., Wang J. “Study onCO_2 reforming of methane to syngas overAl_2O_3–ZrO_2 supported Ni catalysts prepared via a direct sol–gel process.” “Chemical Engineering Science” 59 (2004): 4861-4867.

Luntz A.C., Harris J. “CH, dissociation on metals: a quantum dynamics model.” “Surface Science” 258 (1991): 397-426.

Mark M.F., Maier W.F. “Active Surface Carbon - A Reactive Intermediate in the Production of Synthesis Gas from Methane and Carbon Dioxide.” “Angewandte Chemie International Edition in English” 33 (2003): 1657-1660.

Miao Q., Xiong G., Sheng S., Cui W., Xu L., Guo X. “Partial oxidation of methane to syngas over nickel-based catalysts modified by alkali metal oxide and rare earth metal oxide.” “Applied Catalysis A: General” 154 (1997): 17-27.

Morioka H, et al. “Partial oxidation of methane to synthesis gas over supported Ni catalysts prepared from Ni-Ca/Al-layered double hydroixde.” “Applied Catalysis A: General” 215 (2001): 11-19.

Nandini A., Pant K.K., Dhingra S.C. “Kinetic study of the catalytic carbon dioxide reforming of methane to synthesis gas over Ni-K/CeO_2-Al_2O_3 catalyst.” “Applied Catalysis A: General” 308 (2006): 119-127.

Obalova L., Valaskova M., Kovanda F., Lacny Z., Kolinova K. “Study of the catalytic activity of calcined Ni/Mg/Al (Mn) hydrotalcites for N_2O decomposition.” “Chem. Pap.” 58, (2004): 33-40.

Oberlander R.K. “Aluminas for catalysts.” Academic Press, 1984.

Olsbye U., Akporiaye D., Rytter E., Ronnekleiv M., Tangstad E. “On the stability of mixed M^{2+}/M^{3+} oxides.” “Applied Catalysis A: General” 224 (2002): 39-49.

Osaki T., Masuda H., Mori T. “Intermediate hydrocarbon species for the CO_2-CH_4 reaction on supported Ni catalysts.” “Catalysis Letters” 29 (1994): 33-37.

Oyama S.T. “Novel catalysts for advanced hydroprocessing: transition metal phosphides.” “Journal of Catalysis” 216 (2003): 343–352.

Perry R.H., Green D.W. “Perry's Chemical Engineers' Handbook.” 7th. McGraw-Hill, 1997.

Qin D., Lapszewicz J. “Study of mixed steam and CO_2 reforming of CH_4 to syngas on MgO-supported metals.” “Catalysis Today” 21 (1994): 551-560.

Richardson J.T., Paripatyadar S.A. “Carbon dioxide reforming of methane with supported rhodium.” “Applied Catalysis” 61 (1990): 293-309.

Ruckenstein E., Hu Y.H. “Carbon dioxide reforming of methane over nickel/alkaline earth metal oxide catalysts.” “Applied Catalysis A: General” 133 (1995): 149-161.

Ruckenstein E., Wang H.Y. “Combined catalytic partial oxidation and CO_2 reforming of methane over supported cobalt catalysts.” “Catalysis Letters” 73 (2001): 2-4.

Shishido T., et al. “Partial oxidation of methane over Ni/Mg-Al oxide catalysts prepared by solid phase crystallization method from Mg-Al hydrotalcite-like precursors.” “Applied Catalysis A: General” 223 (2002): 35-42.

Slagtern A., Olsbye U. “Partial oxidation of methane to synthesis gas using La-M-O catalysts.” “Applied Catalysis A: General” 110 (1994): 99-108.

Slagtern S., Olsbye U., Blom R., DahlI M. “The influence of rare earth oxides on Ni/Al_2O_3 catalysts during CO_2 reforming of CH_4.” “Studies in Surface Science and Catalysis” 107 (1997): 497-502.

Solymosi F., Kutsán Gy., Erdöhelyi A. “Catalytic reaction of CH_4 with CO_2 over alumina-supported Pt metals.” “Catalysis Letters” 11 (1991): 149-156.

Somorjai G.A. “Introduction to surface chemistry and catalysis.” New York: Wiley, 1994.

Souza M.M.V.M., Schmal M. “Combination of carbon dioxide reforming and partial oxidation of methane over supported platinum catalysts.” “Applied Catalysis A: General” 255 (2003): 83–92.

Takano A., Tagawa T., Goto S. “Carbon Dioxide Reforming of Methane on Supported Nickel Catalysts.” “J. Chem. Eng. Jpn.” 27 (1994): 727-731.

Takehira K., Shishido T., Wang P., Kosaka T., Takaki K. “Autothermal reforming of CH_4 over supported Ni catalysts prepared from Mg-Al hydrotalcite-like anionic clay.” “Journal of Catalysis” 221 (2004): 43-54.

Takehira K., et al. “Preparation of egg-shell type Ni-loaded catalyst by adopting "Money Effect" of Mg-Al hydrotalcite and its application for CH_4 reforming.” “Catalysis Communications” 5 (2004): 209-213.

Takenaka S., Umebayashi H., Tanabe E., Matsune H., Kishida M. “Specific performance of silica-coated Ni catalysts for the partial oxidation of methane to synthesis gas.” “Journal of Catalysis” 245 (2007): 392-400.

Tang S., Lin J., Tan K.L. “Partial oxidation of methane to syngas over Ni/MgO, Ni/CaO and Ni/CeO_2.” “Catalysis Letters” 51 (1998): 169–175.

Tang S.B., Qiu F.L., Lu S.J. “Effect of supports on the carbon deposition of nickel catalysts for methane reforming with CO_2.” “Catalysis Today” 24 (1995): 253-255.

Tomishige K., Nurunnabi M., Maruyama K., Kunimori K. “Effect of oxygen addition to steam and dry reforming of methane on bed temperature profile over Pt and Ni catalysts.” “Fuel Processing Technology” 85 (2004): 1103– 1120.

Trimm D.L. “The Formation and Removal of Coke from Nickel Catalyst.” “Catalysis Reviews” 16 (1977): 155 - 189.

Tsipouriari V.A., Verykios X.E. “Kinetic study of the catalytic reforming of methane with carbon dioxide to synthesis gas over Ni/La_2O_3 catalyst.” “Catalysis Today” 64 (2001): 83-90.

Vaccari A. “Preparation and catalytic properties of cationic and anionic clay.” “Catalysis Today” 41 (1998): 53-71.

Vermeiren W.J.M., Blomsma E., Jacobs P.A. “Catalytic and thermodynamic approach of the oxyreforming reaction of methane.” “Catalysis Today” 13 (1992): 427-436.

Wang H.Y., Au C.T. “CH_4/CD_4 isotope effects in the carbon dioxide reforming of methane to syngas over SiO_2-supported nickel catalysts.” “Catalysis Letters” 38 (1996): 77-79.

Wu T., Yan Q., Wan H. “Partial oxidation of methane to hydrogen and carbon monoxide over a Ni/TiO_2 catalyst.” “Journal of Molecular Catalysis A: Chemical” 226 (2005): 41-48.

Yan Q.G., Weng W.Z., Wan H.L., Toghiani H., Toghiani R.K., PittmanJr C.U. “Activation of methane to syngas over a Ni/TiO_2 catalyst.” “Applied Catalysis A: General” 239 (2003): 43-58.

York A.P.E., Xiao T., Green M.L.H. “Brief overview of the partial oxidation of methane to synthesis gas.” “Topics in Catalysis” 22 (2003): 345-358.

Zhang J., Wang H., Dalai A.K. “Kinetic studies of carbon dioxide reforming of methane over Ni-Co/Al-Mg-O bimetallic catalyst.” “Ind. Eng. Chem. Res.” 48 (2009): 677-684.

Zhang Y., Li Z., Wen X., Liu Y. “Partial oxidation of methane over Ni/Ce-Ti-O catalysts.” “Chemical Engineering Journal” 121 (2006): 115-123.

Zhang Y., Xiong G., Sheng S., Yang W. “Deactivation studies over $NiO/g\text{-}Al_2O_3$ catalysts for partial oxidation of methane to syngas.” “Catalysis Today” 63 (2000): 517–522.

Zhang Z.L., Verykios X.E. “Carbon dioxide reforming of methane to synthesis gas over supported Ni catalysts.” “Catalysis Today” 21 (1994): 589-595.

Zhu Q., Zhao X., Deng Y. “Advances in the partial oxidation of methane to synthesis gas.” “Journal of Natural Gas Chemistry” 13 (2004): 191-203.

Zhu Q., Zhao X., Deng Y. “Advances in the Partial Oxidation of Methane to Synthesis Gas.” “Journal of Natural Gas Chemistry” 13 (2004): 191-203.

Zhu Y., Chen D., Zhou X., Yuan W. “DFT studies of dry reforming of methane on Ni catalyst.” “Catalysis Today” 148 (2009): 260–267.

Appendix A. Procedure of experiment

A.1 Procedure for preparing catalyst

** Preparation of $Ni_{0.5}Mg_{2.5}Al$ catalyst

1. Clean thoroughly experimental glassware and rinse with deionized water.
2. Measure out 30mL of 1M Ni nitrate with graduate cylinders
3. Measure out 60mL of 1M Al nitrate with graduate cylinders
4. Measure out 150mL of 1M Mg nitrate with graduate cylinders
3. Mix the measured chemicals in a 500mL beaker
4. Pour 240mL of 0.5M $NaCO_3$ into a 1000mL beaker
5. Place a stirring rod in the 1000mL beaker and stir $NaCO_3$ with a stirrer at a speed of 400 rpm
6. Locate the pH meter probe on the wall of the 1000mL considering the height of the solution after mixing all the chemicals.

   CAUTION

   The solution MUST NOT EXCEED the line on the probe

   Also THE TIP OF THE PROBE MUST NOT TOUCH THE STIRRING ROD INSIDE THE BEAKER
7. Place a ring stand behind the stirrer so that the chemicals can be dropped into the 1000mL beaker while it is stirred.
8. Install 2 seperatory funnels with two ring clamps (make sure the clamps are holding the funnels tight)
9. Pour the solution in the 500mL beaker into a 250mL separatory funnel
10. Pour about 100mL of NaOH into a 125mL seperatory funnel
11. Open the cock of the 250 mL seperatory funnel with the catalyst solution. Make sure it is mixed with $NaCO_3$ in the 1000mL beaker drop by drop
12. pH should be kept constant at about 10.0 If it is less than 10.0 open the cock of the 125mL seperatory funnel holding NaOH solution (add this drop by drop)
13. Keep the pH around 10 until all solution runs out
14. Let the solution mix for 30 minutes

15. The solution must be kept in an oven at 110˚C for 12 hours for aging

** Filtration and wash

16. Clean all glassware and rinse them thoroughly with distilled water
17. Assemble funnel to a 1000 mL flask and locate a filter paper in the funnel
18. Connect the vacuum line to the 1000mL and turn on the vacuum pump
19. Pouring some distilled water on the filter paper to check if there is any gap between the funnel and the filter paper
20. Using a spatula, mix the solution thoroughly until there is no separation appeared
21. Start filtering the catalyst solution
22. Fill the 1000mL flask with about 500 mL of distilled water
23. If there is no drop falling in the flask, let the filter cake dry until there are some cracks on the cake
24. Turn off the vacuum pump
25. Carefully remove filter cake from the filter paper and add those back into the 1000 mL beaker which has 500 mL of distilled water
26. Stir the solution until there is no more chunk of the cake (this takes about 20-30 minutes)
27. Repeat steps 2 through 10 until pH of the solution becomes around 7 which shows that there is no more sodium dissolved in the solution. pH of the solution can be measured in two ways. One is after step 11, let the solution separate into catalytic phase and solvent phase and with dip the tip of the pH tape into the solvent part. The other is after step 8, do the ph test with the solution that is filtered.
28. Put the filtered catalyst in oven (at 120℃) for 12 hrs

Appendix B. Procedure for fixed bed reactor

Reactor Preparation

1. Measure 50mg of catalyst and 400mg of silicon carbide
2. Carefully put the catalyst and silicon carbide into a quartz tube and lightly shake the tube to allow the catalyst and silicon carbide to be mixed well. Make sure the surface of the mixture is even (horizontal)
3. Load the sample
    1) Fit O-rings and screws into the upper and lower sides of the tube
    2) Put the tube into the reactor and tight the screws
    3) Carefully place the thermometer in the tube (right above the catalyst surface and it MUST NOT touch the catalyst surface)
4. Start **Leak test**
    1) Check the controller if it is set as **Manual**
    2) Check 2^{nd}, 3^{rd} and 4^{th} channels which are labeled as CH_4/H_2, CO_2 and Air respectively if they are set as 0
    3) Open nitrogen gas valve
    4) Change the channel to 1 and set the nitrogen gas flow to around 80
    5) Close the reactor valve
    6) Wait until pressure inside the reactor becomes 40 kPa. When pressure reaches 40kPa, close the N_2 valve. Change the mass flow controller to **Auto**
    7) Wait about 2~3 minutes to see if there is any leak (if there is a leak, the reactor pressure is lower than 40kPa)
    8) Open the reactor valve, if no leak is detected
5. Insulate each side of the tube
6. Turn on the furnace and reactor controller

Reduction

1. Check that the mass flow meter controller setting is set to **Auto**
2. Open hydrogen, nitrogen gas valves and make sure methane and air valves are closed
3. Go to Labview→"*Input Parameters"*
4. Create a new folder in the C:// drive
4. Set default directory (where to save data) and file name by copying the folder address and pasting into the default directory field

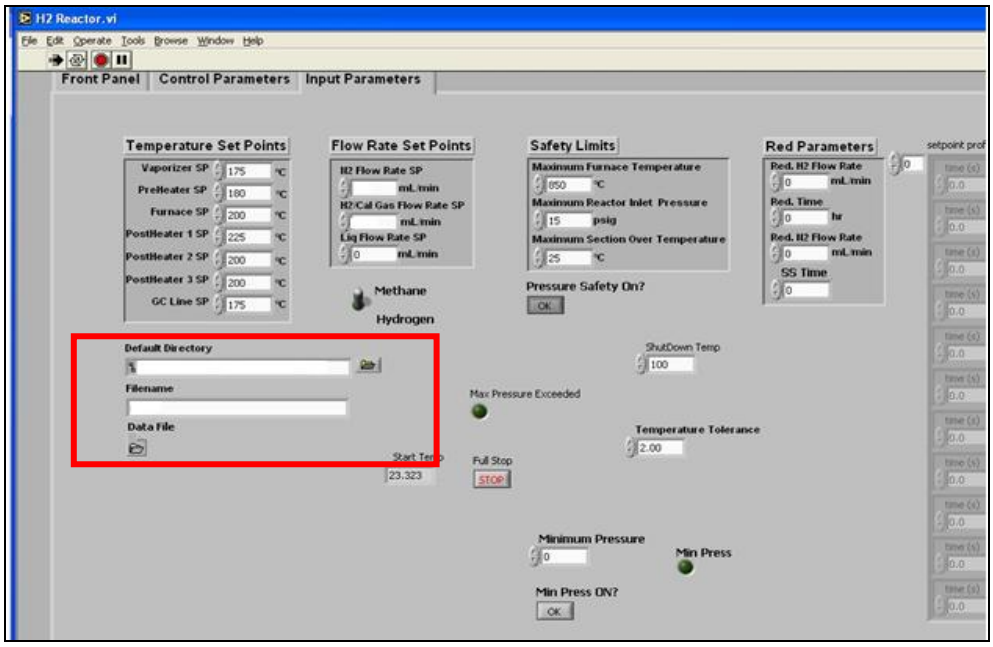

5. Set flow rate for the hydrogen gas and H_2 catalyst. *(The flow rates below refer to a 10% H_2/N_2 dilution)*

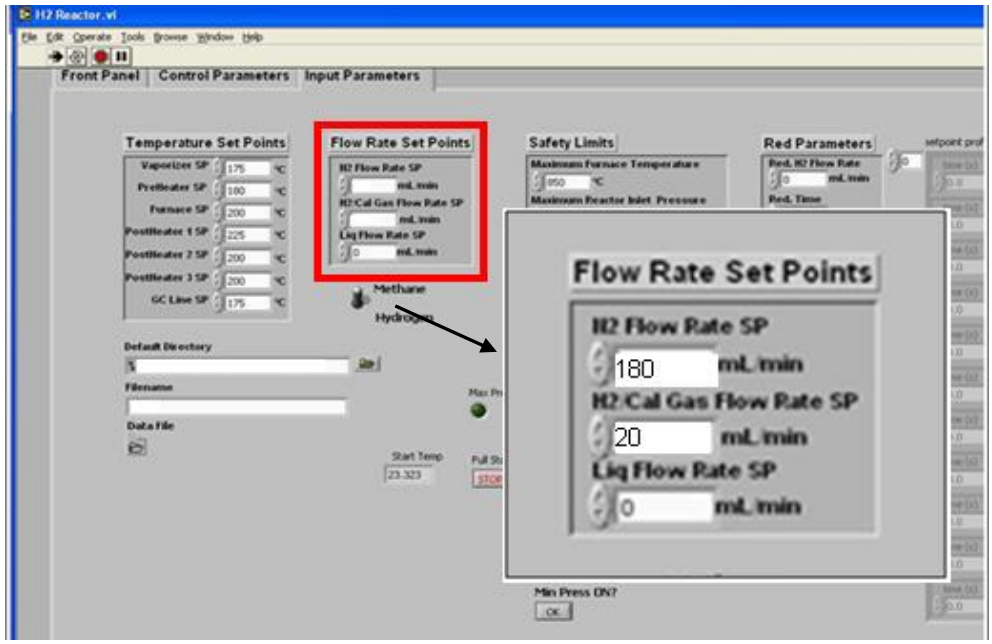

6. Go to "*Front Panel"* and set reaction temperature and make sure reactor setting is at *"Reactor Top TC" (The reaction temperature below refers to a 720℃ reduction.)*

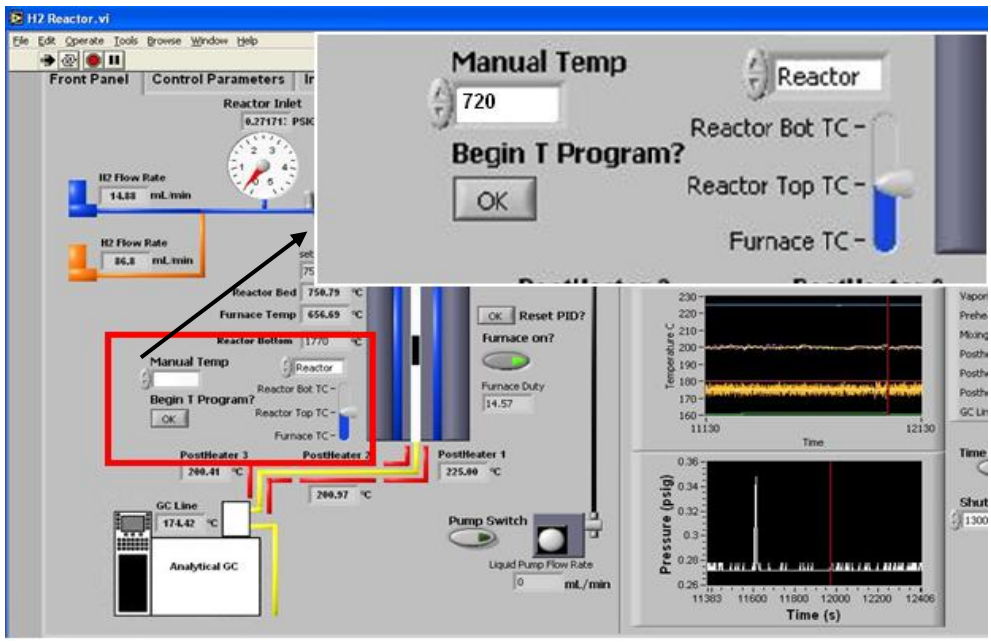

7. Click the first arrow button ("*Running*") on the "*Front Panel*" → *Current Directory*

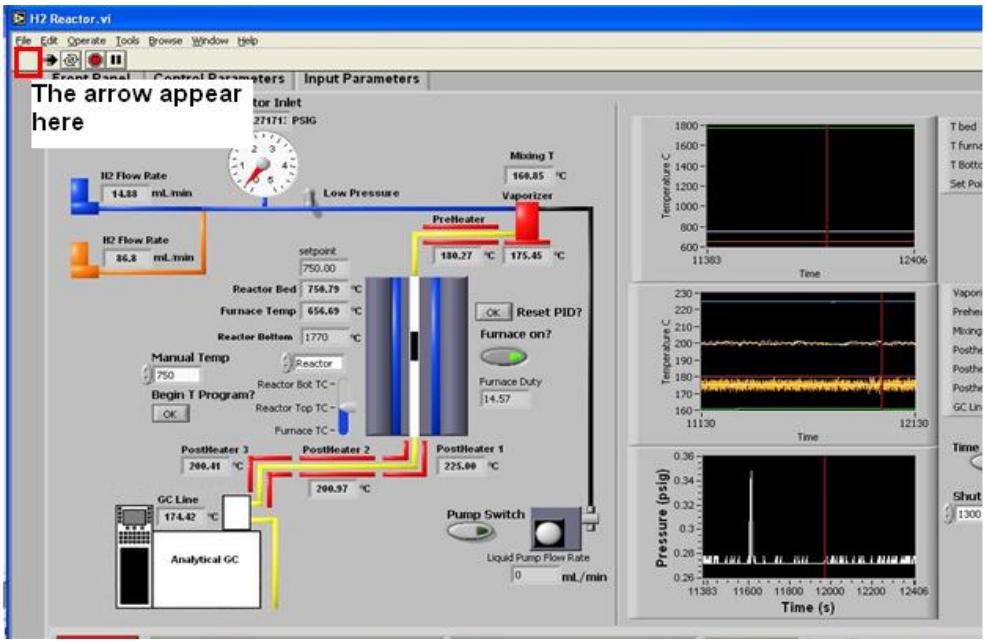

8. Go to GC controller and set sample name (same as the file name used in Labview) and the number of injections (i.e. 20 hours of reduction-each injection takes 30 minutes), then click Data files and set directory where to save GC data (same as the directory set in Labview) In the blank row following flushN2, click none and change and to GA – Clean.

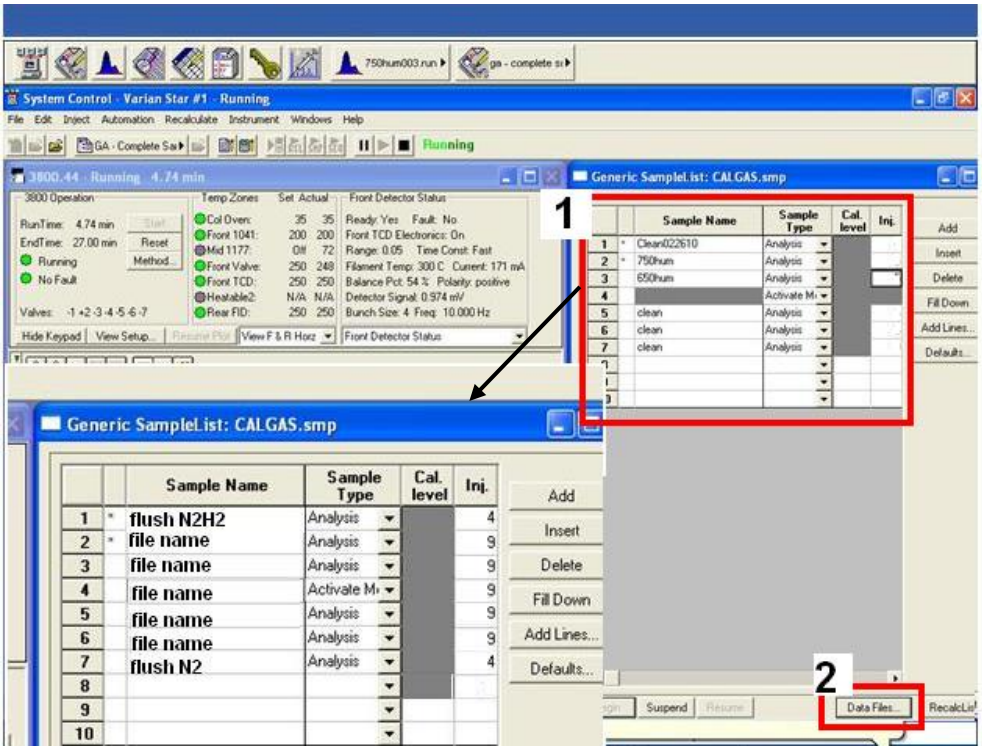

9. Go back to "*Front Panel"* then, wait until "*Reactor Bed*" becomes 420˚C. When the temperature reaches 420˚C, go to GC controller click stop sign

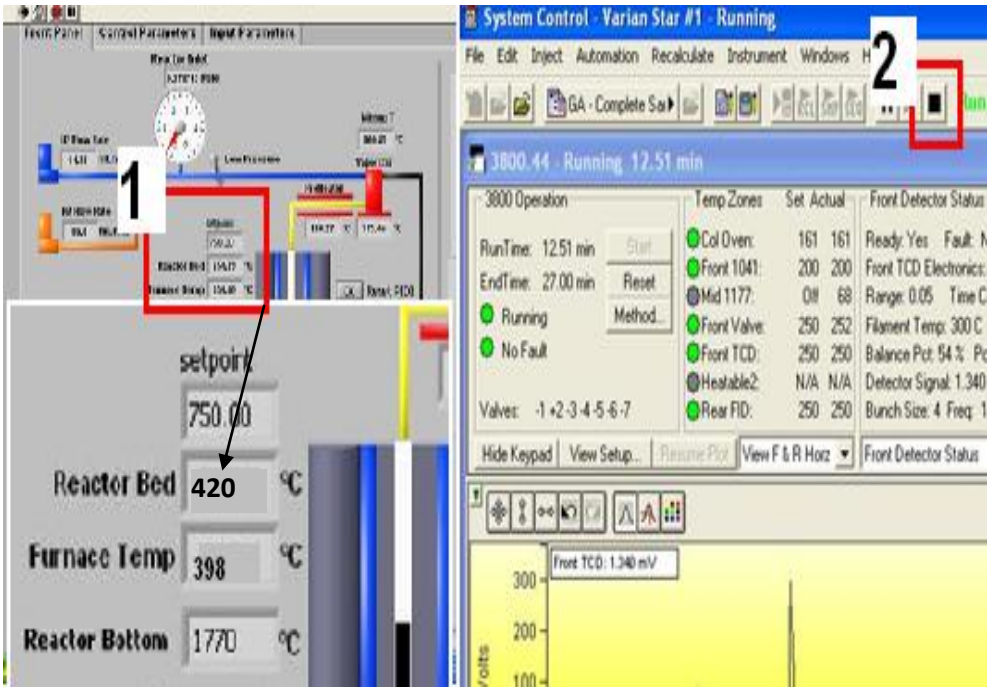

10. After running changes to Computing click Begin → OK → Browse → Select appropriate method (i.e. Complete Sample…) → OK

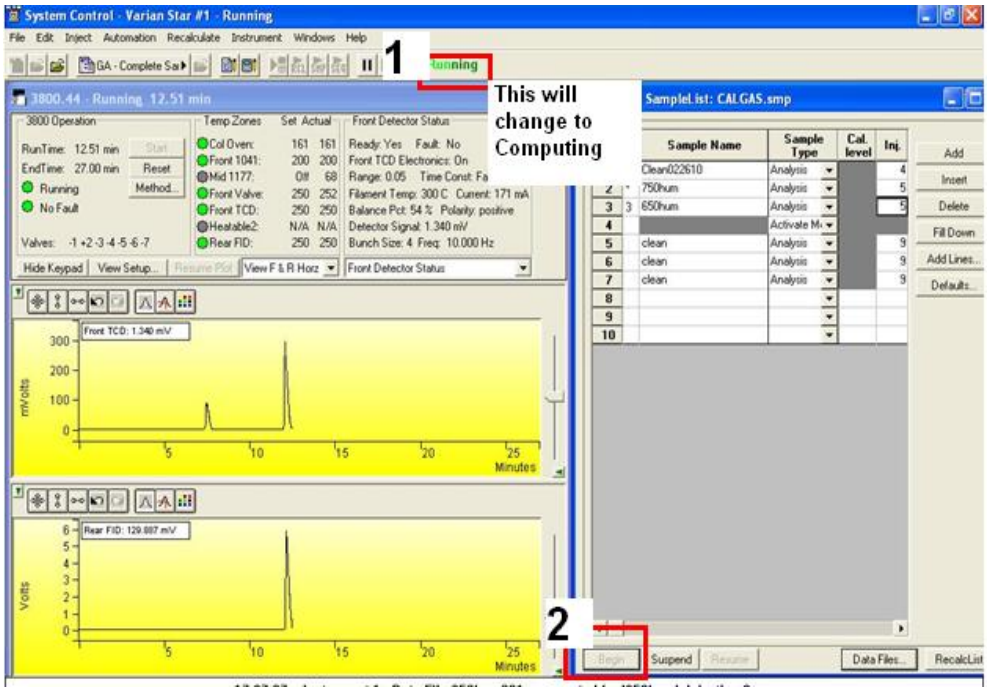

11. Wait until the last injection of reduction finishes

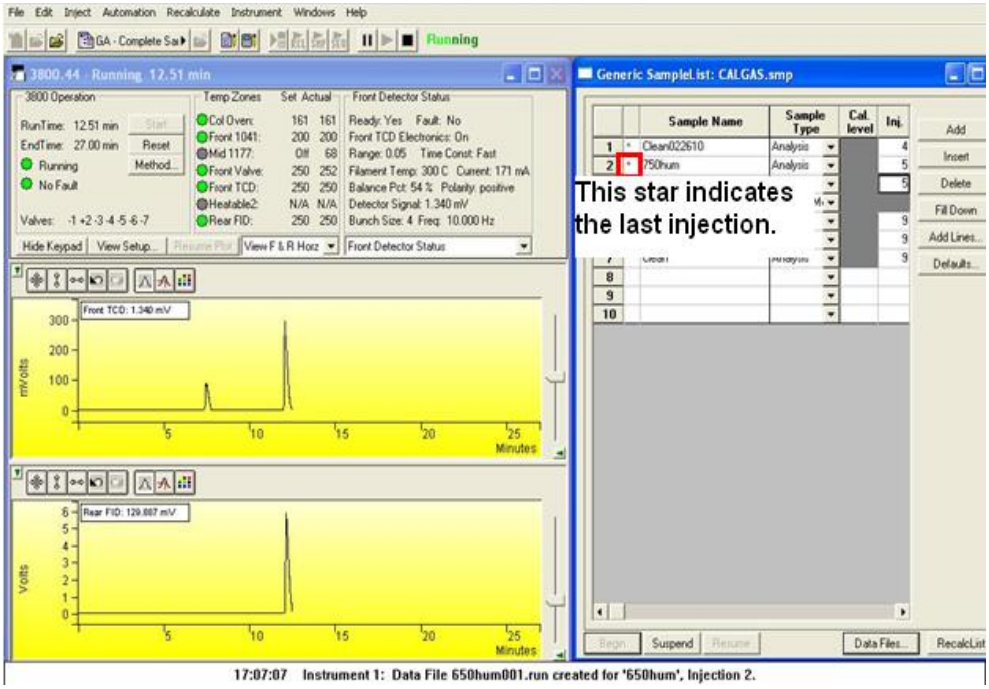

Reaction

1. Reset the “Flow Rate Set Point” in Input Parameter section in Labview to 200 mL/min of N2 and 0 mL/min of H2

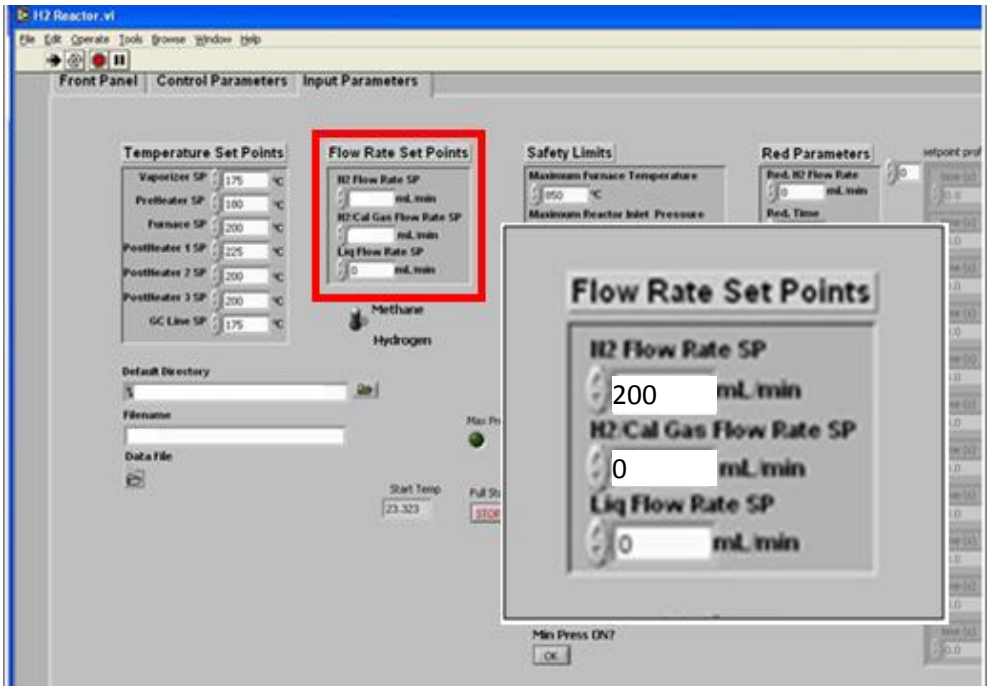

2. Go to “Front Panel” and reset the manual temperature. (Manual temperature for this reaction is set to 700℃).

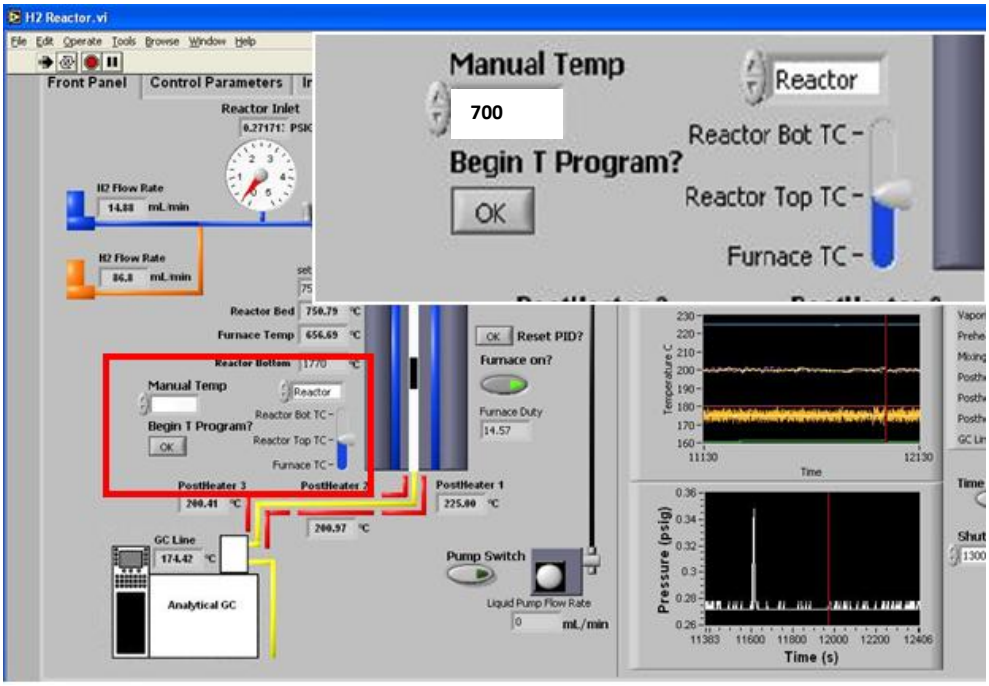

3.

Open appropriate cylinders (i.e. Methane, Carbon dioxide-dry reforming or combined, Air-Partial oxidation or combined)

4. Close the H_2 valve, Open CH_4 and CO_2 valve (dry reforming or combined) or Air valve (partial oxidation or combined)
5. Using mass flow meter controller, change the flow rate of each reactant gas.
   ****Note: the controller must be set as manual**
6. Make sure that the reaction pressure does not exceed **3 psig**
7. When the last injection starts, change the flow rate of the reactants (CH_4 and CO_2 or Air) to 0, except N_2 gas. Then, change the mass flow meter controller setting to **Auto** for cooling down.
8. Close CH_4 and CO_2 or Air valves
9. Close CH_4 and CO_2 or Air cylinders
10. Click the red button in the "*Front Panel*" and check if the reactor bed temperature decreases. Turn off the furnace and reactor controller.

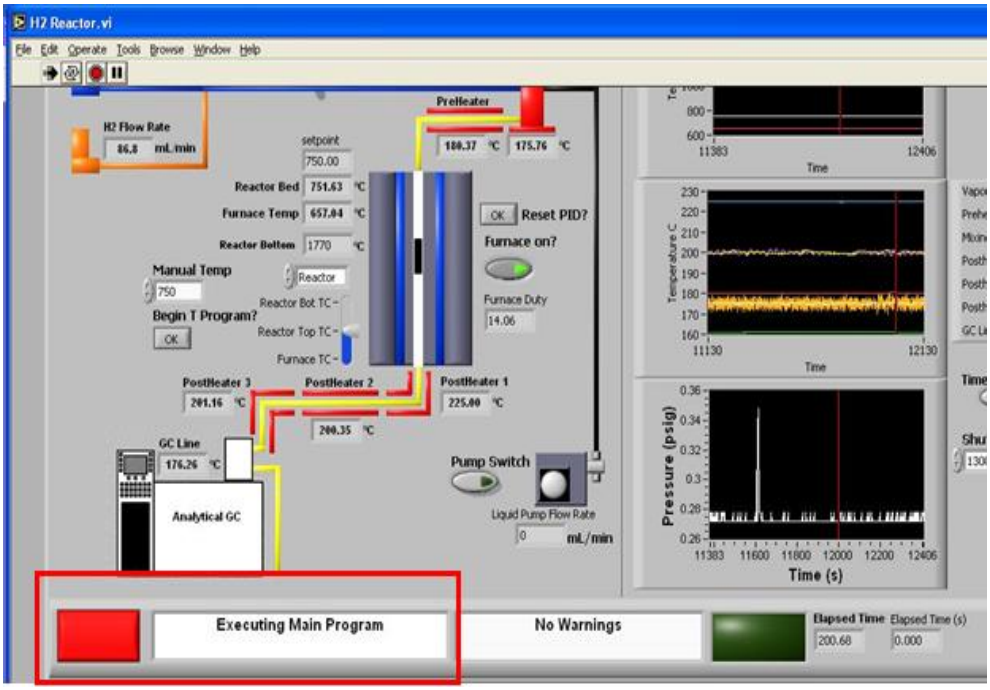

11. When the furnace temperature becomes below 390˚C, slightly open the reactor door.

12. When the reactor bed temperature decreases to around the room temperature, go to *"Input Parameter"* → Click stop

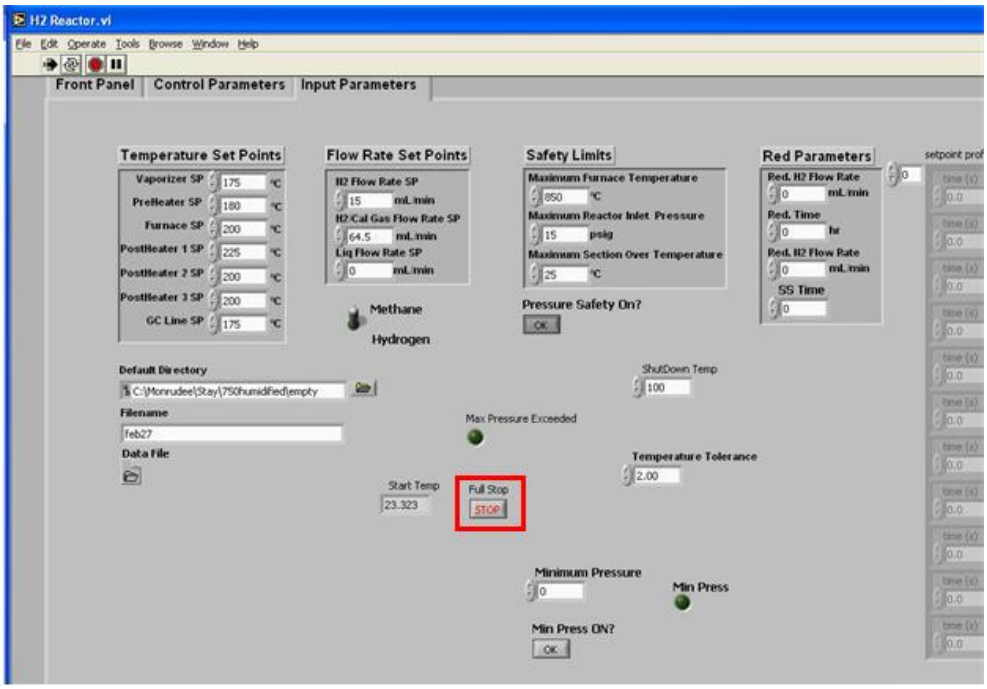

13. Close N_2 valve

SHUTTING DOWN GC IN AN EMERGENCY

1. Set the flow rates to 200 mL/min for N_2 and 0 mL/min for H_2 in the Input Parametres tab

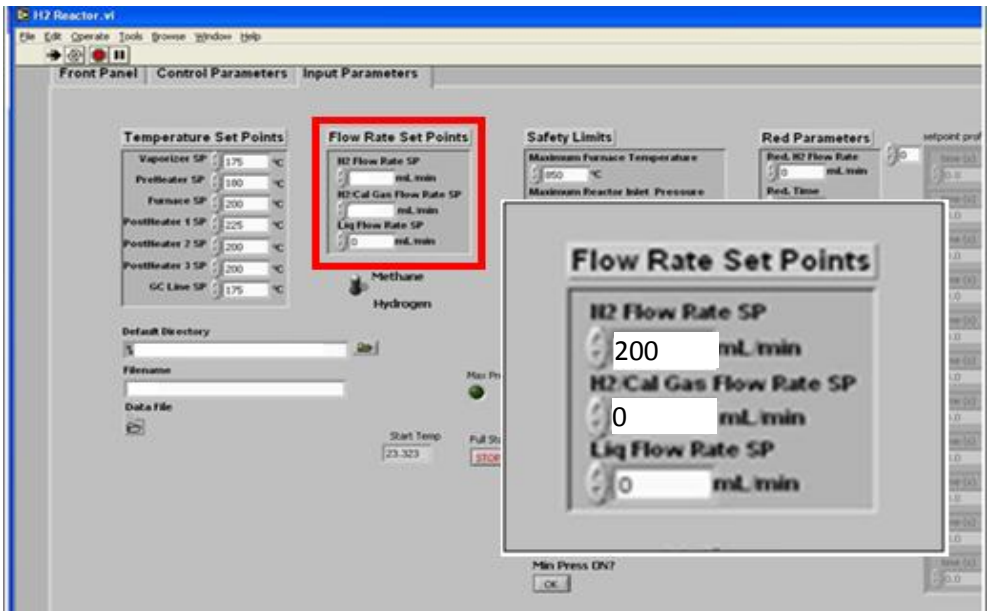

2. Set all flow rates with the exception of N_2 to zero on the mass flow controller (NOTE: should be done on M**anual**)

3. Change the mass flow controller to **Auto**

4. Close the CH_4, H_2 and CO_2 valves

5. Close the CH_4 and CO_2 cylinders if previously opened

6. Click the large red button located at the bottom of the Front Panel

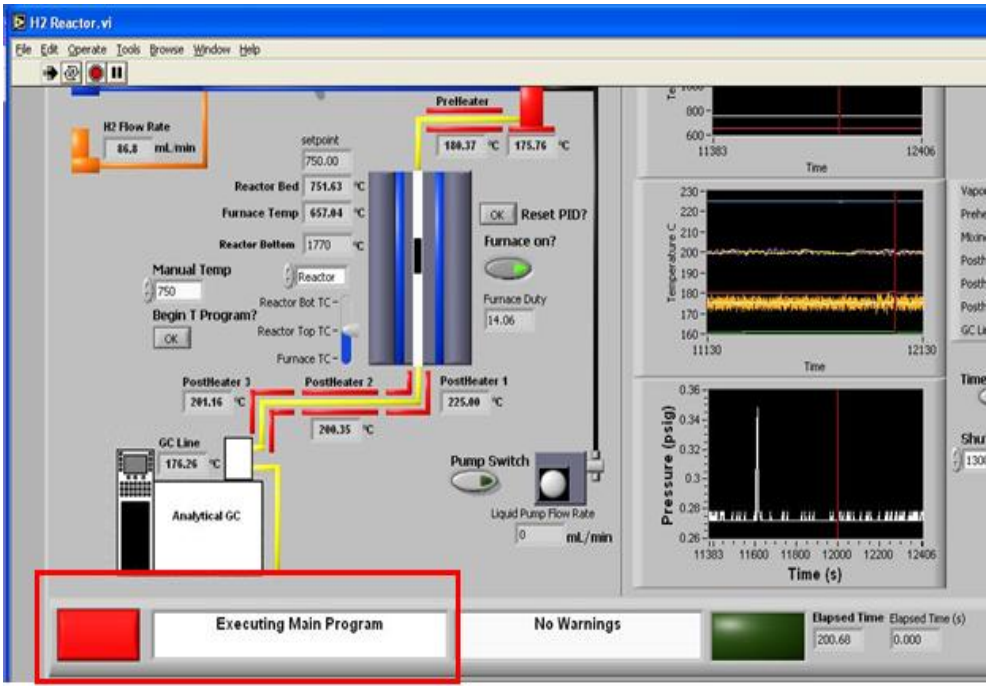

7. In the GC Controller, change the number of injections on the left (i.e. current injection) to the number on the right (i.e. total injections to complete)

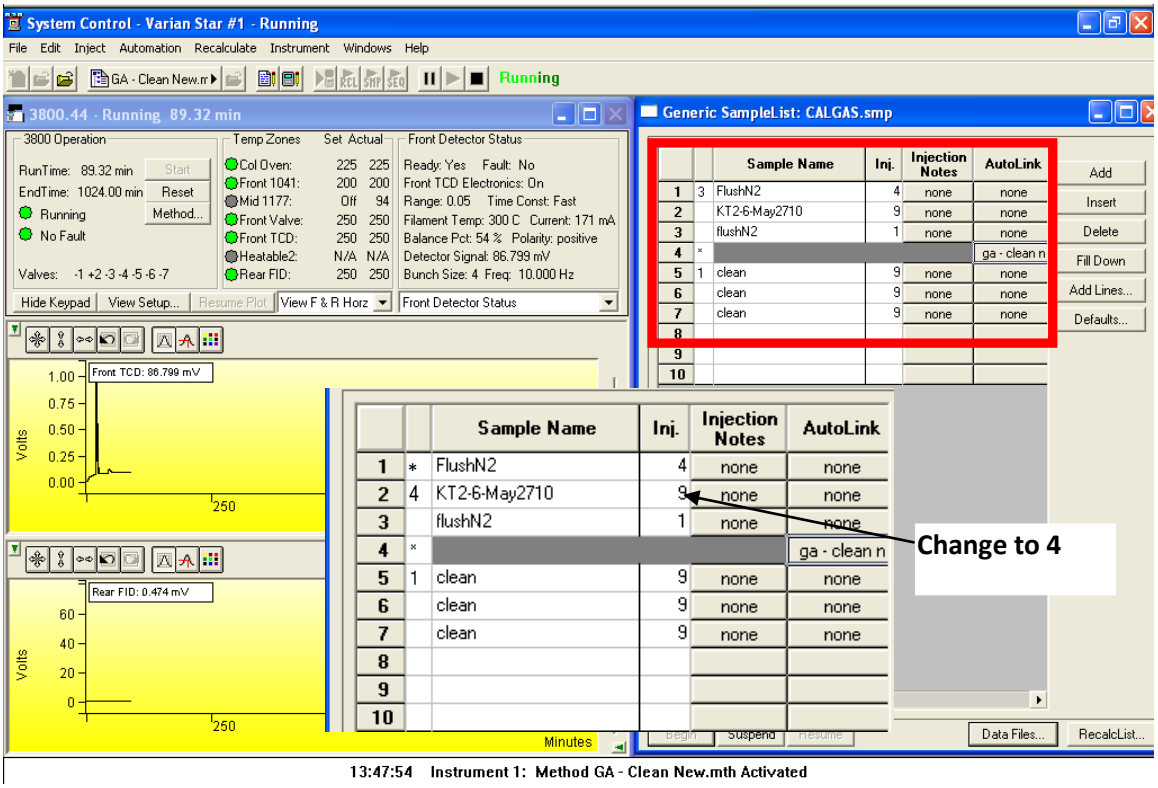

8. In the GC controller, delete all rows before the final flushN2. In the row following the final flushN2, click **none** in the **AutoLink** column and select **GA-Clean Mode** for the method.

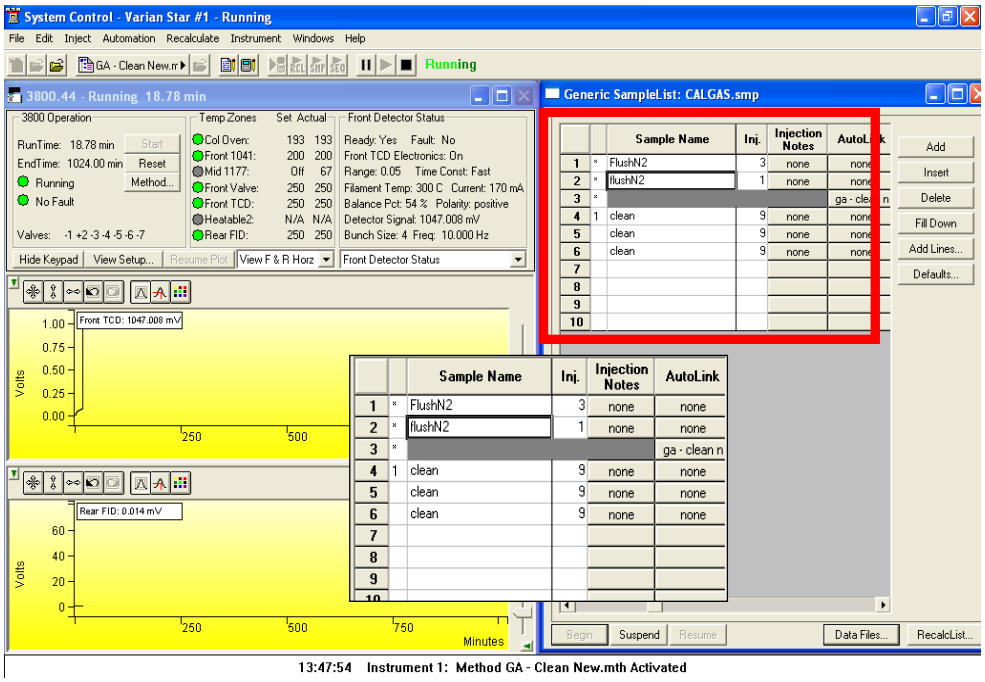

Appendix C. Calibration Data

A.1 Calibration of Mass Flow Controllers (MFCs)

1. MFC for N_2

MFC (#)	Trial #1	Trial #2	Trial #3	Trial #4	Trial #5	ave time	ml/sec	**ml/min**
5.00	53.02	54.12	53.76	52.62	52.16	53.14	0.19	**11.29**
10.00	25.04	25.57	26.01	26.57	25.74	25.79	0.39	**23.27**
20.00	13.65	12.72	13.12	13.17	12.96	13.12	0.76	**45.72**

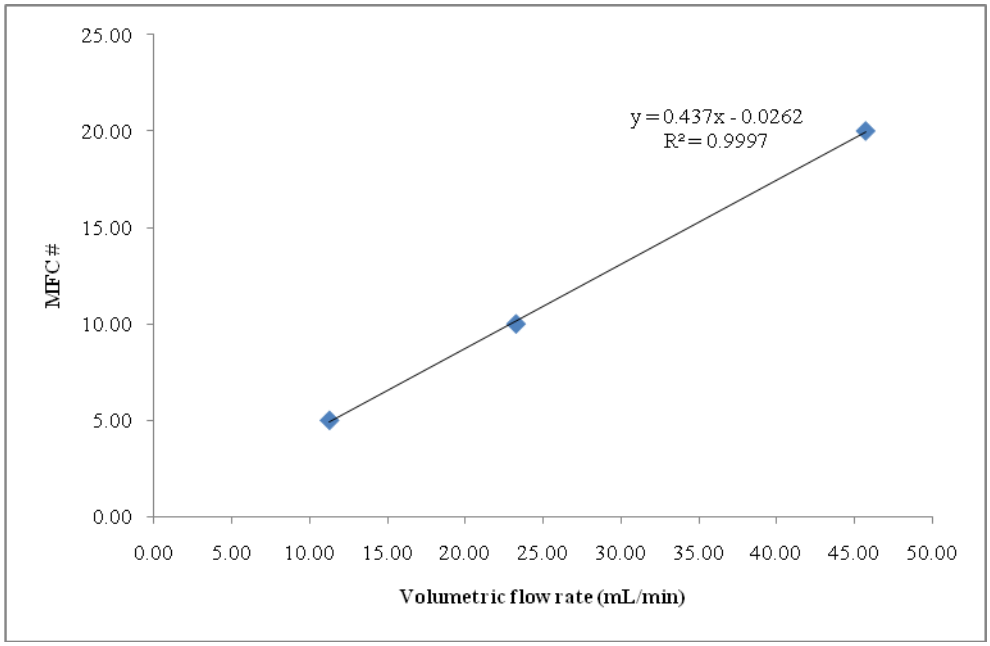

2. MFC for H2

MFC (#)	Trial #1	Trial #2	Trial #3	Trial #4	Trial #5	ave time	ml/sec	**ml/min**
5.00	32.04	32.58	32.44	32.55	32.04	32.33	0.31	**18.56**
10.00	22.06	22.27	22.39	23.76	22.64	22.62	0.44	**26.52**
20.00	14.03	13.83	14.03	14.12	14.14	14.03	0.71	**42.77**
30.00	10.89	10.70	10.86	11.15	11.26	10.97	0.91	**54.68**
40.00	8.43	8.39	8.43	8.62	8.43	8.46	1.18	**70.92**
50.00	6.96	6.89	6.67	7.01	6.93	6.89	1.45	**87.06**
60.00	5.80	5.74	5.75	5.68	5.71	5.74	1.74	**104.60**
70.00	5.14	5.12	5.19	5.12	5.11	5.14	1.95	**116.82**

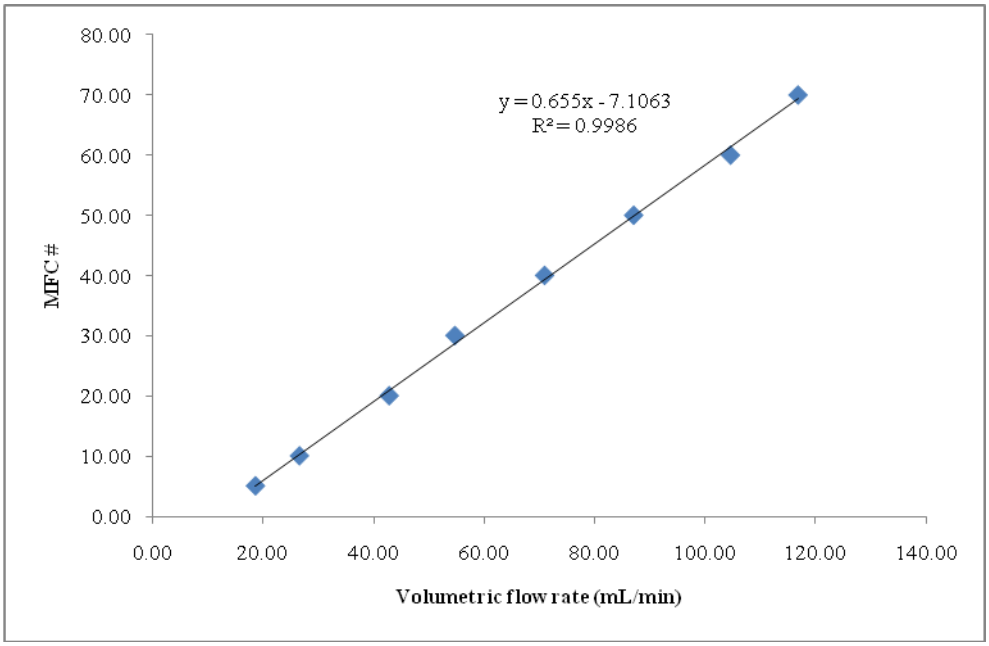

3. MFC for CO_2

MFC (#)	Trial #1	Trial #2	Trial #3	Trial #4	Trial #5	ave time	ml/sec	**ml/min**
8.00	90.52	92.33	91.52	89.92	89.16	90.69	0.11	**6.62**
10.00	65.84	66.76	65.68	67.58	66.62	66.50	0.15	**9.02**
20.00	30.02	29.43	28.13	28.24	29.04	28.97	0.35	**20.71**

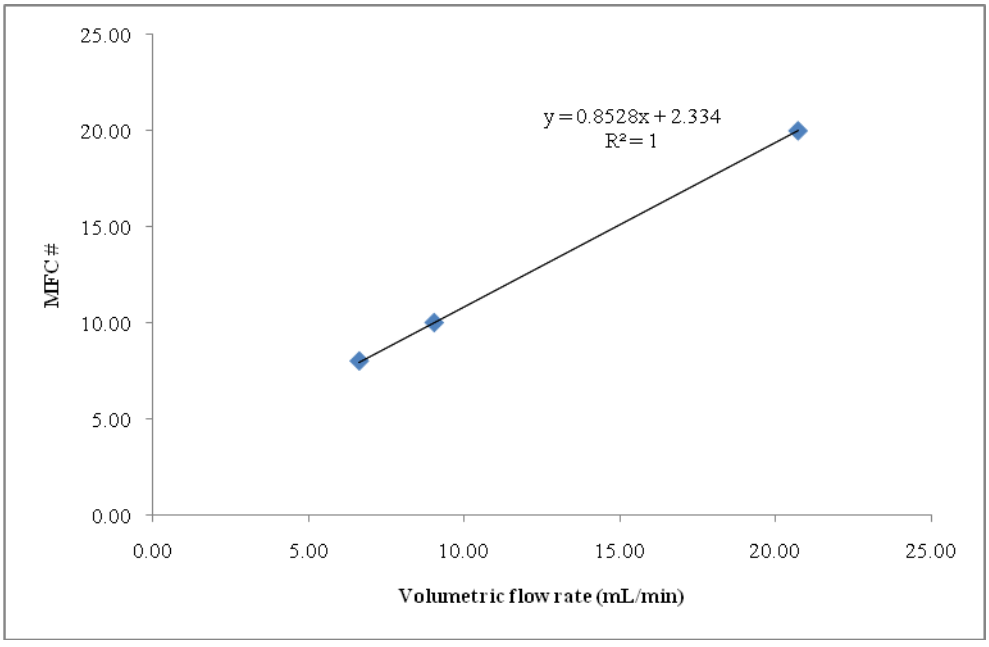

4. MFC for Air

MFC (#)	Trial #1	Trial #2	Trial #3	Trial #4	Trial #5	ave time	ml/sec	**ml/min**
5.00	64.86	64.83	65.93	64.96	64.75	65.07	0.15	**9.22**
10.00	29.62	29.52	29.33	28.53	29.15	29.23	0.34	**20.53**
20.00	14.18	14.22	14.68	15.22	14.57	14.57	0.69	**41.17**

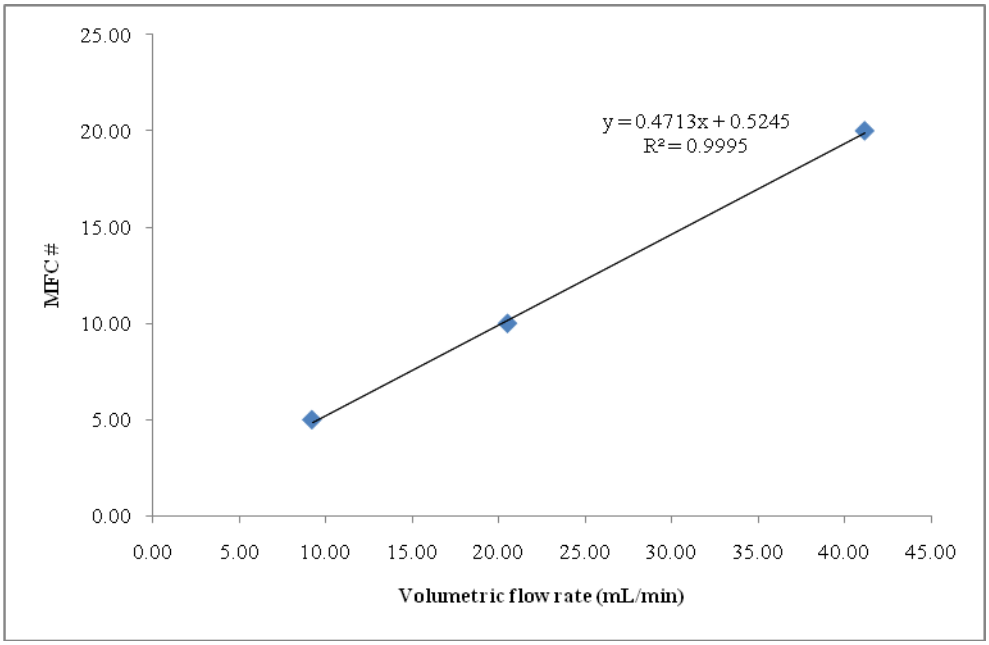

5. MFC for CH_4

MFC (#)	Trial #1	Trial #2	Trial #3	Trial #4	Trial #5	ave time	ml/sec	ml/min
5.00	42.36	45.15	43.15	43.54	43.43	43.53	0.23	**13.78**
10.00	30.64	30.78	30.64	29.82	29.92	30.36	0.33	**19.76**
20.00	19.65	19.34	19.48	19.34	19.33	19.43	0.51	**30.88**

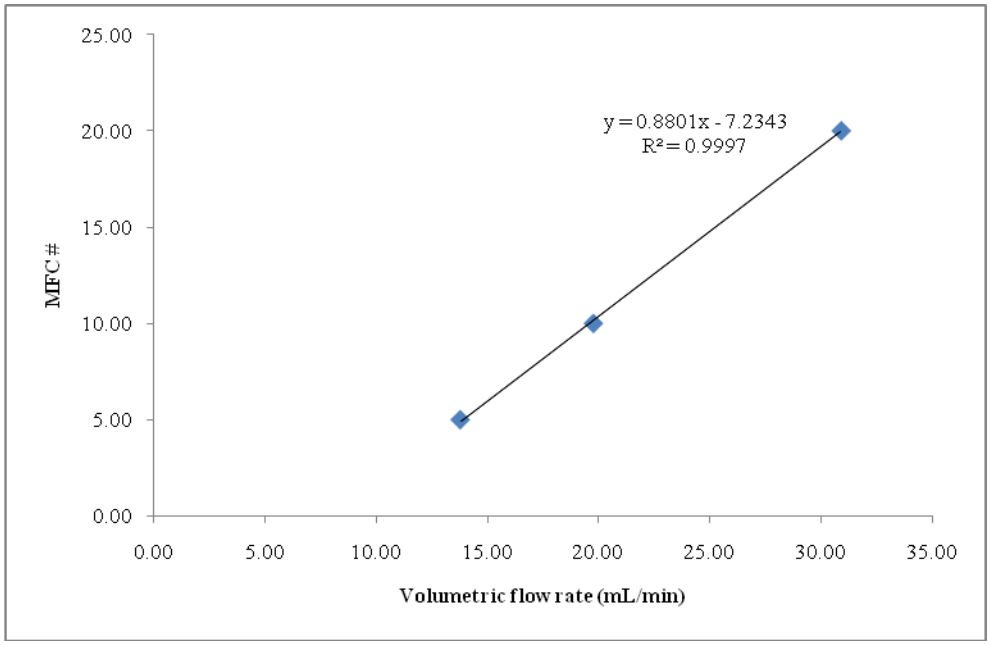

Appendix D. Sample calculations

1. Catalyst performances

Input Gas Compositions				
Total gas flow rate:		200.000	mL/min	
N2 dilution:		60	%	
N2 flu rate:		120	mL/min	
Total reaction gas flow rate:		80.000	mL/min	
Input Gas	Ratio	vol%/min	mL/min	mol/min IN
CH4	1	0.50	40.00	0.001636929
CO2	1	0.50	40.00	0.001636929
O2	0	0.00	0.00	0
N2			120.00	0.004910787
Total	2	1.00	200.00	

Based on the GC result, the methane conversion (X_{CH4}), yield of H_2 (Y_{H2}), yield of CO (Y_{CO}), and H_2/CO ratio were obtained.

$$X_{CH4} = \frac{n_{CH4,in} - n_{CH4,out}}{n_{CH4,in}} \quad \text{[Eq. 51]}$$

$$Y_{H2} = \frac{n_{H2,out}}{2 \times n_{CH4,in}} \quad \text{[Eq. 52]}$$

$$Y_{CO} = \frac{n_{CO,out}}{n_{CH4,in} + n_{CO2,in}} \quad \text{[Eq. 53]}$$

$$H_2/CO\ ratio = \frac{n_{H2,out}}{n_{CO,out}} \quad \text{[Eq. 54]}$$

$$C\ balance = \frac{n_{CH4,out} + n_{CO2,out} + n_{CO,out}}{n_{CH4,in} + n_{CO2,in}} \quad \text{[Eq. 55]}$$

Example: CO_2 reforming of CH_4 over $Ni_{0.5}Mg_{2.5}Al$ catalyst

Injction	Period	GC Area					vol%/min OUT					mol/min OUT					Carbon balance		Conversion (%)	Yield (%)		Ratio
#	(hr)	H2	N2	CO	CH4	CO2	N2	CH4	CO2	H2	CO	N2	CH4	CO2	H2	CO	mol/min OUT	%	CH4	H2 / CH4 input	CO / CH4+CO2 input	H2/CO
1	0.5	12630	2494338	1145430	202748	199195	47.34	4.58	3.21	23.38	21.04	0.00491	0.0004750	0.00033 2577	0.00242 5827	0.00218 2769	0.002990 3	100.5	73.402	67.922	73.340	1.111
2	1.0	12640	2495072	1143050	204584	201809	47.35	4.62	3.25	23.40	21.00	0.00491	0.0004790	0.00033 656	0.00242 7102	0.00217 7664	0.002993 2	100.6	73.178	67.958	73.168	1.115
3	1.5	12610	2494116	1143938	204629	201314	47.33	4.62	3.24	23.35	21.01	0.00491	0.0004793	0.00033 5912	0.00242 2107	0.00218 0144	0.002995 3	100.6	73.162	67.818	73.252	1.111
4	2.0	12622	2492462	1148234	201580	198364	47.30	4.55	3.19	23.37	21.09	0.00491	0.0004727	0.00033 152	0.00242 6017	0.00218 9643	0.002993 9	100.6	73.530	67.927	73.571	1.108
5	2.5	12611	2493464	1142539	204315	200908	47.32	4.61	3.23	23.35	20.99	0.00491	0.0004787	0.00033 5363	0.00242 2915	0.00217 8056	0.002992 1	100.5	73.195	67.841	73.182	1.112
6	3.0	12617	2493445	1144493	204031	200438	47.32	4.61	3.22	23.36	21.02	0.00491	0.0004780	0.00033 4632	0.00242 4111	0.00218 1757	0.002994 4	100.6	73.231	67.874	73.306	1.111
7	3.5	12568	2495934	1140128	206858	204200	47.37	4.67	3.28	23.27	20.94	0.00491	0.0004839	0.00034 0178	0.00241 2163	0.00217 1435	0.002995 5	100.6	72.900	67.540	72.959	1.111
8	4.0	12548	2496285	1141237	206345	203611	47.37	4.66	3.27	23.23	20.96	0.00491	0.0004827	0.00033 9213	0.00240 7913	0.00217 3229	0.002995 2	100.6	72.968	67.421	73.019	1.108
9	4.5	12448	2496931	1138540	208703	206250	47.38	4.71	3.31	23.04	20.92	0.00491	0.0004879	0.00034 3243	0.00238 7718	0.00216 7608	0.002998 8	100.8	72.678	66.855	72.831	1.102
10	5.0	12500	2498792	1136508	209041	206403	47.42	4.72	3.31	23.14	20.88	0.00491	0.0004883	0.00034 3234	0.00239 618	0.00216 2226	0.002993 8	100.6	72.655	67.092	72.650	1.108
11	5.5	12504	2498253	1137462	208605	206456	47.41	4.71	3.32	23.14	20.90	0.00491	0.0004874	0.00034 3388	0.00239 7463	0.00216 4472	0.002995 3	100.6	72.704	67.128	72.725	1.108
12	6.0	12455	2499469	1136021	209270	207024	47.43	4.72	3.32	23.05	20.87	0.00491	0.0004887	0.00034 4112	0.00238 6748	0.00216 0745	0.002993 6	100.6	72.633	66.828	72.600	1.105
13	6.5	12407	2501270	1131820	212396	209826	47.46	4.79	3.37	22.96	20.79	0.00491	0.0004954	0.00034 8234	0.00237 5707	0.00215 1346	0.002995 0	100.6	72.259	66.519	72.284	1.104

Appendix E. Aspen Plus™ simulation

Thermodynamic properties for partial oxidation, CO_2 reforming and oxidative CO_2 reforming of CH_4 at different temperatures were simulated by using ASPEN Plus™ software. The details and procedures are listed below with pictures.

1. Process diagram

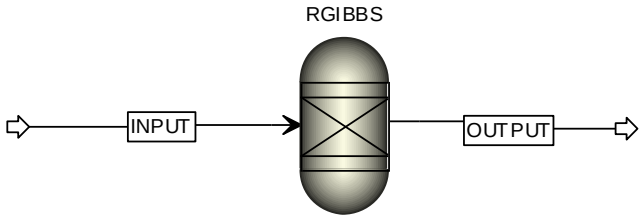

2. Setup

- Units of measurement: SI unit

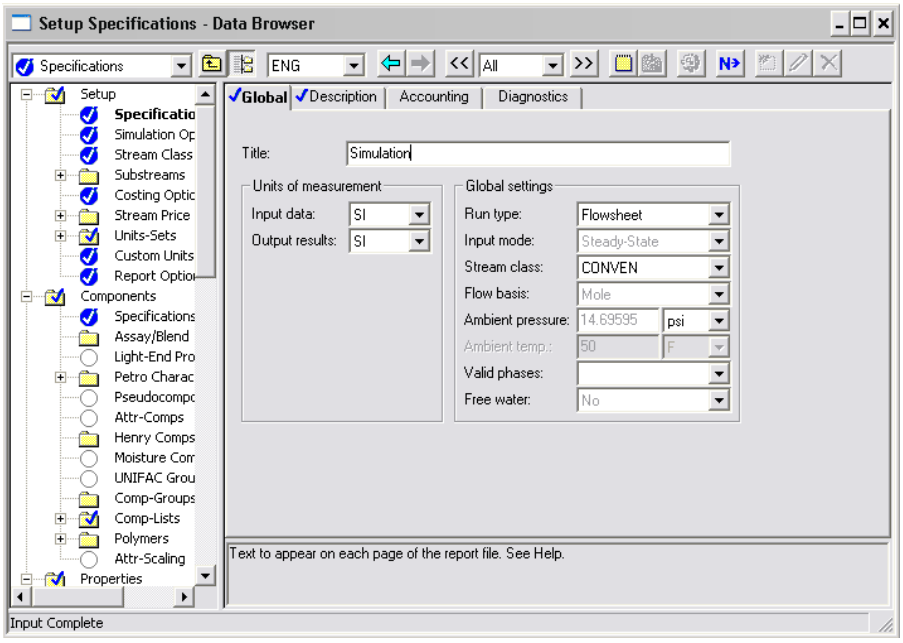

3. Properties

- Process type: ALL
- Base method: IDEAL

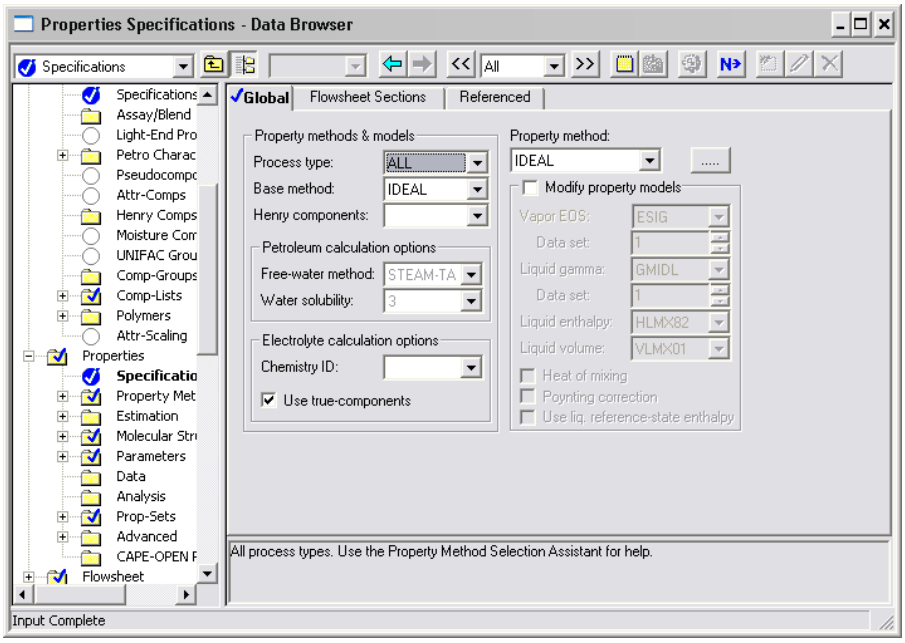

4. Components

- Component ID: CH_4, O_2, CO, H_2, CO_2, H_2O, and N_2

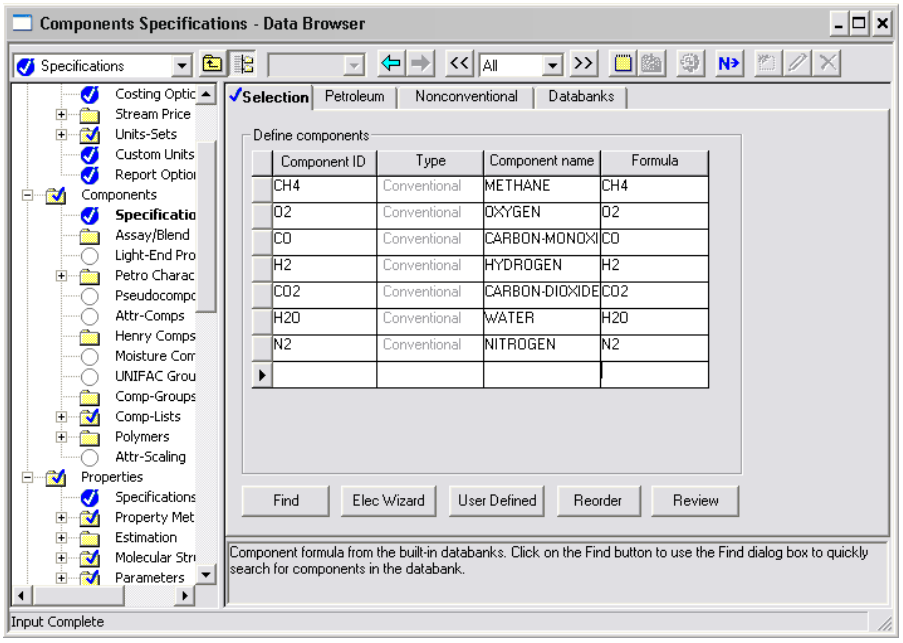

5. Input stream

- Temperature: range in 200-900℃ *(Temperature of the input stream and the reactor should be identical)*
- Pressure: 1atm
- Total flow: 100 kmol/sec
- Composition of input gas ($CH_4/O_2/CO_2/N_2$) by mole-fraction
    - Partial oxidation of CH_4: 0.26/0.13/0/0.6
    - CO_2 reforming of CH_4: 0.2/0/0.2/0.6
    - Oxidative CO_2 reforming of CH_4: 0.218/0.036/0.145/0.6

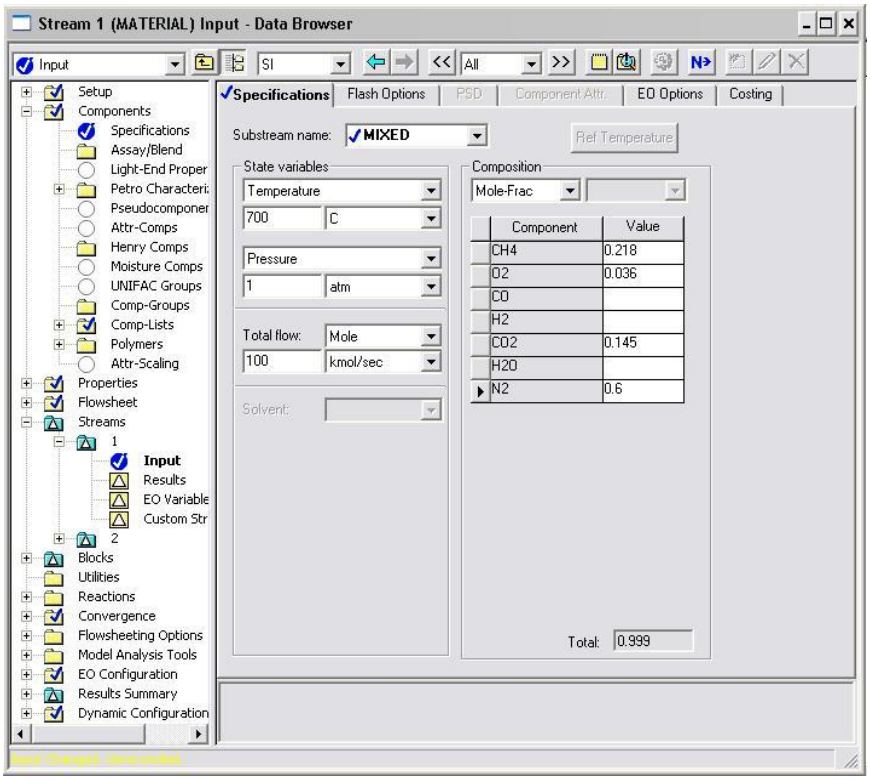

<Example for the oxidative CO_2 reforming of CH_4 at 700℃>

6. Reactor (Gibbs reactor)

- Pressure: 1atm
- Temperature: range in 200-900℃ *(Temperature of the input stream and the reactor should be identical)*